

**THE STUDY OF ELECTRICAL ENERGY UTILIZATION
FROM THREE RENEWABLE ENERGY
RESOURCES IN THE PUBLIC AREA OF A CONDOMINIUM**

WICHAI PETTONGKAM

**A DISSERTATION SUMMITTED IN PARTIAL FULFILLMENT OF THE
REQUIREMENTS FOR THE DEGREE OF DOCTOR OF ENGINEERING
PROGRAM IN ENERGY AND MATERIALS ENGINEERING
(INTERNATIONAL PROGRAM)**

FACULTY OF ENGINEERING

RAJAMANGALA UNIVERSITY OF TECHNOLOGY THANYABURI

ACADEMIC YEAR 2018

**COPYRIGHT OF RAJAMANGALA UNIVERSITY
OF TECHNOLOGY THANYABURI**

**THE STUDY OF ELECTRICAL ENERGY UTILIZATION
FROM THREE RENEWABLE ENERGY
RESOURCES IN THE PUBLIC AREA OF A CONDOMINIUM**

WICHAI PETTONGKAM

**A DISSERTATION SUMITTED IN PARTIAL FULFILLMENT OF THE
REQUIREMENTS FOR THE DEGREE OF DOCTOR OF ENGINEERING
PROGRAM IN ENERGY AND MATERIALS ENGINEERING
(INTERNATIONAL PROGRAM)**

FACULTY OF ENGINEERING

RAJAMANGALA UNIVERSITY OF TECHNOLOGY THANYABURI

ACADEMIC YEAR 2018

**COPYRIGHT OF RAJAMANGALA UNIVERSITY
OF TECHNOLOGY THANYABURI**

Dissertation Title The Study of Electrical Energy Utilization from Three Renewable Energy Resources in the Public Area of a Condominium

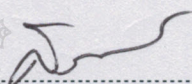
Name-Surname Mr. Wichai Pettongkam

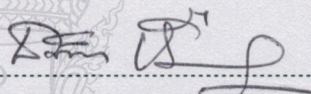
Program Energy and Materials Engineering

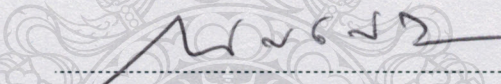
Dissertation Advisor Assistant Professor Wirachai Roynarin, Ph.D.

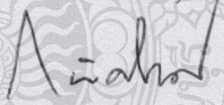
Academic Year 2018

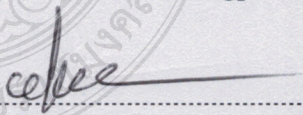
DISSERTATION COMMITTEE


..... Chairman
(Assistant Professor Sorapong Pavasupree, Ph.D.)


..... Committee
(Assistant Professor Tanit Ruangrunghaikul, Ph.D.)


..... Committee
(Mr. Narongchai O-Charoen, Ph.D.)


..... Committee
(Assistant Professor Kiattisak Sangpradit, Ph.D.)


..... Committee
(Assistant Professor Wirachai Roynarin, Ph.D.)

Approved by the Faculty of Engineering, Rajamangala University of Technology Thanyaburi in Partial Fulfillment of the Requirement for the Degree of Doctor of Engineering

..... Dean of Faculty of Engineering
(Assistant Professor Sivakorn Anghong, Ph.D.)

December 6, 2018

Dissertation Title	The Study of Electrical Energy Utilization from Three Renewable Energy Resources in the Public Area of a Condominium
Name – Surname	Mr. Wichai Pettongkam
Program	Energy and Materials Engineering
Dissertation Advisor	Assistant Professor Wirachai Roynarin, Ph.D.
Academic Year	2018

ABSTRACT

The Royal Thai Government Policy emphasizes renewable energy utilization in the high potential areas such as Pathum Thani Province in the center part of Thailand. This study presents the use of renewable energy such as solar, water and wind energy on the rooftop of a high-rise building situated in Pathum Thani Province. The building characteristics show the annual average wind speed of 3.97 m/s, the annual rainwater stored on the rooftop is 354 m³/y, and the annual average solar energy is 5.37 kWh/m².

The study of hydropower energy from a waterfall was reconsidered and applied to be used in this study using rainwater flowing from the rooftop to drive a Pico Turgo Turbine. The rooftop was restructured to store 57.6 m³ of rainwater flowing down through a pipe of 21 m head to drive the 1 kW Pico Turgo Turbine. The turbine was equipped with four 10 mm diameter nozzles at 17° angle of attack, a 430mm runner diameter, and 21 buckets with a total capacity of 0.007 m³. The Computational Fluid Dynamics (CFD) is the simulation technique that showed the water turbine electricity output 1,037W, the experimental result 950W, and the theoretical calculation 1,310W. The CFD simulation showed the efficiency 79.21%, whereas the experimental result 72.51%. The CFD technique was also used to determine the suitable wind turbine location on the building rooftop. This indicated an appropriate installation point where a small building and surrounding terrain could increase the magnitude and velocity vector affecting the turbine characteristics. The HOMER software was used to simulate the Hybrid Renewable Energy System between wind and solar electrical energy outputs and evaluated with the experimental on-site data recorded. The HOMER simulation indicated power production 47% being generated from PV solar system, about 8% from the wind turbine, and 45% fed in from the local grid. The renewable fraction of this system was approximately 0.524. The experimental data showed 42.38% of the annual power production which was derived from PV system and 5.87% from the wind turbine system, indicating the potential to reduce annual dependence on grid electricity by 51.75%.

This study explains the data of electrical energy produced from different renewable energy systems installed in the building. The results showed that the electrical energy output costs produced from the Hybrid Renewable Energy System were proved unsatisfied compared to the single renewable energy system. The CFD data of the Horizontal Wind Turbine Machine installed on the rooftop illustrate huge and various problems from its turbine characteristics as well as the building characteristics, while the Pico Turgo Water Turbine machine was proved unsuitable to be used in high rise buildings because of its installation cost and unstable rainwater supply.

Keywords: PV solar panel, micro wind turbine, Pico Turgo water turbine, renewable energy on high rise building, hybrid renewable energy system (HRES), computational fluid dynamic (CFD), HOMER software

Acknowledgments

Joining the D.Eng Program at Rajamangala University of Technology Thanyaburi enables me to grow in so many directions, as an academic and a person.

For this thesis, first , I would like to express my sincere gratitude to my advisor Assistant Professor Dr. Wirachai Roynarin and Mr. Decha Intholo for the valuable of guidance and encouragement which help me throughout my research.

Secondly, I would like to thank to the thesis committees, Assistant Professor Dr. Sorapong Pavasupree, Associate Professor Dr. Jakkree Srinonchat, Associate Professor Dr. Kiattisak Sangpradit, and Dr. Amphol Arphathanakorn for their valuable comments and helpful suggestions.

Finally, I am most thankful for my family who always support and encourage me in every endeavour. Without their love, patience, and encouragement, I would not be who I am today.

Wichai Pettongkam



Table of Contents

	Page
Abstract.....	(3)
Acknowledgements.....	(4)
Table of Contents.....	(5)
List of Table.....	(6)
List of Figures.....	(7)
CHAPTER 1 INTRODUCTION.....	11
1.1 General Overview.....	11
1.2 Objectives.....	11
1.3 Overview.....	12
1.4 Dissertation Overview.....	13
1.5 Utilization of the Dissertation.....	14
CHAPTER 2 THEORY AND LITERATURE REVIEW.....	15
2.1 Understanding of Energy and Power.....	15
2.2 Renewable Energy Potential Resources in Thailand	18
2.3 Wind Turbine Configuration.....	24
2.4 PV Energy.....	30
2.5 Water Energy.....	31
2.6 Hybrid Renewable Energy System (HRES) System.....	38
2.7 HOMER Software for HRES Simulation Description.....	40
CHAPTER 3 METHODOLOGY.....	45
3.1 Introduction.....	45
3.2 Methodology.....	46
3.3 Homer Commercial Program Calculation.....	68
3.4 Experimental Site Testing.....	74
CHAPTER 4 RESULTS AND DISCUSSION.....	79
4.1 Pico-Water Turbine Energy Result.....	79
4.2 Homer Hybrid System Simulation Result.....	94
CHAPTER 5 CONCLUSIONS.....	103
5.1 Recommendation and Contribution.....	104
5.2 The Interesting Knowledge Found in this Study.....	104
Bibliography.....	106
Appendices.....	112
Appendix A CFD Design Usability.....	113
Appendix B Original Location of Wind Turbine CFD Result as Wind Flow from SW.....	118
Appendix C New Location of Wind turbine CFD Result as Wind Flow from SW.....	121
Appendix D List of Publications.....	124
Biography.....	126

List of Tables

	Page
Table 2.1	Wind data in Suvarnabhumi airport Thailand as measured by the Windfinder website..... 20
Table 2.2	The features of various PV product..... 30
Table 2.3	Classification of hydro power of capacity..... 31
Table 2.4	Classification of hydro power of head..... 31
Table 2.5	Groups of water turbines. 32
Table 3.1	Boundary conditions of the pico turgo turbine..... 62
Table 3.2	Grid convergence..... 65
Table 3.3	Load of public commonly use area electricity at the high-rise Pier93 67
Table 3.4	Technical specifications of a PV panel..... 74
Table 3.5	Technical specifications of the micro wind turbine..... 75
Table 4.1	Power of the Turgo water turbine from theoretical calculations, CFD simulations, and experimental tests..... 79
Table 4.2	Power from wastewater..... 81
Table 4.3	Velocity magnitude from SSW wind flow direction at point (A-K) of 3 m from rooftop level..... 88
Table 4.4	Rotation of micro wind turbine between including terrain obstacle and not including terrain obstacle from the SSW wind flow direction..... 92
Table 4.5	Rotation of micro wind turbine between the original and new locations from the SSW wind flow direction..... 93
Table 4.6	Results of a simulation of a hybrid PV-wind energy system operating on the PIER 93 building..... 96
Table 4.7	Results of a simulation of a hybrid PV-wind energy system operating on the PIER 93 building..... 97
Table 4.8	HOMER simulation results of monthly energy purchased..... 98
Table 4.9	Power production (simulated with HOMER and experimental) of the renewable energy sources in a hybrid wind-PV energy system installed on the PIER 93 building 98

List of Figures

	Page
Figure 2.1	PV cell generating electricity..... 17
Figure 2.2	The Wind potential in Thailand..... 19
Figure 2.3	Feature and characteristics of monsoon in Thailand..... 19
Figure 2.4	Wind rose at Suvarnabhumi Airport Thailand..... 21
Figure 2.5	Determination of flat terrain..... 22
Figure 2.6	Schematic of a momentum wake. Reproduced by the permission of Alternative Energy Institute..... 22
Figure 2.7	Global solar irradiation map of Thailand..... 23
Figure 2.8	Annual average global and diffuse solar radiation in Thailand..... 23
Figure 2.9	General components of HAWT..... 25
Figure 2.10	Ideal power curve of a wind turbine..... 26
Figure 2.11	Model H-type VAWT..... 27
Figure 2.12	Different sizes of wind turbines..... 28
Figure 2.13	Typical application of wind turbine sizes..... 28
Figure 2.14	Micro wind turbine..... 29
Figure 2.15	Micro wind turbine circuit..... 29
Figure 2.16	Crystalline silicon solar cells..... 30
Figure 2.17	Turbine application range chart..... 33
Figure 2.18	Bucket of Turgo turbine..... 34
Figure 2.19	(a) Earliest design of Giovanni Branca and (b) Sketch of the Turgo type design..... 35
Figure 2.20	Design of a typical Turgo runner..... 35
Figure 2.21	CFD simulation of Turgo runner..... 36
Figure 2.22	(a) Bucket of Turgo turbine and (b) Velocity triangles..... 37
Figure 2.23	General HRES architecture..... 38
Figure 2.24	On-grid PV-wind turbine HRES..... 38
Figure 2.25	PV-wind-biomass hybrid power supply system..... 39
Figure 2.26	Typical schematic of an HRES in HOMER..... 40
Figure 2.27	Block diagram of a standalone hybrid energy system..... 43
Figure 2.28	Standalone PV-wind hybrid system..... 43
Figure 2.29	I–V and P–V characteristics of a PVG..... 44
Figure 3.1	Conceptual design of a stand-alone HRES..... 45
Figure 3.2	The research step..... 46
Figure 3.3	(a) Pathum Thani province, Thailand and (b) High-rise PIER 93 building located in the Pathum Thani province 47
Figure 3.4	Annual average global and diffuse radiations in Thailand between 1964–2008..... 48
Figure 3.5	Wind data measurement at the PIER 93 building 49
Figure 3.6	The resource data from wind, solar and water..... 49
Figure 3.7	Daily wind speed for each month of 2017 at the PIER 93 building. 51
Figure 3.8	Process flowchart..... 51

List of Figures (Continued)

		Page
Figure 3.9	(a) PIER 93 high-rise building, (b) Roof gutter area, and (c) water storage area on rooftop	52
Figure 3.10	Tool bar of CFDdesign commercial program for New model simulation.....	54
Figure 3.11	CFDdesign commercial program assessment tool for Mash error checking	54
Figure 3.12	Material selection for a micro wind turbine.....	55
Figure 3.13	CFDdesign Material selection of Building, Building Terrain and Wind turbine	55
Figure 3.14	The boundaries conditions setup of building terrain for SSW direction wind flow input.....	55
Figure 3.15	Meshing of the simulation model.....	56
Figure 3.16	Solving the CFD method.....	57
Figure 3.17	Layout of the terrain at PIER 93. (a) Google view, (b) 2D model, and (c) 3D model.....	57
Figure 3.18	3D model grid cell creations. (a) Terrain, (b) Roof top of the PIER 93 building, and (c) micro wind turbine.....	58
Figure 3.19	Boundary conditions. (a) Velocity inlet from the SSW direction and (b) Pressure outlet at the outlet side.....	59
Figure 3.20	CFD simulation method.....	60
Figure 3.21	Turgo turbine computational domain and boundary conditions.....	63
Figure 3.22	Bucket grid dependency of the Turgo turbine. (a) Coarse mesh, (b) Medium mesh, and (c) Fine mesh.....	63
Figure 3.23	Grid density of the turgo turbine nozzle, cup, and rotating region	64
Figure 3.24	Grid dependency of the Pico Turgo turbine.....	64
Figure 3.25	Pico Turgo turbine. (a) Prototype buckets and (b) Prototype buckets with runner.....	65
Figure 3.26	3D model of pico turbine testing. (a) 3D model connected set connecting to PMG, (b) 3D water circulation system connecting with water pumping, (c)real prototype testing apparatus, and (d) Water flow impacting the turbine blade.....	66
Figure 3.27	Two renewable energy system concept design.....	67
Figure 3.28	HOMER commercial program.....	68
Figure 3.29	Selecting the real side location of the PIER 93 building.....	68
Figure 3.30	Monthly input average of the wind velocity.....	69
Figure 3.31	Input primary load input of the PIER 93 building.....	69
Figure 3.32	Specifications of the PV Inputs.....	70
Figure 3.33	Input specifications of a wind turbine.....	70
Figure 3.34	Wind speed daily profile of the HOMER program at 14 °N, 100 °E	71
Figure 3.35	Simulation model of the hybrid PV and wind system.....	72

List of Figures (Continued)

	Page
Figure 3.36 Energy inputs for the wind turbine and solar photovoltaic array (a) Power curve of the micro wind turbine and (b) Global solar radiation at the study site (14 °N, 100 °E).....	73
Figure 3.37 PV array installation at the PIER 93 building.....	74
Figure 3.38 Micro wind turbine installed at the PIER 93 building.....	75
Figure 3.39 PV-wind hybrid inverter.....	76
Figure 3.40 PV-wind hybrid inverter circuit.....	76
Figure 3.41 Experimental hybrid system installed on the rooftop of the PIER 93 building. (a) Hybrid system on the rooftop, consisting of a wind turbine and solar PV panels, (b) PV panels installed on the rooftop of a high-rise building, and (c) Hybrid system control panel.....	77
Figure 3.42 Battery bank. (a) Battery capacity curve and (b) Battery.....	78
Figure 4.1 Comparison of power output between theoretical, CFD, and Experimental Results.....	80
Figure 4.2 Rotation of runner and water head.....	80
Figure 4.3 Power curve of Pico turgo water turbine on differences nozzle diameter.....	81
Figure 4.4 Streamline of water flow in a bucket.....	82
Figure 4.5 Velocity contours on turgo water turbines. (a) Flow and (b) Vector velocities.....	83
Figure 4.6 Velocity distribution. (a) Rotating region and (b) Buckets.....	83
Figure 4.7 Flow velocity contours of pico turgo turbines. (a) Top, (b) Middle, and (c) Bottom buckets.....	84
Figure 4.8 Isosurfaces of velocity in the bucket.....	84
Figure 4.9 Pressure and velocity profiles for the top, middle, and bottom buckets. (a) Velocity and (b) Pressure profiles.....	85
Figure 4.10 Flow velocity contours of the turgo water turbine. (a) Top, (b) Middle, and (c) Bottom buckets.....	86
Figure 4.11 Velocity investigation point on the rooftop.....	86
Figure 4.12 Velocity distribution on the rooftop from the SSW wind flow direction (a) Height 0–26 m from the rooftop and (b) Height 0–3 m from the rooftop.....	87
Figure 4.13 Cross-section velocity area of the ESE and SSW directions at each WT installation point.....	88
Figure 4.14 Velocity contour of the cross-section area of the SSW section from the SSW wind flow direction.....	89
Figure 4.15 Velocity and vector contour of the cross-section wind flow area of the ESE section from the SSW wind flow direction.....	90

List of Figures (Continued)

	Page	
Figure 4.16	Wind turbine velocity curve from the SSW wind flow direction of WT1, WT2, WT3, and WT4 (a) Including terrain obstacle, (b) Not including terrain obstacle, and (c) Percentage of angular velocity differences.....	91
Figure 4.17	Micro wind turbine installation point. (a) Original and (b) New location points.....	92
Figure 4.18	Percentage of angular velocity differences from the SSW wind flow direction.....	93
Figure 4.19	Electricity production of HOMER simulation result of hybrid PV-wind system. (a) Wind turbine and (b) PV simulation results..	94
Figure 4.20	Average daily power output profiles by month for case study hybrid power (a) Wind turbine power output (b) PV power output	95
Figure 4.21	Monthly averages of energy output from the case study HRES, as calculated using HOMER.....	96
Figure 4.22	Comparison between HOMER simulation and experimental on-site values for monthly micro wind turbine power production (Feb. 2016–Jan. 2017).....	99
Figure 4.23	Comparison between HOMER simulation and experimental on-site values for monthly solar photovoltaic power production (Feb. 2016–Jan. 2017).....	99
Figure 4.24	Site measurement data of monthly average electricity production, measured on-site of a hybrid PV-wind energy system installed at the PIER 93 building.....	100
Figure 4.25	HOMER result of monthly profiles of power purchased from the grid into a hybrid wind-PV energy system installed on the PIER 93 building.....	101
Figure 4.26	Monthly profile of power production hybrid PV-wind energy system from HOMER simulation result.....	101
Figure 4.27	Cost comparison of renewable energy system.....	102

CHAPTER 1

INTRODUCTION

1.1 General Overview

Solar, water, and wind energies are used as renewable energy resources globally [1]. Generally, the wind and solar energies are combined in remote areas using battery storage [2]. The operation of solar and wind energy systems has become increasingly popular due to their modular and environment-friendly nature [3]. For high-rise buildings located in urban areas, roof-mounted micro wind turbines can be a suitable source of energy because they make less noise than large wind turbines [4]. In a wind turbine, the cut-in speed point should be low so that it can be effective in power production [5, 6].

The electrical energy in a high-rise building is mainly used in two areas: privately owned area and commonly used public area. The energy usage in a private area can be controlled by an individual user in accordance with his life style, requirements, and willingness to pay. The energy usage in a public or commonly used area is an important study because of the significant amount of energy consumed. This area, which consists of office, corridor, stairway, fence, parking, security, etc., requires more light illumination and electrical utility supply to operate continuously, 24 hours a day. There is another problem to consider of the waste and mismatch electrical energies consumed in the building. Therefore, achieving the appropriate type of energy resources is the primary concern. All these will lead to the management and optimization of energy usage in the public area

In this study, we will use all three types of renewable sources. The wind turbine machine, the water turbine machine, and the photovoltaic (PV) cell are used to generate electrical energy from wind, water, and solar radiation, respectively. The renewable energy sources are the solution to overcome the electricity cost problems using renewable energy along with energy from fossil fuels.

The renewable energy is plentiful but unstable depending on the environmental circumstances. The directive uses of these energies become more advance in technology to reduce the effect of unstable power. The modern technology of devices and the renewable energy producing machines are more advance, easy to install, and friendly to user.

1.2 Objectives

This dissertation is focused on the following topics:

1.2.1 To review the literatures related to this topic

1.2.2 To understand the theory of three different types renewable energy resources

1.2.3 To design a power generation system from wind energy, solar energy and water energy for the case study high-rise building

1.2.4 To design and testing the hybrid power generation system of wind and solar energy.

1.2.5 To design and testing power generation system of water turbine.

1.2.6 To verify, evaluate, and analyze this experiment, by compiling conclusions and recommendations

1.3 General Overview

The optimization of the three renewable energies for an eco-smart building is studied using the renewable energy from wind, water, and solar energies produced by wind turbine, water turbine, and PV cell, respectively. This study is conducted at the case study building to collect the information of each individual load and total load required

The calculation and design of a suitable type of renewable energy will be studied to generate electrical energy and inject it into the system to replace the electrical energy generated from fossils.

The physical construction and civil work characteristics of the building are very important and critical. The area around the rooftop of a building is useful to collect and reserve the water from the rain before penetrating to the water turbine. This roof top area should be rearranged for this purpose.

The roof top area also benefits from installing a low wind speed wind turbine and PV array.

There are many processes in this methodology, mention as follows mentioned below:

1.3.1 Select the high-rise building for this case study.

1.3.2 Study the physical and civil characteristic of the building for weight and height limitation, electrical wiring diagram, plumb system diagram, roof structure size and area, and the rain gutter size and area.

1.3.3 Study the functioning of the building to indicate electricity usage in privately owned and public areas.

1.3.4 Measure the power consumption load of all electrical appliances in the public area to evaluate the individual W/h and total W/h (power consumed per hour).

1.3.5 Study and evaluate the original electrical single-line diagram.

1.3.6 Study and calculate the cost of electricity for future comparison.

1.3.7 Study the three renewable energy systems, i.e. wind, water, and solar energies. This will enable us to select the suitable and appropriate type and sizing of each renewable technique for this building.

1.3.8 Study the theory and the used of hybrid technology to combine altogether the different type of renewable energy technologies.

1.3.9 Study and verify the statistic of sun irradiation, wind characteristic, and rainwater quantity from local authority.

1.3.10 Calculate in detail the power generated from each renewable energy source selected to inject into the system.

1.3.11 Redesign the original single-line diagram and modify the energy sources from both fossil energy and selected renewable energy.

1.3.12 Seek and/or fabricate the renewable energy type selected.

1.3.13 Integrate and install the system/hybrid system.

1.3.14 Monitor, analyse, and evaluate the power generation and consumption.

1.3.15 Arrange and publish the procedure, experimental analysis, conclusion, and recommendation.

1.4 Dissertation Overview

CHAPTER 1 INTRODUCTION

The first chapter is an introduction of the background and general statement of the problem, purpose, scope, overview, and utilization of the dissertation topic.

CHAPTER 2 THEORY

The second chapter concludes the theories required to gain more understanding of each related renewable technology and applying them to the system to be designed.

CHAPTER 3 METHODOLOGY

The third chapter describes the overall methodology to achieve the goal of this dissertation, starting from the measuring system designed to measure the load consumption lead to indicate the total energy required. Further, it covers the explanation of fabrication, assembly, and installation of the system design; and the operation, monitoring, and analysis by a mathematical software program.

CHAPTER 4 RESULTS AND DISCUSSION

The fourth chapter explains the designated system design and the results of energy consumption. The evaluation and comparison of the energy consumption measurement and the feasibility result of each renewable source are also investigated. The discussion on the advantages and disadvantages of the renewable energy system, and other details to prove how energy can be managed and utilized are also covered in this chapter.

CHAPTER 5 CONCLUSIONS

The fifth chapter is the conclusion of the purpose, problems, and methodology of this study, which indicates the benefit of managing and optimizing energy usage in a high-rise building. Furthermore, it discusses the recommendation of using this study effectively against social problems, such as global warming because of carbon emission, and for other building investments in terms of energy cost.

1.5 Utilization of the Dissertation

The aim of this dissertation is to be a complete study and experimentally explain how to develop three renewable energy sources for an eco-smart building. The experimental analysis is derived from theory and the existing problem of energy used and wasted in a building. The system designed and installed will enable a viewer to verify and adjust the adjacent details, to fulfil their requirements, such as energy cost against installation cost effectiveness. Finally, this study is expected to provide a comparison figure indicating the beneficial contribution of reducing the carbon dioxide emission that affects the global warming issue



CHAPTER 2

THEORY AND LITERATURE REVIEW

Human life requires and uses energy. The world is driven by energy and power consumption in various kinds. However, some energy is limited and not cost effective. The effort to use renewable energy sources to generate electricity has increased globally. Renewable energy sources are natural energy sources including wind, solar, hydropower, and geothermal energies that can be recycled and have been very popular as an alternative energy for electric power generation sources. Renewable energies are known as green energy because they reduce pollution and global warming problems.

2.1 Understanding of Energy and Power

2.1.1 Renewable Energy

The instant natural environment can create renewable energy flow in the world. The development of renewable energy is essentially a policy-driven development directed at improving energy security, defensive to the climate, and encouraging to the economic development.

2.1.2 Wind Energy

Wind energy is an indirect form of solar energy in which uneven solar irradiation on earth, because of its shape and rotation, causes temperature and spatial air pressure differences. The differences and local earth terrain (land, sea, and forest) effect create air movement, i.e. winds. The wind energy harnessing mechanisms has to keep going on for utilization in transportation and other applications, such as pump water grind grains, in the following centuries [1–4].

In 2011, the total installed capacity reached approximately 240 GW and the new installed capacity was around 40 GW as compared to that in 2010 [5]. Around 1887, Scotland developed the first wind turbine, which converted wind energy to electrical energy for providing electricity to a single house. In the early 1990s, most of the installed wind turbines generated 300 kW; however, no 1–3 MW grid-connected turbines were installed; while 5–6 MW wind turbines were installed in few areas. The high strength of blades, high performance of generators, and high controller system are major factors that rapidly developed the wind power technology.

Wind maps show that the annual wind speed distribution and wind energy, the weather system, and local land terrain has never made wind steady at any site, Wind velocity fluctuates by minutes, hour, day, and season. The weibull distribution function is used with shape parameter k and scale parameter c for defining the statistical wind speed variation

Wind speed has the weibull distribution with shape parameter $k=2$, which is specifically known as the Rayleigh distribution and given as follows with wind speed v

$$f(v) = \frac{\pi v}{2\bar{v}^2} \exp\left[-\frac{\pi}{4}\left(\frac{v}{\bar{v}}\right)^2\right] \quad (2.1)$$

Where $f(v)$ = Weibull probability density function of wind speed

\bar{v} = mean speed (m/s)

v = instantaneous wind speed (m/s)

Generally, the height of 10 m is used for recording the wind speed. Wind shears, such as hills or mountains, have significant wind flow characteristics. The wind speed profile is functional to the ground-level surface and height as expressed in the following:

$$v_2 = v_1 \left(\frac{h_2}{h_1}\right)^\alpha \quad (2.2)$$

Where v_1 = wind speed, h_1

v_2 = wind speed, h_2

α = coefficient ground friction surface

2.1.3 Solar Energy

The earth energy consumption from solar radiation is around 15 TW and human can use only 0.01 % of this. The most common energy resource is the solar energy, using PV cells which convert sunlight to electricity with radiation of the sun being the main source. Solar energy is a sustainable energy and can reduce used of fossil energy; thus, low cost and high efficiency of the PV technology is a global goal nowadays. Wind energy is an indirect form of solar energy in which uneven solar irradiation on earth

Variety in urban design form complex architectures, including building obstruction and complex terrain.

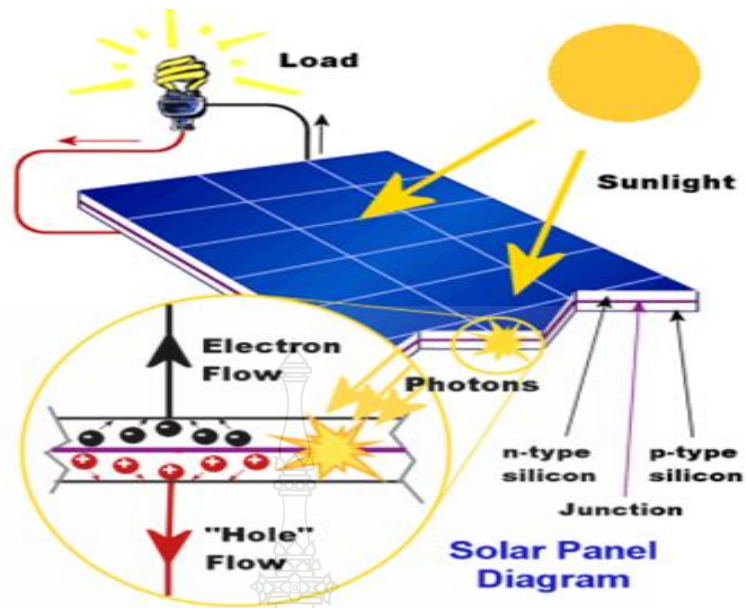


Figure 2.1 PV cell generating electricity [4]

Semi-conducting materials are used for PV cells construction Figure 2.1 shows a PV cell generating electricity. The photons from the sun are attracted to the electrons of the semi-conducting materials and then absorbed to finally generate electricity flow through the load.

2.1.4 Hydropower Energy

Hydropower is among various renewable energy resources, irrigation and machine devices are developed for hydro-powers, such as sawmills textile mills, power houses, and others [6].

Theoretical hydropower power available can be calculated from the following equation:

$$P_h = \eta_{TG} \rho g Q H_{net} \quad (2.3)$$

where P_h is power (watts)

η_{TG} is the turbine efficiency ($0 < 1$)

ρ is water density (1000 Kg/m^3)

Q is water flow rate (m^3/s)

g is gravity acceleration (9.78 m/s^2)

H_{net} is the net head

Determining the flow rate and available net head is the main task for hydropower development. The net head (effective head for turbine) is the difference of the gross head and hydraulic losses before entering the turbine. The flow rate of a given river can be measured using gauge meters, area velocity, and other parameters [8-11].

2.1.5 Hybrid Energy

Hybridization of energy sources increases the overall reliability of a system because one energy source can compensate for another as required. However, proper component selection and sizing are essential in the design of such systems. Several studies have shown that in addition to improving energy reliability, hybrid renewable energy systems (HRES) also increase global sustainability. A study of PV distributed generation (PV-DG) hybrid systems was conducted using 12 isolated, off-grid HRES installed for rural electrification in the Jujuy province of Argentina [12]. Comparison of the stand-alone and grid-connected hybrid systems in Turkey was also made [13]. In India, hybrid PV and wind energy systems are becoming popular and beginning to penetrate the renewable energy market, because HRES are cost-effective in remote areas where extending the grid supply would be expensive [14,15].

2.2 Renewable Energy Potential Resources in Thailand

2.2.1 Wind Energy Resources in Thailand

To justify the utilization of wind turbines in cities, potential problems, such as noise and urban design requirements need to be mitigated, and their performance needs to be maximized. One approach to maximize this performance is to develop wind turbines with lower cut-in speed to deal with the slow average wind speed in urban areas. However, the extra cost of wind turbines with low cut-in speed may not be offset by the consequent energy gain, making them potentially economically inefficient. The wind potential in Thailand, as classified by the World Bank is considered mostly poor to fair, as shown in Figure 2.2.

The wind resource map of Southeast Asia shown in Figure 2.2 was created for the World Bank by True Wind Solutions using Metso Map, a mesoscale atmospheric simulation system. Although the map should present an accurate overall picture of wind resources in Southeast Asia, the resource estimates for any particular location should be confirmed by local measurements.

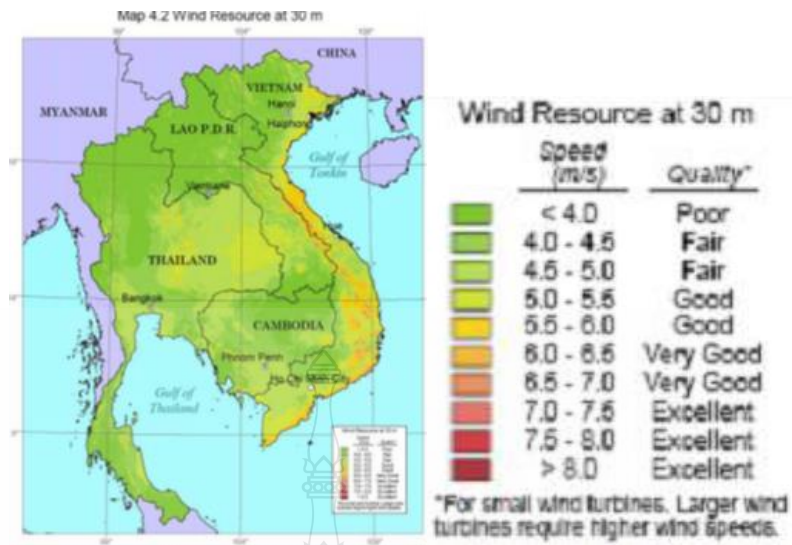


Figure 2.2 The Wind potential in Thailand [16]

The annual monsoon pattern of any given location is very important. The direction and characteristics of monsoon in Thailand is shown in Figure 2.3.

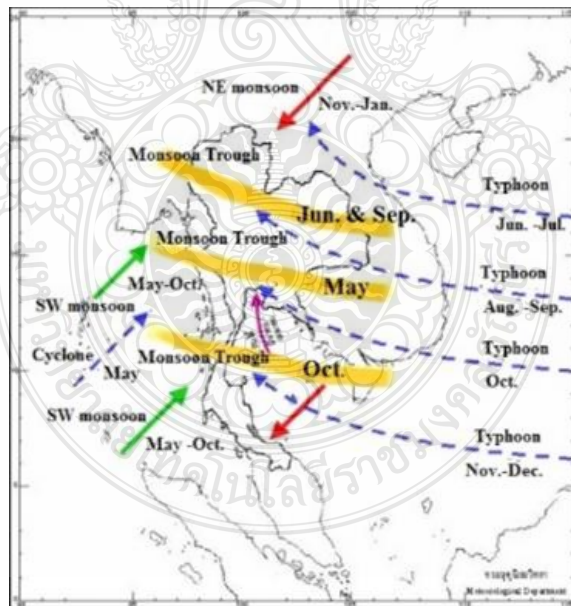
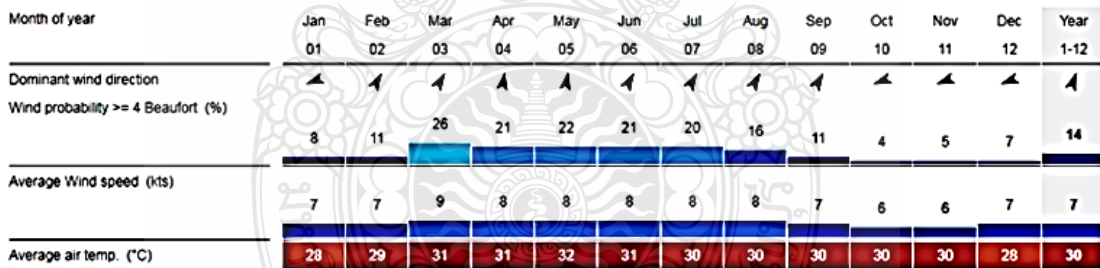


Figure 2.3 Feature and characteristics of monsoon in Thailand[17]

The wind data of the study area was measured and collected by the department of meteorology in Pathum Thani measuring station. The annual wind data is presented in Table 2.1. The monthly average wind speed in the minimum is 2.05 m/s and the maximum are 6.55 m/s. The annual average wind speed is 3.95 m/ s, which is sufficient for utilizing the wind energy in the selected area. From wind speed data, due to the cold season under northeast monsoon and tropical cyclone during November–January resulting average wind speed at 2.54 m/s was measured. In March–April, the hot weather in summer under southwest monsoon and tropical cyclone resulting average wind speed at 4.70 m/s was measured. From May–October, under rainy season, with the effects of tropical cyclone and southwest monsoon, the average wind speed of 4.54 m/s was measured and was recorded as the highest wind speed of the measuring year.

Table 2.1 Wind data in Suvarnabhumi airport Thailand as measured by the wind finder website [17]

M/Y	Ave(m/s)	M/Y	Ave(m/s)	M/Y	Ave(m/s)
Jan	3.60	May	4.12	Sep	3.6
Feb	3.60	Jun	4.12	Oct	3.09
Mar	4.63	Jul	4.12	Nov	3.09
April	4.12	Aug	4.12	Dec	3.60
Annual Ave.					3.82



Wind data for the study area was measured and collected by the Wind finder website at Suvarnabhumi airport measuring station. The annual wind data for this location is presented in Table 1. The minimum and maximum monthly average wind speeds are 3.09 m/s and 4.63 m/s, respectively. The annual average wind speed of the selected area is 3.82 m/s, which is sufficient for utilizing the wind energy. In the cold season from November–January, including the northeast monsoon and tropical cyclone, an average wind speed of 3.43 m/s was measured. From February–April, with hot summer weather, the southwest monsoon, and tropical cyclone, the average wind speed was measured as 4.12 m/s. In the rainy season from May–October, in which the effects of tropical cyclone and the southwest monsoon are felt, an average wind speed of 3.86 m/s was measured and recorded.

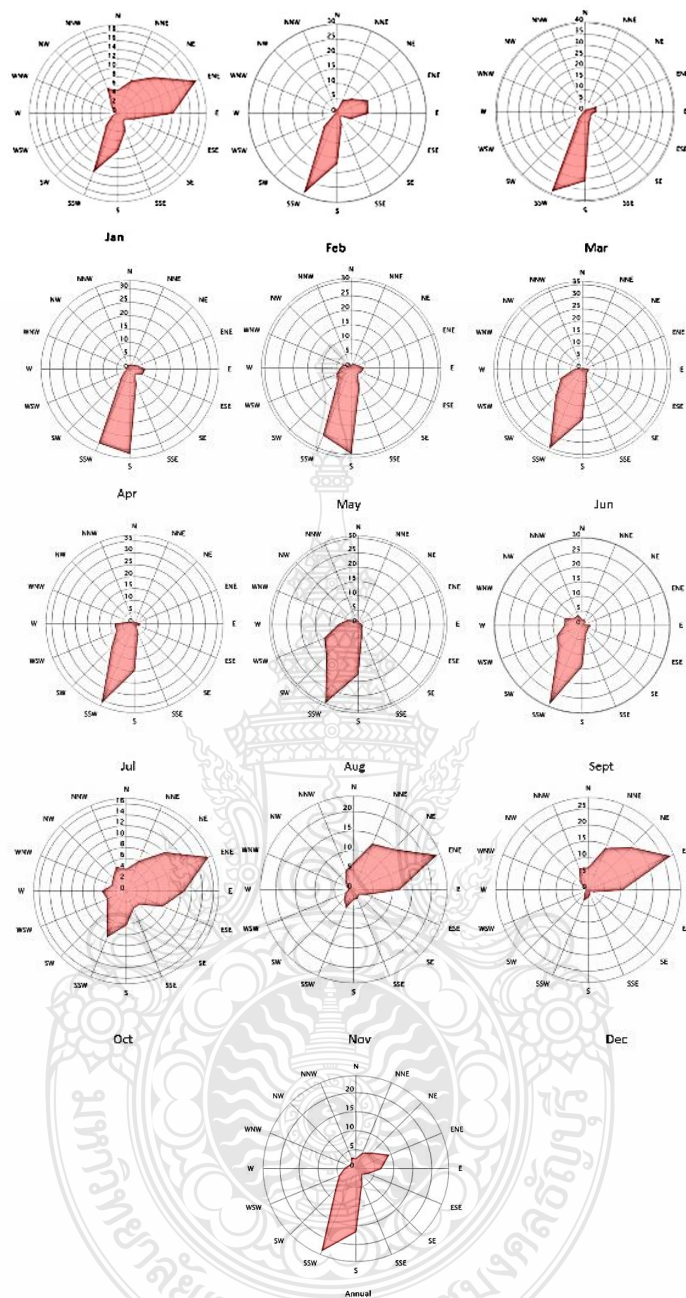


Figure 2.4 Wind Rose Data at Suvarnabhumi Airport Thailand [17]

Figure 2.4 shows that the wind rose data are based on real observations from the weather station collected at Suvarnabhumi Airport in Samut Prakan, Thailand from Wind finder. The PIER93 building located at Pathum Thani province is near the Suvarnabhumi airport; thus, the data will assume for calculation of this study. Mostly, the wind flow direction of Thailand is from south-southeast direction (SSW) and east-northeast direction, which is shown in the annual wind rose.

The terrain is mostly divided into flat and non-flat terrain. The effect of terrain to wind flow must be considering when wind turbine is installed. As shown in Figure 2.5, the Hub-High of wind turbine should be high 3 h of the hill height.

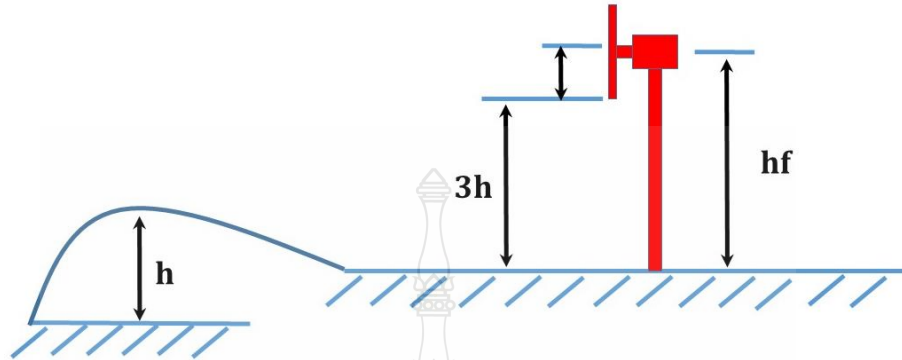


Figure 2.5 Determination of flat terrain [18]

When wind flows over an obstacle, the recirculating wake flow region (eddy) will be generated at the downstream side of the obstacle, and the velocity of wind flow will increase at the top of the obstacle, as shown in Figure 2.6.

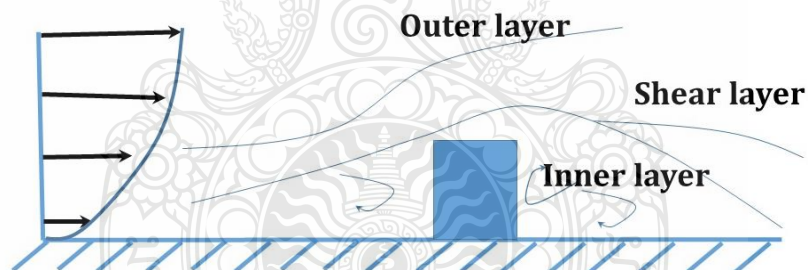


Figure 2.6 Schematic of a momentum wake. Reproduced by the permission of Alternative Energy Institute [18]

2.2.1 Solar Energy Potential Resources in Thailand

The global solar radiation incident on the area of Thailand is shown in Figure 2.7 As illustrated; the highest solar irradiation (19–20 MJ/m² d) was measured in the middle area of Thailand. The annual average global radiation of Thailand during 1964–2008 is 6.82 MJ or 4.672kWh/m²/d as shown in Figure 2.8. The selected study area located at 14 °N, 100 °E. In such area, the highest average energy in April of each year is 5.458kWh/d and the lowest in September, with the average energy 4.161 kWh/d.

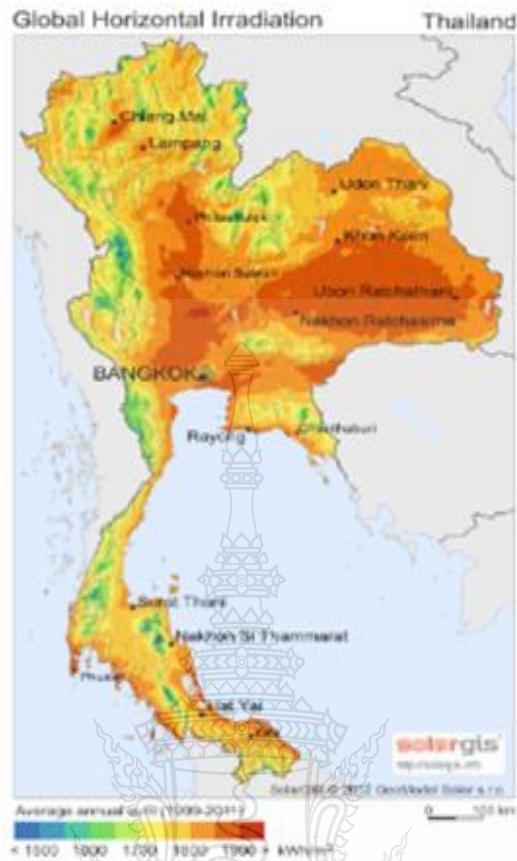


Figure 2.7 Global solar irradiation map of Thailand [19]

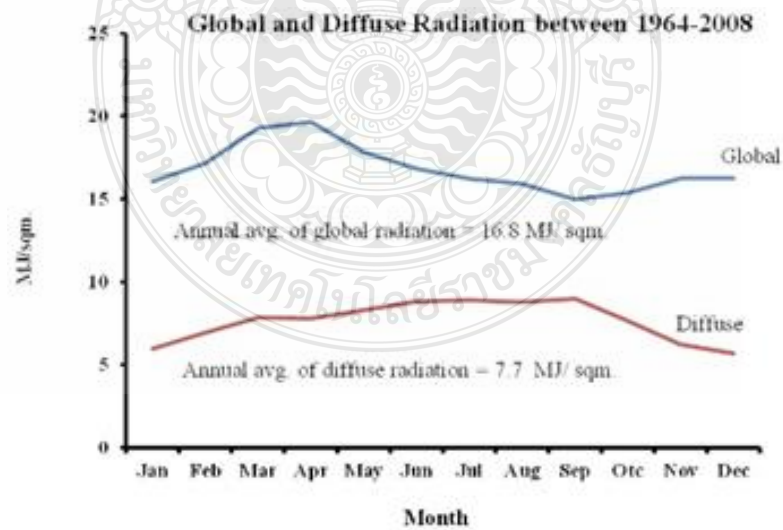


Figure 2.8 Annual average global and diffuse solar radiations in Thailand [19]

2.3 Wind Turbine Configuration

2.3.1 Wind Turbine Type

Wind turbine has several configurations, but mostly in commercialization used the drag type and lift type wind turbines, the 90% of wind turbine is the lift type and horizontal axis type wind turbine [8]. While the drag type turbine is use wind, force pushes on a surface of wind turbine blade, the drag type turbine easy to build but efficiency lower than lift type [9–11]. Wind turbine lift type, force from wind flow perpendicular with wind turbine blade including both horizontal axis wind turbine (HAWT) and vertical axis wind turbine (VAWT). Wind turbine type is a rotor HAWT.

The main advantages of HAWT are good aerodynamics performance and versatility of application. However, there are complex electro-mechanical transform equipment, such as gearbox, shaft, generator, and yawing system. In the VAWT, the rotor axis lies vertically, and the blades sweep a cylindrical or conical plane, which is perpendicular to the air flow and parallel to the rotor axis. The electro-mechanical transforms equipment, such as gearbox, shaft, and generator, are mostly placed on ground that are easy to operate

In the VAWT, the rotor axis lies vertically, and the blades sweep a cylindrical or conical plane, which is perpendicular to the air flow and parallel to the rotor axis. The main advantages are all the dynamic electro-mechanical equipment will be placed on the ground and yawing mechanism is not needed.

Most common and modern wind turbines use the HAWT design. The poor efficiency and high material demand of the vertical axis systems are the determining factor for the market shares dominance taken by the horizontal axis system.

The wind turbine output is greatly affected by its aerodynamics performance and the aerodynamics is determined mainly by the geometry of the blades. The shape of the aerodynamic profile is a decisive factor for blade performance.

2.3.2 HAWT Wind Turbine Type

The wind power system includes one or more wind turbine units operating electrically in parallel. Irrespective of the size and operation type (with-grid or off-grid), each turbine consists of three main components called tower, nacelle, and hub; these components include respective constituents in them, as shown in Figure 2.9 below

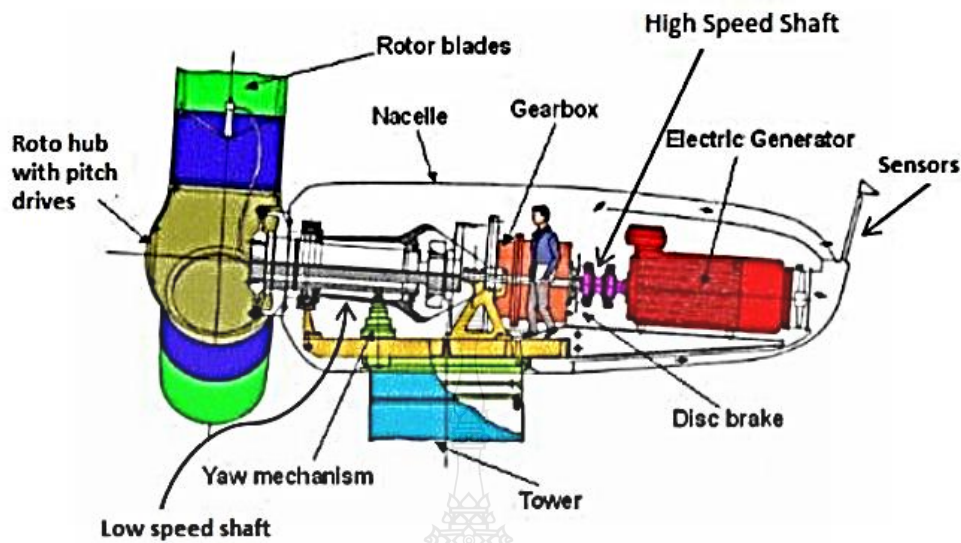


Figure 2.9 General components of HAWT [20]

Tower: The tower use to support and hold the nacelle and the hub of wind turbine.

Nacelle: Nacelle consists of main electro-mechanical equipment, such as shaft with mechanical gear, gear box, electrical generator, yaw mechanisms, and sensors, which helps for power generation, as shown in Figure 2.9 above.

Shaft: It is used for connecting and transferring the mechanical energy to either directly to the generator or through gearbox and high-speed shaft to the generator. In slow speed generator, there is only low speed shaft but in high speed generators case, there are low speed and high-speed shafts on both sides of gearbox.

Gearbox: It is needed in high speed generator cases and it will step up the slow speed coming through low speed shaft. Further, the gearbox will transfer the mechanical energy to the generator through the high-speed shaft.

Generator: It is equipment which converts the mechanical energy to electrical energy. According to the wind system required design, there are two main types of generators; low speed generator and high-speed generator. Each of them has its own vantage points.

Yawing mechanism: It keeps the upwind turbine facing the wind while the wind changes direction

Sensors: They are installed either over the top of the nacelle such as wind vane, anemometer and thermometer, or inside the nacelle such as thermometer and other mechanical and electrical parameters monitoring and regulating devices

Besides, the disc brake is installed for stoppage when needed, and the controlling mechanism also installed there to control and regulate the turbine components as required.

Hub: The hub helps to interconnect the blades (two or three) in it and rotate together for driving the shaft (low speed shaft). The hub consists of pitch drives for each blade for controlling the pitch angle.

The power of wind turbine as below

$$P_{mech} = \frac{1}{2} \rho A v^3 C_p \quad (2.4)$$

The electrical output power can be described in equation

$$P_{mech} = \frac{1}{2} \eta_T \rho A v^3 C_p \quad (2.5)$$

Where η_T is the total efficiency of transmission and conversion

The maximum theoretical power coefficient C_p of wind turbine is 0.45 approximately [21-23] and on an average achieves 0.3 approximately. The relationship between power output and wind speed incoming are significantly understand use for design control system, or optimization system. The power curve is plotted for specifies power can extract from the incoming wind, as shown in Figure 2.10 contains an ideal wind turbine power curve

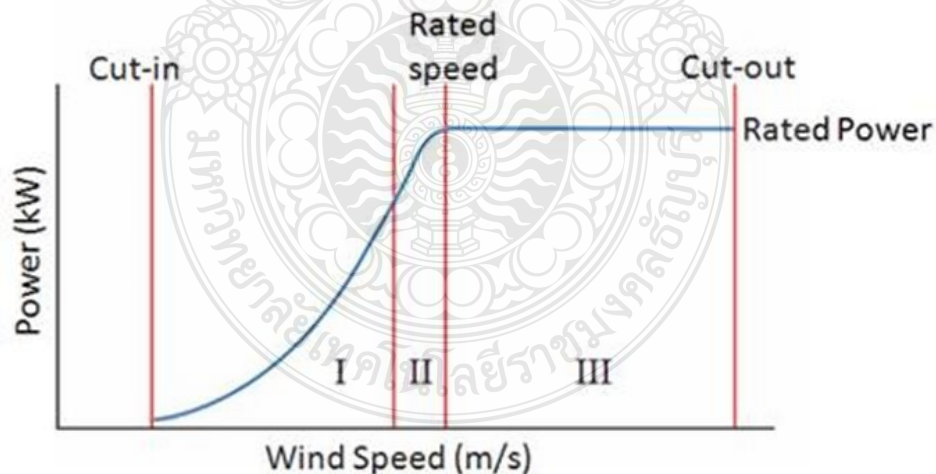


Figure 2.10 Ideal power curve of a wind turbine [24]

The cut-in point on power curve is the wind turbine blade being rotating and beginning generating the power. When the wind velocity is increasing the power production will be increasing together. The rated power point on power curve is the maximum of power which wind turbine machine can generate even the wind speed increasing. The cut-out power point is the point of wind machine is stop rotating.

2.3.3 VAWT Wind Turbine Type

The air flow orientation perpended with turbine's axis called the VAWTs wind turbine type. The model H-type VAWT is shown in Figure 2.11. The energy is captured by frontal area of wind turbine blade, VAWTs diameter is smaller than those of HAWTs and can be installed closely together, which means that it can be increase the power density of a wind farm [25].



Figure 2.11 Model H-type VAWT [25]

2.3.4 Micro Wind Turbine

Micro wind turbines include VAWTs and HAWTs [26]. The three bladed HAWTs type is mostly using in today [27]. The mostly electricity power is generated from micro wind turbine approximately 1–10 kW and diameter about 1.5–3.5 m. In the urban area including complex terrain that induce complex wind flow direction, rapidly flow of gust wind therefore micro wind turbine suitable for this case cause micro wind turbine rapid response for complex flow direction and wind speed.

Figure 2.12 shows the hub-height of HAWTs versus the difference size of wind turbine diameter. Generally, the micro wind turbine tower is constructed no taller than 10 m while the MW wind turbine tower can be installation more than 100 m. The typical applications of wind turbine sizes are shown in Figure 2.13.

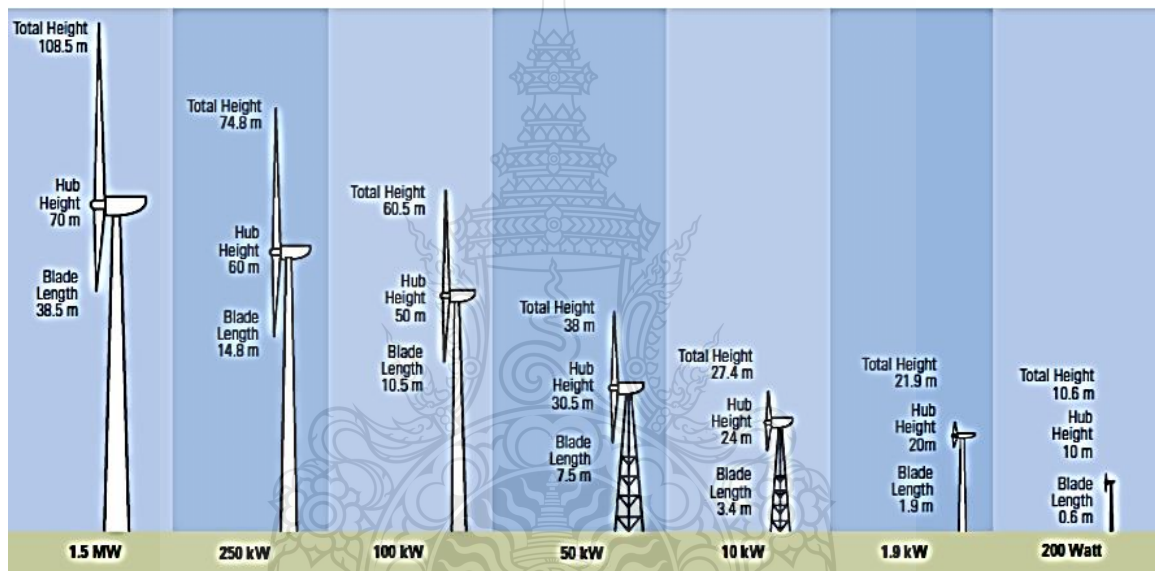


Figure 2.12 Different sizes of wind turbines [27]

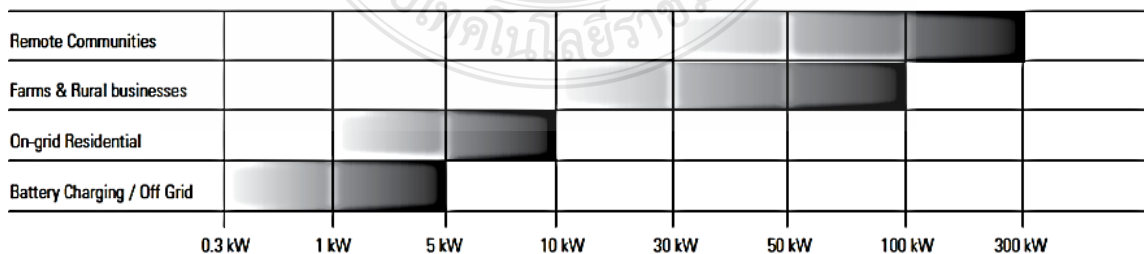


Figure 2.13 Typical application of wind turbine sizes

Figure 2.14 shows the different types of micro wind turbines; however, the micro wind turbine not popularly use for electricity generation because low efficiency which approximately 3–6 %. Although the micro wind turbine is not popularly installed in a wind farm; however, in the urban or complex terrain area need wind turbine which rapid respond wind flow direction, therefore the micro wind turbine is suitable for this case.



Figure 2.14 Micro wind turbines [28]

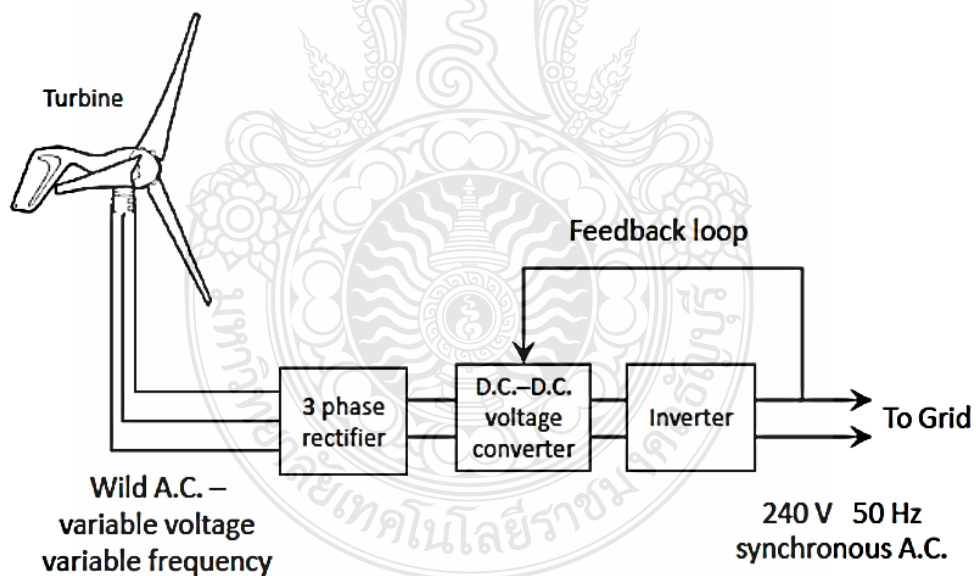


Figure 2.15 Micro wind turbine circuits [29]

Figure 2.15 shows a micro wind turbine circuit. Generally, micro wind turbines generate AC power 3 phase. Most micro wind turbines are used for battery charging of off-grid system; however, sometimes it can be developed for on-grid systems.

2.4 PV Energy

The sun energy is a free natural energy which abundantly available everywhere in the world. This energy calls renewable energy (RE), electricity power from the sun can be generated by PV cell system [30-32]. Recently, the PV cell material obtains two type which is crystalline PV and thin film PV [33-36]. The efficiency of PV cell depends on manufacturing company and processing, the summarizes of PV type and product as shows in Table 2.2

Table 2.2 The features of various PV products

PV Type	Material (silicon)	Cell Efficiency	Thickness (mm)	Color
Crystalline	Mono	21.50%	0.2-0.3	Dark blue
	Poly	16.50%	0.24-0.3	Blue
Thin film	Amorphous	10.50%	1-3	Reddish brown
	CIS	14.00%	2-4	Dark gray
	Cadmium	10.00%	3	Reflective dark green

2.4.1 Crystalline PV Type

Figure 2.16 shows the PV type of crystalline silicon (C-Si) which including two types that are mono-crystalline and polycrystalline. The crystalline silicon (C-Si) process use the temperature above 1000 centigrade for de-oxidation and purification of crystalline silicon. Normally, this type uses wafers ranging between 10–15 cm then interconnected into modules, the mono-crystalline energy efficiency can over 20% while polycrystalline about 16.5%.

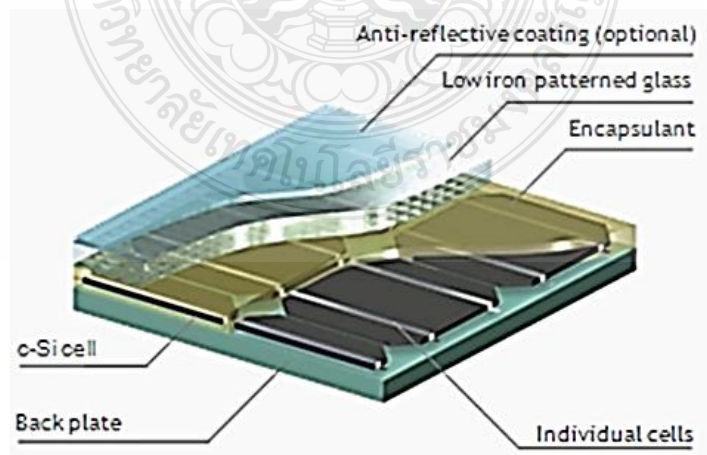


Figure 2.16 Crystalline silicon solar cells [37]

2.4.2 Thin-film PV Type

The materials that are used for PV cell thin film type obtain amorphous silicon, copper indium diselenide (CIS) and cadmium telluride (CdTe). The layer of this type is approximately 0.001 mm, which includes processes, such as vaporous, deposition, electrolytic baths, and sputter processes. The process requirement needs the temperature lower than crystalline PV production, the temperature 200–600 centigrade. As the thin film process uses the energy for production less than crystalline PV production and also including the efficiency lower than that 10%; however, the thin film price lower than crystalline PV and more flexible shape and the material laminated is various can be used cover that mean various design for customer requirements. In year 2011 thin film PV price is approximately \$1.37/watt.

2.5 Water Energy

For thousands of years, water energy has been used by humans. The water energy is used as potential energy for electricity generation process. When the potential energy of water is used, the head of water and flow rate are significant parameters to produce electricity [30]. Mostly, the energy from water using turbine for energy capture which have many types of water turbine, Turgo turbine type, cross flow turbine type, Pelton turbine type etc. The sizing of capacity turbine can consider in Table 2.3 and the quantity of electricity production is depending on head and flow rate of water.

Table 2.3 Classification of hydro power of capacity [38]

Type	Capacity(kW)
Pico water turbine	2 - 30
Micro water turbine	31 - 100
Mini water turbine	101 - 2,000
Small water turbine	2,001 - 2,500
Large water turbine	>2,500

The classifications of hydro power plant can use 'Head' of water to classify the power plant is given in Table 2.4.

Table 2.4 Classification of hydro power of head [39]

Type	Head(m)
High head of hydro power	>100
Medium head of hydro power	30 - 100
Low head of hydro power	2 - 30

The kinetic energy is generated by water under pressure from the reservoir; water pressure is transported by the penstock pipe. The loss in penstock pipe has two types, first is head loss which due to friction of roughness of wall pipe, length and diameter of pipe that decrease velocity of water. Second is minor loss that results from changes in geometry or added components to a piping system along with major losses are responsible for pressure drops along a pipe and generally as you increase flow by 10%, the minor losses increase by 20% [40]. The head of water depends on the water level height as by Equation (1) and the hydrostatic pressure.

$$P_g = \rho gH \quad (2.6)$$

where ρ is the density of water, g is gravity acceleration, H is the head of water, and Bernoulli's equation can be applied with steady state flow and the flow is laminar flow type and considering the fluid is incompressible, the viscosity that can eliminate because viscosity is very low, over all condition,

$$P + \frac{1}{2}\rho v^2 + \rho g z = const \quad (2.7)$$

The significant equipment hydro power is a turbine that converts energy of water into the rotating shaft power. The turbine type selection depends mainly on two characteristics: available head and flow. Running speed of the generator is designed from turbine speed that depends on the type of turbine and demand of electricity. Table 2.5 presents a basic turbine classification that including three types of turbine water head including low water head, medium water head, and high-water head.

Table 2.5 Groups of water turbines [41]

Turbine runner	High Head	Medium water Head	Low water Head	Ultra-Low water Head
Impulse	Pelton Turgo	Cross-flow Turgo	Cross-flow Multi-jet- Turgo	Water-wheel
		Multi-jet Pelton		
Reaction		Francis Pump-as- turbine	Propeller Kaplan	Propeller Kaplan

2.5.1 Impulse Turbine Types

The design of impulse turbines is simple; thus, this turbine type is widely used as micro-hydro [42]. The advantage is turbine tolerance design can more than reaction turbines that mean suitable for water including large particles in the water flow. The pressure difference between inlet and outlet of Impulse turbines are not including.

The Turgo turbine, which is an axial type impulse turbine, has only rarely been used for small units. The cross-flow turbine is an impulse turbine used for small units only. The efficiency of the cross-flow turbine has been measured in laboratory to be around 80% while efficiency of the Turgo turbine has been reported to be close to 90% which medium head applications [43].

The non-dimensional between the water head and power output and speed of water turbine shaft is considered for selecting hydro turbines [44]. Figure 2.17 shows the water head and water flow rate for selecting the water turbine type. The Pelton water turbine and Turgo water turbines suitable for high heads while the cross-flow water turbine and radial (Francis) water turbines is suitable for medium water head.

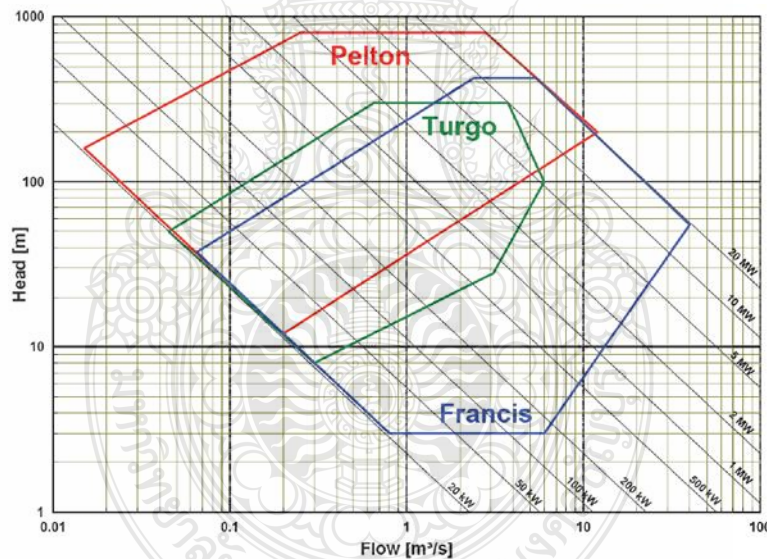


Figure 2.17 Turbine application range chart [45]

Pico Turgo water turbine type can be used for electricity power generation under the 5 kW range. Recently, many commercial products less than 5 kW of water turbine is used the Pico water turbine type.

2.5.2 Low-head Pico-hydro

A low head pico-hydro has been largely neglected as compared to the medium and high head due to higher initial costs resulting from lower power density [46]. Although, there is demand of electricity in developing countries that has an abundance of low head water resources, a push toward renewable energy has made these types of schemes more appealing in recent years. In low head pico-hydro research has been flexible designed, while the cross-flow turbines are cheap, easy to manufacture, and work for a wide range of flow conditions [47]. The lower head already demands a higher flow rate, meaning larger more expensive penstocks; low turbine efficiency further exacerbates the low power density issue

2.5.3 Turgo Turbine

The impulse of water turbine type is Turgo type. The Turgo turbine type can be upward of 82% of mechanical efficiency when the test at the laboratory conditions. However, at general real side of installation location, the efficiency approximately 40% [48]. The high pressure of water at outlet side is converted from the water head which thought the nozzle device. The blade of Turgo turbine similar cup, water jet attacks the cup which connected the turbine runner and generally the water jet attack angle approximately 17–20°.



Figure 2.18 Bucket of Turgo Turbine

Figure 2.18 shows the 3D shape of a Turgo turbine type. Turgo turbine type is fast achievement emigration of the water [49]. Turgo turbine type is minimal maintenance and suitable for pico-hydro off-grid installations more than Pelton turbine type [50] and less the airtight housing than Pelton turbine type, although single or multiple nozzles can be used and the head water ranging from 15–300 m is can used for application.

Figure 2.19(a) shows the design of a Turgo water turbine in the sixteenth century [51] which obtaining one water jet, as shown in Figure 2.19(b). Comparing the Pelton and Turgo water turbine types, the specific speed of a Turgo water turbine type is higher than that of a Pelton water turbine type.

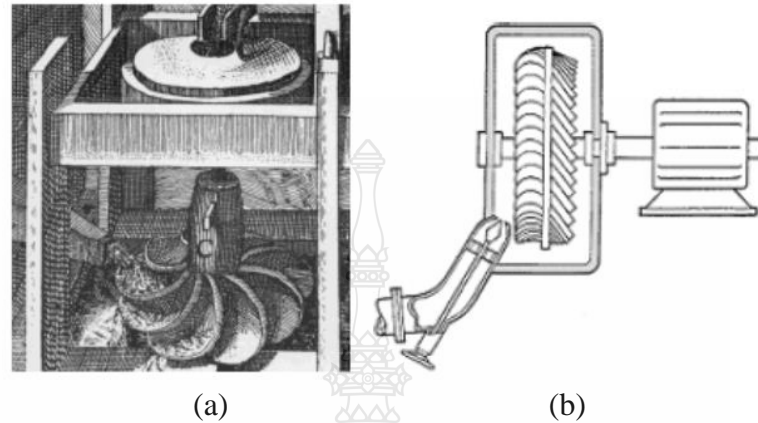


Figure 2.19 (a) Earliest design of Giovanni Branca and (b) sketch of the Turgo type design [52]

- In 1919, Eric Crewdson designing the first Turgo impulse turbine
- In 1920, Turgo turbine was tested by Dr. A. H. Gibson, maximum efficiency was 83.5% at head of 200 feet, producing 106 HP, 640 rpm
- In 1936, Gilkes reduced the D/d ratio to 4.5:1 for improving the efficiency, as shown in Figure 2.20
- In 1971, a one-dimensional theory was developed that explains the relatively low efficiencies of the inclined jet
- In 2011, Anagnostopoulos use CFD for the implementation of Turgo blade surfaces exhibit a complex 3D shape, as shown in Figure 2.21

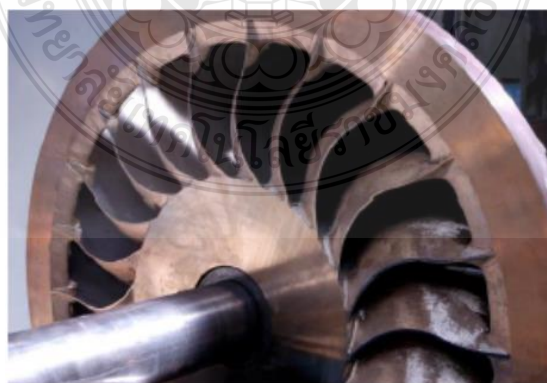


Figure 2.20 Design of a typical Turgo runner [53]

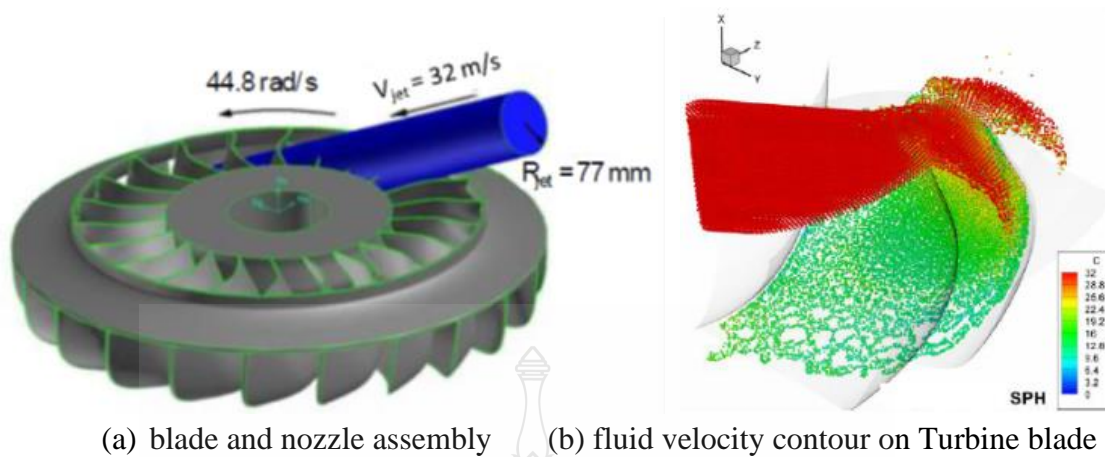


Figure 2.21 CFD simulation results of Turgo runner [53]

2.5.4 Runner Design and Parameterization

The runner design can use the hydraulic head H , with elevation z , and pressure p , combined with velocity v as below

$$H = z + \frac{p}{\rho g} + \frac{v^2}{2g} \quad (2.8)$$

Where ρ is the fluid density and g is gravity, mean velocity of the free jet,
Using

$$c = \varphi \sqrt{2gH} \approx 0.97 \sqrt{2gH} \quad (2.9)$$

where φ is the efficiency of the nozzle, generally approximate 0.97-0.98.
The flow rate Q and the jet diameter d , as below:

$$Q = \frac{\pi}{4} d^2 c \quad (2.10)$$

At the best efficiency point the runner speed is as follows:

$$u_1 \approx (0.46 - 0.47)c \quad (2.11)$$

The runner diameter is

$$D_s = \frac{60u_1}{\pi n} \quad (2.12)$$

The Bezier curve is used for creating the blade curve design, and n is the runner speed in rpm. The radial distance is r and the runner peripheral velocity is u_1 . The maximum efficiency generated when the flow exits of water from nozzle with zero circumferential velocity. The equation for characteristics of the turbine is described as turbine power P , and the gross head H_g combined with the system efficiency η as Equation 6 as below.

$$P = T\omega = \eta\rho gQH_g \quad (2.13)$$

Where the power of Turgo water turbine is described as P and the torque which is generated from water jet as T . Another parameter is ω describing the angular velocity, while the density and gravitational are described as ρ and g , respectively.

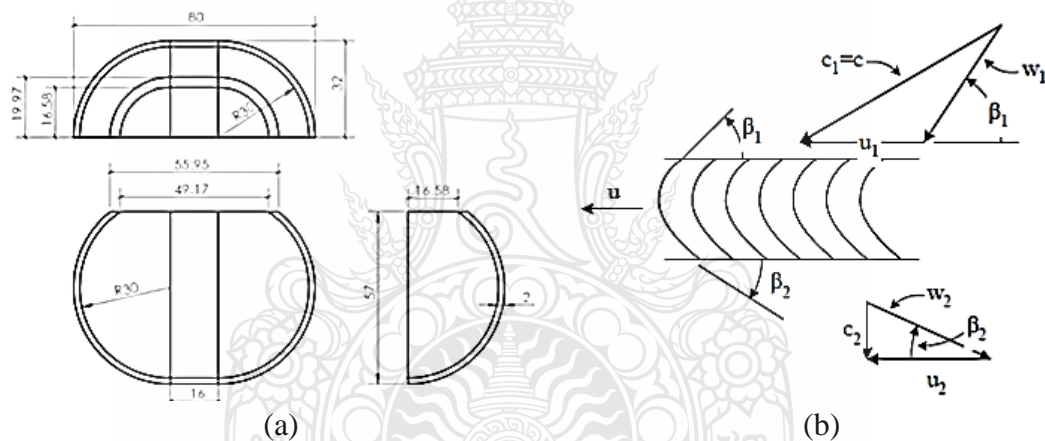


Figure 2.22 (a) Bucket of Turgo turbine and (b) velocity triangles

The water jet impact the bucket can be described as velocity triangles, as shown in Figure 2.22. The friction of piping and valve can reduce the water jet velocity; also the power will be reduced.

2.6 Hybrid Renewable Energy System (HRES) System

A system including more than two types of renewable sources is called as 'Hybrid System'. The renewable energy can be off-grid or on-grid system depending on the design of the case suitable area side. An HRES is shown in Figure 2.23. It can support the AC load type or DC load type or both types.

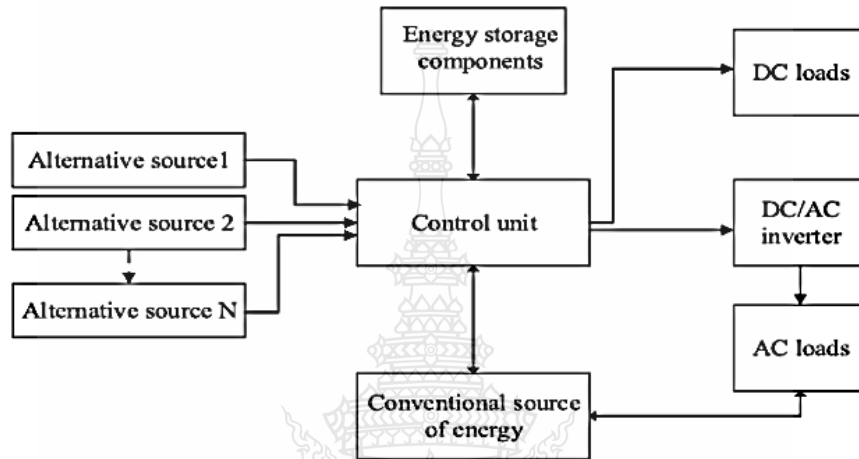


Figure 2.23 General HRES architecture [54]

An energy storage system can also be included or excluded in the HRES. An example of an on-grid PV-wind turbine HRES is shown in Figure 2.24. For renewable energy sources utilization, the feasibility studies of potential and optimal of the hybrid renewable energy generation system were conducted all over the world.

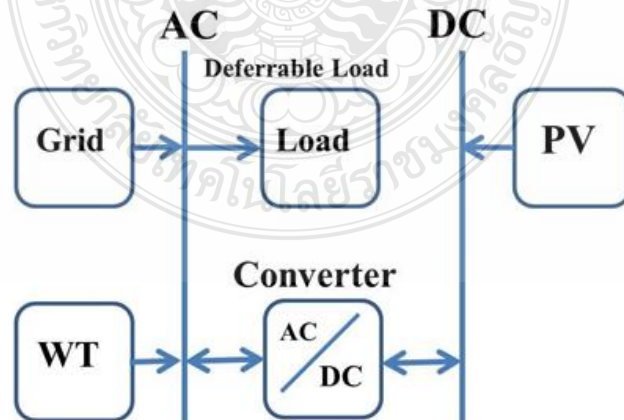


Figure 2.24 On-grid PV-wind turbine HRES [55]

The PV-diesel based hybrid systems have complementary characteristics as follows [56–62]:

- Working cost of PV system is minimum as compared to Diesel Generator
- O & M cost minimum as compared to Diesel Generator
- Reduces battery storage requirement
- Better dependability
- Less emissions
- System autonomy
- Accuracy analysis
- Reduce generation costs and increase the reliability of energy supply
- Maximize the techno-economic benefits
- Find out the number of storage days

A hybrid system is usually composed of three sustainable energies, such as wind power, solar power, and biomass power [63], as shown in Figure 2.25.

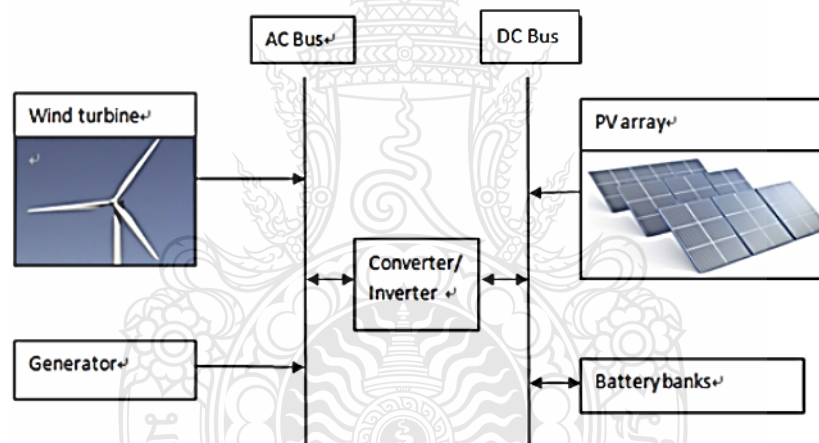


Figure 2.25 PV-wind-biomass hybrid power supply system [64]

2.6.1 Methodology for a Hybrid System

The term 'hybrid' is used to refer to something made by combining different features, and similarly the hybrid energy systems consist of a combination between renewable energy sources and fossil fuels in conjunction with batteries to circumvent the intermittence, the seasonal and periodical variations, of the renewable energy. Hybrid systems are promising to supply sustainable energy for small grids and standalone systems where one energy source is not enough for the expected load [65].

The design of PV based hybrid systems [66–71] and PV-Wind based hybrid system [72–77] to assess the practical performance of the system using distinct methodology. For a standalone hybrid system in which their significant load depends on

the intermittent energy sources (solar or/and wind); a reliable backup system is necessary and supplied by storage equipment (battery banks) and diesel generators. These backup systems will also help to optimize the sizing of the hybrid system. There are several kinds of hybrid systems which will be developed by combining solar, hydro, wind and diesel in different scheme according to the available resources in the site.

There are numerous methods to optimize the technical and economic possible combination of different renewables sources ranging from simple Excel based to the computer optimization program. In this thesis work, HOMER is utilized for optimization and sensitivity analysis.

2.7 HOMER Software for HRES Simulation Description

The HOMER software was developed at the National Renewable Energy Laboratory (NREL), United States [78]. Although the HOMER software has been used in many studies, a brief description on it is presented in the review papers [79-83]. HOMER is a powerful tool for designing and planning an HRES to determine optimal size of its components through carrying out the techno-economic analysis. Many resources, such as WT, PV array, fuel cells, small hydropower, biomass, converter, batteries, and conventional generators, are modelled using HOMER. The HOMER program also considers HRES in grid-connected and stand-alone modes. Figure 2.26 shows the typical configuration of an HRES designed in HOMER. The required input data for simulation with HOMER and a comprehensive frame work to show how optimal sizes of HRES's equipment is determined by HOMER are described in this section

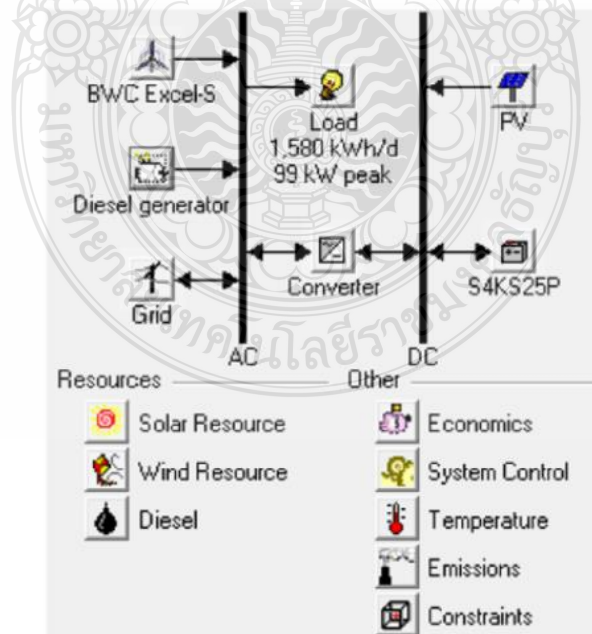


Figure 2.26 Typical schematic of an HRES in HOMER [84]

The meteorological data are wind speed, solar radiation, temperature, and stream flow which are fed into the software in the form of monthly averages or time series data. HOMER uses these inputs data to calculate the output power of WT, PV array and hydropower. The load profile of each region is the most important factor in the simulation and optimization. Some locations, such as universities, hospitals, hotels, and industrial towns, have real load consumption data, which are appropriate for simulation. These real data are fed into HOMER as time series data. However, in some regions especially remote and rural areas that the real load consumption data are not available, the load profile should be forecasted with notice to the specification of that region. These data are fed into HOMER as a daily profile and HOMER uses the minimum power balance constraint.

When comparing the cost of electricity from fuel cost of Diesel Generator, we apply the HOMER energy micro grid power design software to perform energy balance simulations and to optimize the size of the system components. The result can be showed that a wind turbine with the hydrogen energy storage system is a feasible solution.

In addition, analysis using Hybrid emphasized system design with little focus on the prefeasibility analysis of renewable energy system. HOMER gives more detailed information than the statistical models screen and provides the optimization and sensitivity analysis with limited input based on the literature reviews, the HOMER software is taken for the purposes of this study to carry the feasibility assessment.

The combined generation of electricity by wind and solar energy is a very attractive solution for isolated regions with high levels of yearly wind energy and insolation. A computer model is developed for the simulation of the electricity system of a Mediterranean island, including a wind power plant, a PV power plant and a storage system. Various parameters calculated in the simulation can be used to improve the configuration of the system and to estimate the cost of the electrical energy unit.

In recent studies, many new resources are considered, such as biogas has been used as a fuel resource for generators in [85] and flywheel has been used as an energy storage in [86].

2.7.1 Equipment Modelled in HOMER

Various HRES's equipment modelled in HOMER and used in different articles is presented. Loads, components, and grid are three types of the HRES's equipment, which are modelled in HOMER. HRES should meet the load requirements in each time step. Electrical, thermal, and hydrogen loads are modelled in HOMER. The electrical loads are primary and deferrable loads. The primary loads are the electrical load that must be met in certain time while deferrable load is thee electrical load that must be met with in sometime period, but the exact time is not important. In HOMER, each part of HRES that can produce, deliver, convert, or save energy is named as a component.

Ten components are modelled in the HOMER. WT, PV, and small hydropower are three renewable energy and non-dispatch able resources. Generators, grid, and boiler are three dispatch able resources. Converter and electrolyzed are components that convert electrical energy to other forms. AC and DC power a reconverted to each other using converters and electrolyzes consume AC or DC power and generate hydrogen through electrolyzing water. Batteries and hydrogen tanks are components that store energy. HRES that are modelled in the articles have used different components for simulation. In some articles, fuel cells are used as generators.

Grid is modelled in the HOMER in three modes, namely, grid-connected, stand-alone, and compares stand-alone system with grid extension. In grid connected mode price and sell back of electricity should be fed into HOMER in two types, real time prices and scheduled rates. In compare stand-alone system with grid extension mode, breakeven grid extension distance will be calculated using three inputs including capital, operation and maintenance cost and grid power price. The breakeven grid extension distance

2.7.2 PV-wind Hybrid Standalone Power Generation System Configuration and Method

A hybrid solar-wind power generation system consists of a PV system, a wind power system, a battery bank, rectifiers, an inverter, and serves the load demand. The single source system like PV energy system or wind energy system requires battery backup and DG unit in standalone system to achieve better performances, which affects hybrid system cost, reliability, cost of energy and environmental emission [87-89].

The electric power is generated by the PV modules and the wind turbines (WT). It is used to satisfy the power demand while the excess is used to charge the battery bank. The energy sources are connected to the direct current (DC) bus via the generators. The energy losses during conversion and charging and discharging of the battery are considered (refer Figure 2.27). The connection of all energy sources to a DC bus simplifies power management. The choice of the DC bus is based on the fractions of the energy generation from renewable sources (The energy production by the PV system and by the wind system are 62% and 38%, respectively, of the total energy production.).

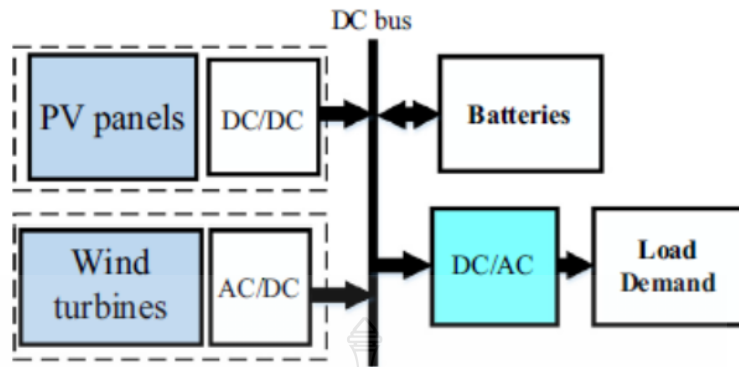


Figure 2.27 Block diagram of a standalone hybrid energy system [90]

PV generators (PVG) have maximum power points (MPP) corresponding to meteorological conditions. In a wind generator (WG) when the wind speed varies considerably, the variable speed generation (VSG) is more noticeable than fixed speed systems. In these systems, a maximum power point tracking (MPPT) adjusts the system's quantity to maximize turbine power output. In PV-wind stand-alone systems, MPPT algorithms are usually implemented on both DC-DC and AC-DC converters, while battery banks are required to store surplus energy, as shown in Figure 2.28

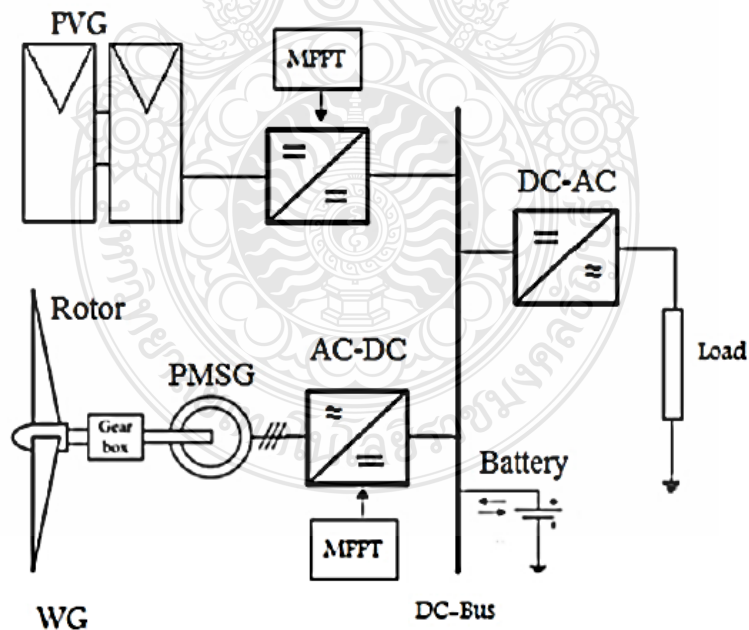


Figure 2.28 Standalone PV-wind hybrid systems [91]

Figure 2.29 shows I–V and P–V characteristics of a PVG, the MPPT methods can be classified into conventional and advanced methods. The conventional methods require a prior knowledge of the characteristic of the system or are based on mathematical relationship which does not meet all meteorological conditions. Therefore, they cannot precisely track the MPP of PV generator or the Wind generator at any at any meteorological conditions. Intelligent MPPT methods logic and artificial neural networks (ANN) are more efficient; however, they are more complex compared to the conventional techniques that are generally simple, cheap and less efficient. In this study, an alternative approach has been proposed using optimized fuzzy logic controllers to control the PV-wind system

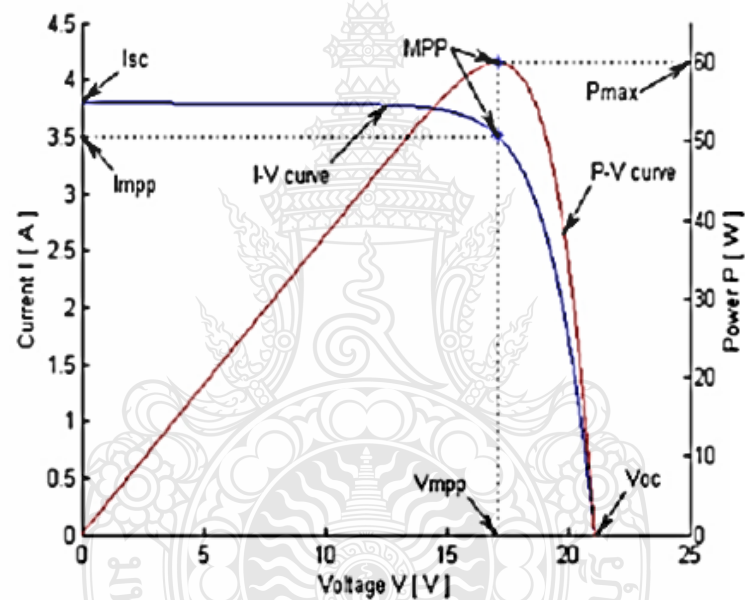


Figure 2.29 I–V and P–V characteristics of a PVG [92]

CHAPTER 3 METHODOLOGY

In this study, the feasibility study to design an on-grid renewable energy system combining PV, water turbine, and wind turbine systems, having a power capacity to supply electricity to the offices of a high-rise building has been studied

3.1 Introduction

Figure 3.1 shows the conceptual design criteria of a stand-alone HRES apply to lighting load. First, study and collecting data of building load requirement then design the renewable system. Integrating effectively production and management of three renewable energy use in PIER 93 building. The renewable energy refers to the wind, water, and solar energies produced by wind turbine, water turbine, and PV cell, respectively.

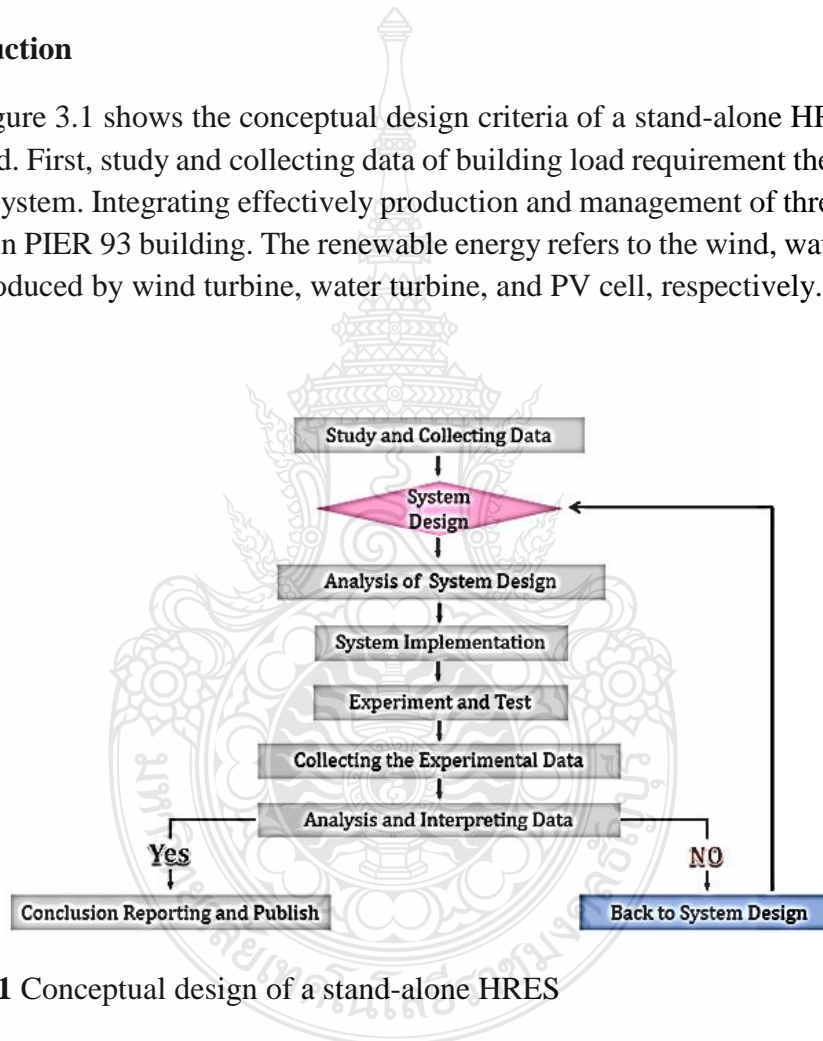


Figure 3.1 Conceptual design of a stand-alone HRES

Figure 3.1 shows the conceptual design criteria of a stand-alone HRES apply to lighting load. The major design criteria are energy hybrid stand-alone. The minor design criteria are to evaluate the renewable energy for the grid tie system for the power load. Design the system and equipment of an appropriate renewable power in an adequate load demand

3.2 Methodology

The step of metrology of this research as follow

1. Siting Designated and Criteria
2. System design, components selection and assembly
3. System Simulation algorithm of Homer Program and CFD Technique.
4. System implemented, experiment and test
5. Experiment Results analysis discussion and conclude
6. Compiling paper publishing in the int'l. journal
7. Conference at the relevant international conferences
8. Integrated results and compile the Dissertation

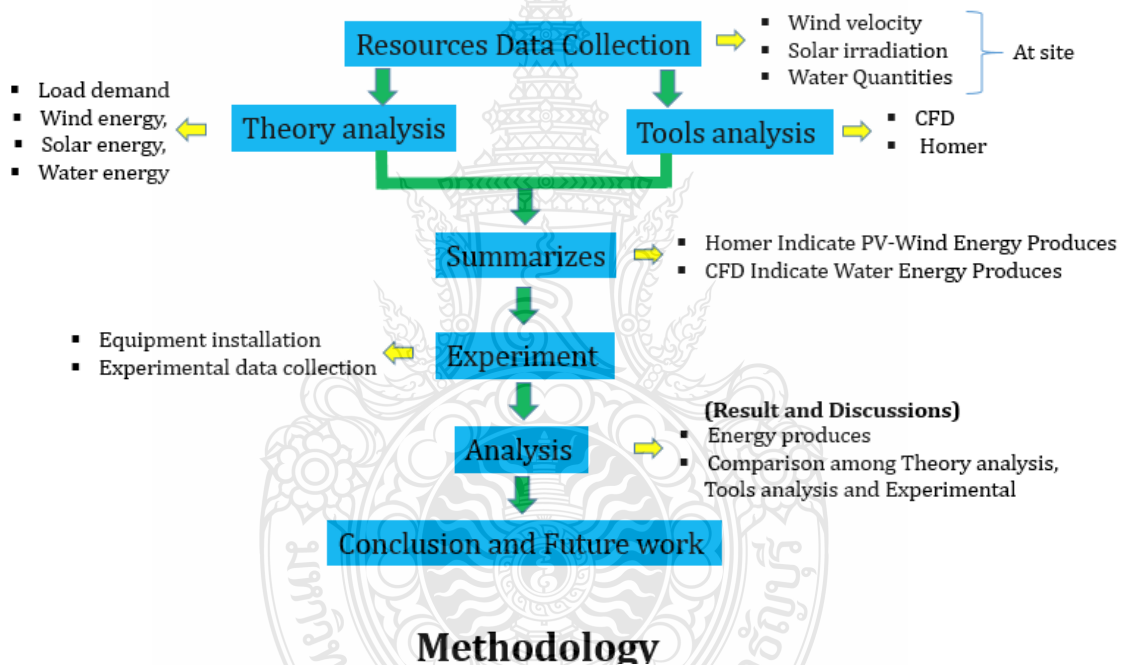


Figure 3.2 The research step

The resources data collection is shown in Figure 3.2. The data including wind velocity, solar irradiation and water quantities where collected at site. This research used the tools for simulation that including CFD commercial program and HOMER commercial program. After that is analyzed by theory about load demand, wind energy, solar energy and water energy. Next step is summarizing the data, the result show that HOMER indicates PV-Wind Produces while CFD indicate water energy produces. The experimental must use for verifying the data from CFD and HOMER simulation result. The result form experimental will compare and discuss about power production and finally whole result will be conclusion.

3.2.1 Location of Study Area

The PIER 93 building is located in Pathum Thani in the middle area of Thailand. Pathum Thani province area is approximately 12778.3 square kilometers or 7986429 hectares. The location of the Pathum Thani province is shown in Figure 3.3



Figure 3.3 (a) Pathum Thani province, Thailand and (b) High-rise PIER 93 building located in the Pathum Thani province

At the site location that consider How to develop three RE System from solar, Wind and Water energy producing electricity for Public Area of condominium and How to develop rooftop space available for Water reservoir, Solar PV and Micro Wind Turbine Machine

3.2.2 Solar Energy Potential

The global solar radiation incident on the area of Thailand is shown in Fig. 2.4. As illustrated in Figure 2.5, the highest solar irradiation (19–20 MJ/m² d) was measured in the north-eastern area of Thailand, i.e. in the Nakhon Ratchasima, Chaiyaphum, Khon Khean, Mahasarakham, Buriram, Surin, Srisakhet, Roi Et, Yasothon, and Ubon Ratchathani provinces, because of their dry plateau (6). Annual average global radiation of Thailand during 1964–2008 is 6.82 MJ or 4.672kWh/m²/d. as shown in Figure 3.4

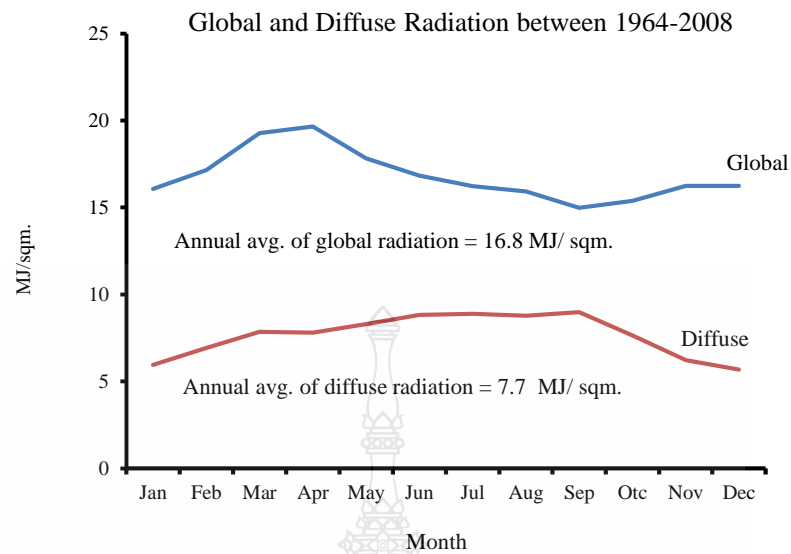


Figure 3.4 Annual average global and diffuse radiations in Thailand between 1964–2008

The proper location has the highest potential to utilize solar energy for electric power generation. The selected study area located at 14 °N, 100 E has the high potential for generating electricity from solar energy, as shown in Figure 2.6. In such area, the highest average energy in April of each year is 5.458kWh/d and the lowest in September, with the average energy 4.161 kWh/d.

3.2.3 Wind Energy Data Measurement

To utilize wind energy to generate electricity, annual monsoon characteristic of selected location is very important. The direction and speed of the wind at a selected location must be continuously measured to obtain the correct wind data for analyzing the potential of wind energy to generate electricity. Wind data of study area was measured and collected by site measurement at PIER 93 building on rooftop station, as shown in Figure 3.5. Wind data of 2017 is shown in Figure 3.6.



Figure 3.5 Wind data measurement at the PIER 93 building

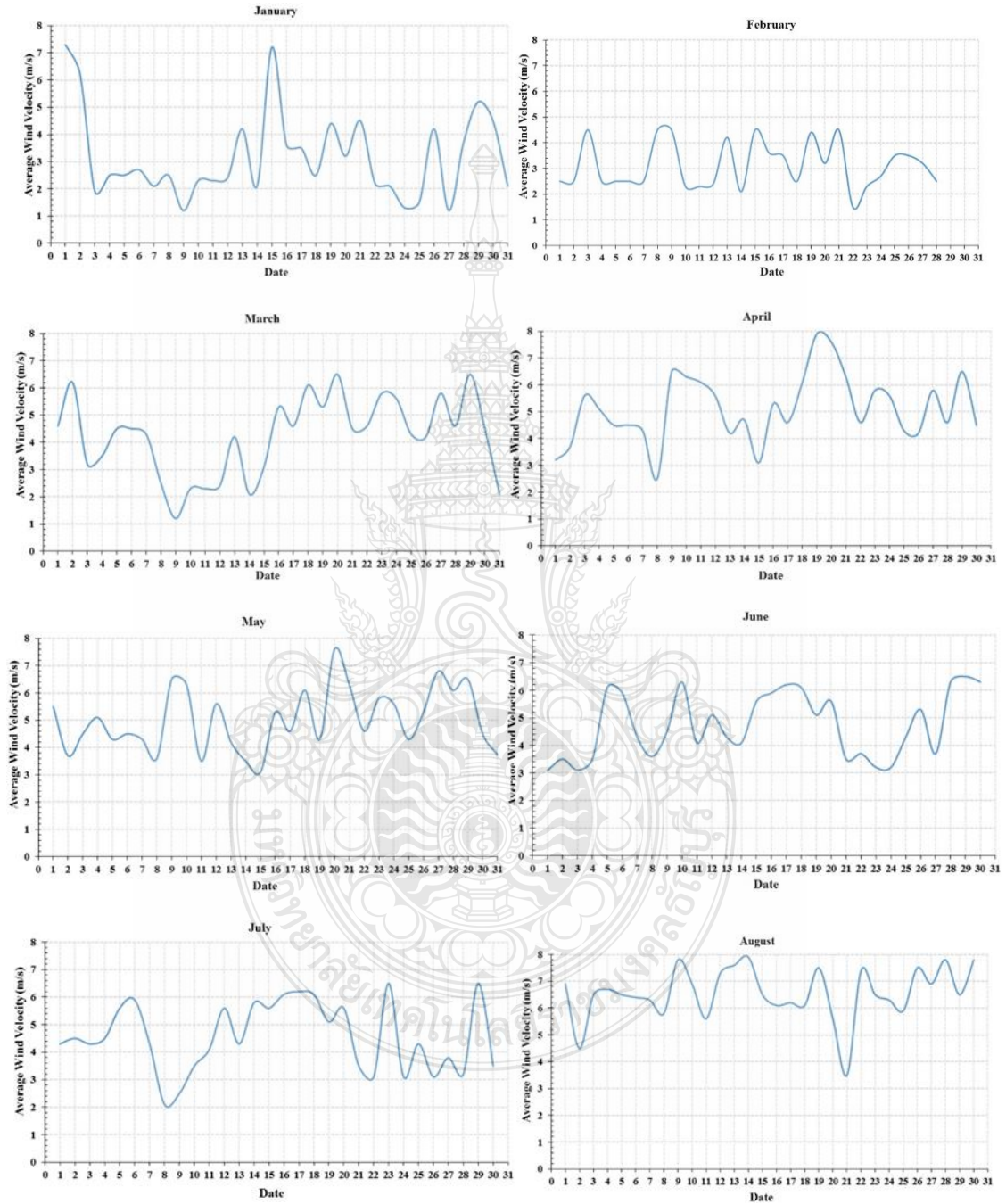
The monthly average wind speed in the minimum is 2.01 m/s and the maximum are 6.55 m/s. The annual average wind speed is 3.94 m/s, which is enough for utilizing the wind energy in the selected area.

	Wind(m/s)	Solar (MJ/m ²)	Water (mm)
Jan	3.6	16.1	20
Feb	3.6	17.5	60
Mar	4.63	19.6	70
Apr	4.12	18.2	42
May	4.12	17.5	150
Jun	4.12	16.8	210
Jul	4.12	16.1	300
Aug	4.12	15.5	250
Sept	3.6	15.8	45
Oct	3.09	15.9	30
Nov	3.09	16.2	35
Dec	3.6	16.3	20
Ave.	3.82	16.2	102.67

Figure 3.6 The resource data from wind, solar and water

Figure 3.6 shows the three-renewable energy from which is from wind, water and solar energy.

As illustrated in Figure 3.6, the annual average wind speed measured was observed to be suitable for designing an on-grid HRES



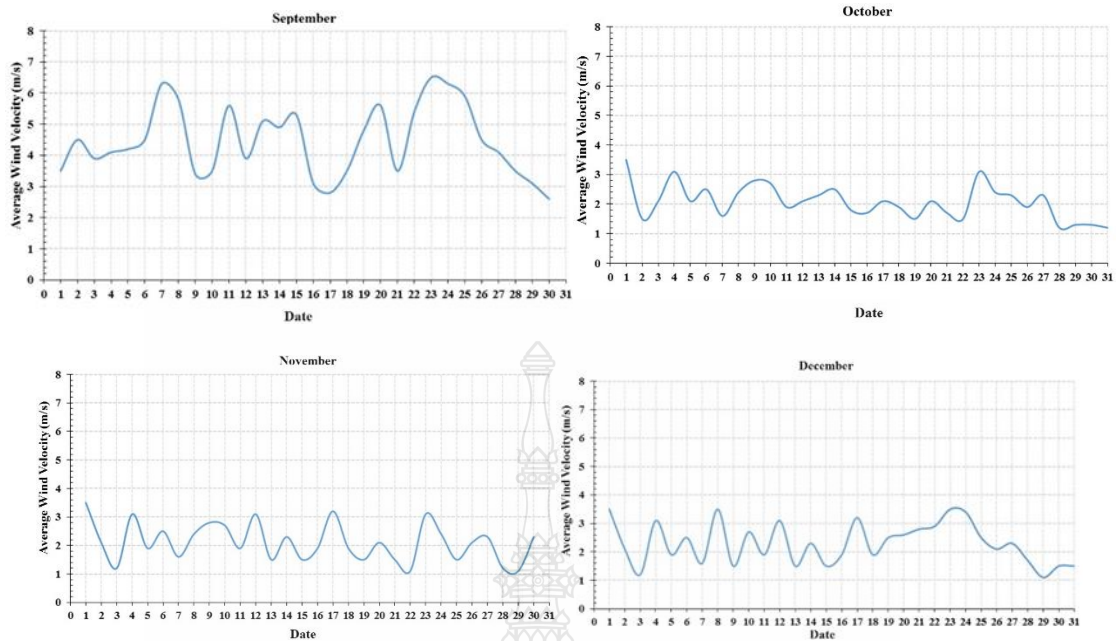


Figure 3.7 Daily wind speed for each month of 2017 at the PIER 93 building

3.2.4 Water Turbine Data Calculation

The different location and condition are important parameters for water turbine installation and specification. Therefore, before select the turbine should consider environmental requirements and selection process method, as shown in Figure 3.8 below

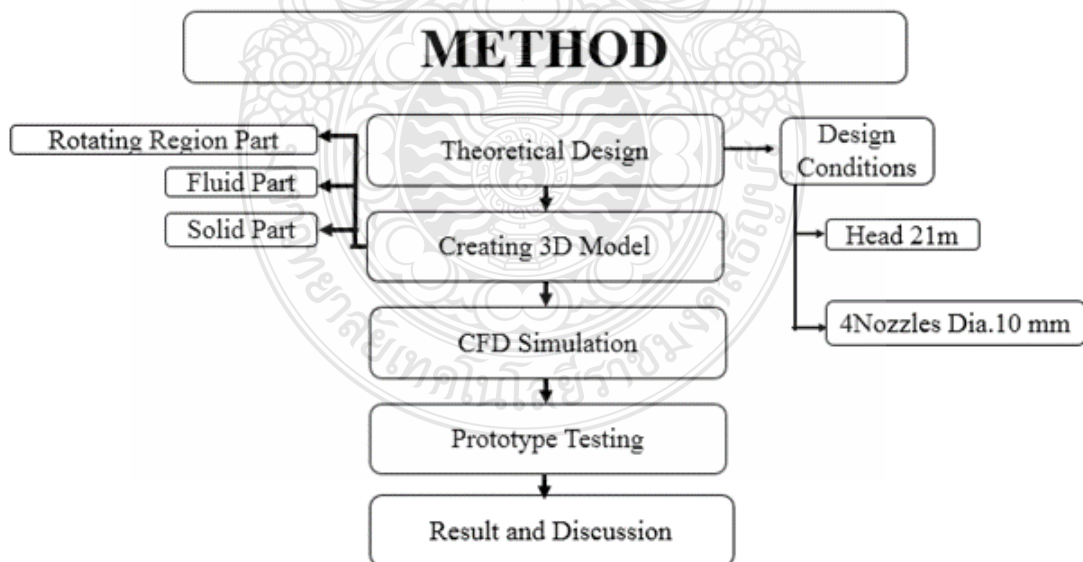


Figure 3.8 Process flowchart

Figure 3.9(a) shows the PIER 93 building with the rooftop as such that it can be used as a rain water reservoir for rainwater storage, which uses water flow along the piping from rooftop into the water turbine blade installed at the first floor of the PIER 93 building, as shown in Figure 3.9(b). The rainwater storage is approximately 57.6 m³ at the rooftop, as shown in Figure 3.9(c), and the annual rainfall stored on the rooftop is approximately 354.15 m³/y.

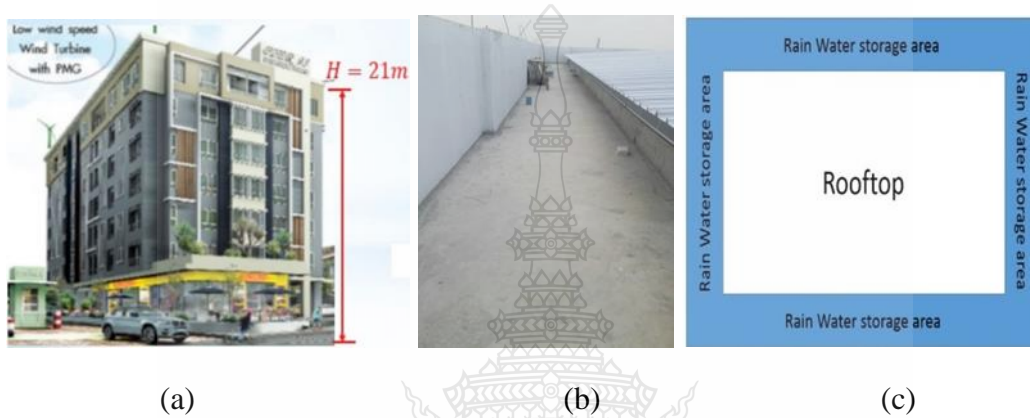


Figure 3.9 (a) PIER 93 high-rise building, (b) Roof gutter area, and (c) Water storage area on rooftop

3.2.5 Quantitative Theoretical Analysis of the Pico Turgo Turbine

The 10 mm diameter of four nozzle is designed for this case of this research, including the condition of flow rate approximately 0.0062 m³/s or 22.3 m³/h and using 21 m high; thus, the water jet velocity can be calculation as below

$$c = \varphi \sqrt{2gH}$$

$$= 0.97 \sqrt{2 \times 9.81 \times 21} = 19.7 \text{ m/s} \quad \text{where } H = 21 \text{ m}, \varphi \approx 0.97$$

The flow rate of the four nozzles is

$$Q = \frac{\pi}{4} d^2 c$$

$$Q = \frac{\pi}{4} \times 0.01^2 \times 19.7$$

$$Q_K = 0.0015 \text{ m}^3/\text{s} \times 4 = 0.0062 \text{ m}^3/\text{s}$$

The velocity of the runner is

$$u_1 \approx (0.46 - 0.47)c$$

$$u_1 \approx (0.46 - 0.47) \times 19.7 \approx 9.1 \text{ m/s}$$

Using a generator of 400 rpm, the runner diameter is

$$D_s = \frac{60u_1}{\pi n} = \frac{60 \times 9.1}{\pi \times 400} = 0.43 \text{ m}$$

Thus, the power can generate

$$\begin{aligned} P &= \rho g Q H \\ &= 998 \times 9.81 \times 0.0062 \times 21 = 1,310 \text{ kW} \end{aligned}$$

The annual volume rainfall is 354.15 m^3 . Therefore $1.31 \text{ kW} \times 15.87 \text{ h} = 20.78 \text{ kWh/year}$. In these research conditions, the maximum head is 21 m and selected four nozzles of 10 mm diameter. The runner of the Pico Turgo turbine is designed and calculated from this condition. The potential energy of water head is converted to kinetics energy attack to turbine blade which connected the runner turbine shaft to drive the generator. The 3D model is first created using CFD simulation, and the flow contour is investigated to estimate the RPM and torque of the turbine.

3.2.6 Computational Fluid Dynamics (CFD)

This study uses the CFD method two times for simulation, first for the Pico Turgo water turbine model and second for the micro wind turbine installed at the rooftop of the PIER 93 building model. CFD simulation method for micro wind turbine

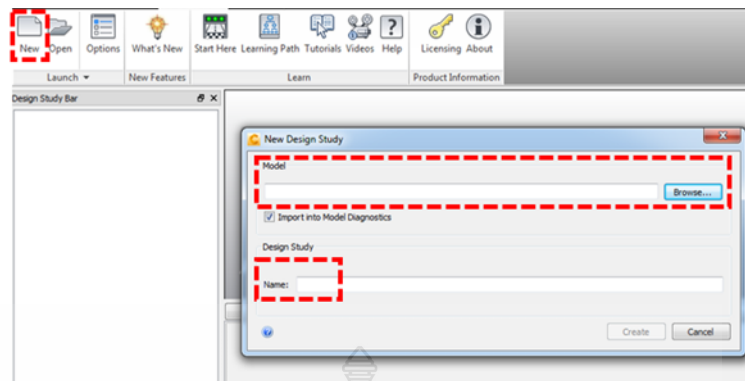


Figure 3.10 Tool bar of CFDdesign commercial program for new model simulation

Figure 3.10 shows the CFD menu and the first step for using the CFD commercial program. The supported file for the CFD design commercial program and simulation is the xt file.

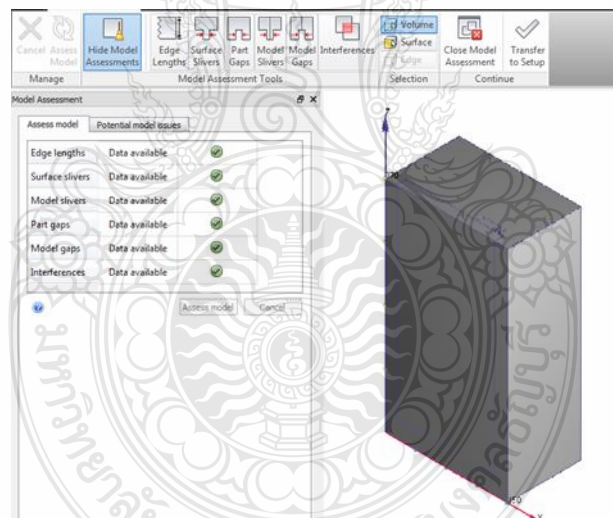
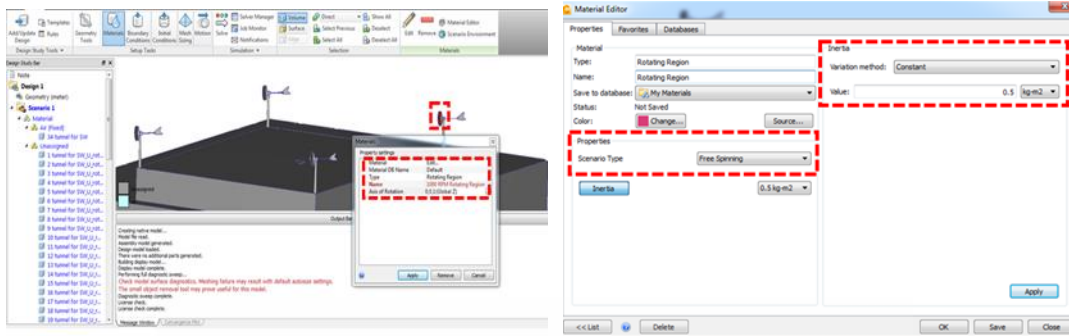


Figure 3.11 CFDdesign commercial program assessment tool for mesh error checking

Figure 3.11 shows the CFD design commercial program assessment. This program will check the model for suitable simulation including, edge length, surface sliver, model sliver, part gap, model gap, and model interface.

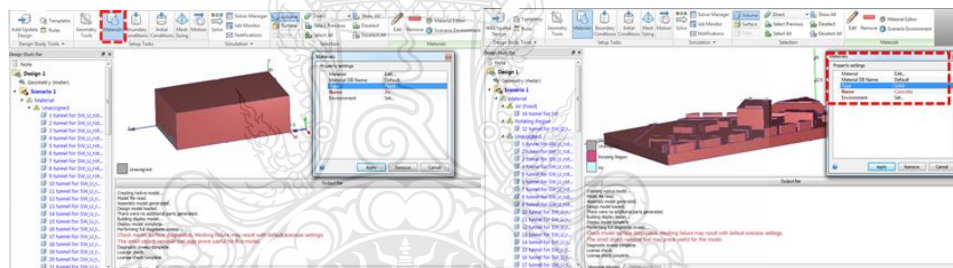


(a)

(b)

Figure 3.12 Material selections for a micro wind turbine

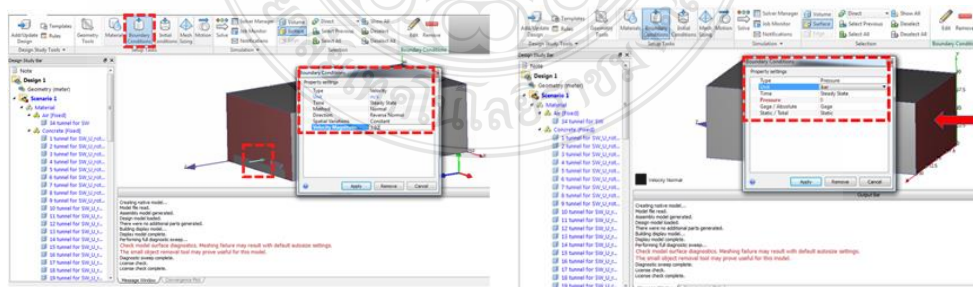
Figure 3.12 shows the material selection for a micro wind turbine. The materials of wind turbine simulation include static part and dynamic part. The static part including wind turbine hub, wind turbine tower while the dynamic part including wind turbine blade and wind turbine rotating region. The rotating region uses the free spin type and 0.5 kg/m² of the wind turbine blade moment inertia with constant.



(a)

(b)

Figure 3.13 CFDdesign Material selection of building, building terrain and wind turbine



(a)

(b)

Figure 3.14 The boundaries conditions setup of building terrain for SSW direction wind flow input

Figure 3.13 shows the material selection for air flow. The fluid surrounding for this simulation is the air. The air properties are including in CFD design program. At the surrounding terrain and PIER 93 building material is concrete.

Figure 3.14 shows the boundary condition setup for the inlet and outlet sides. At the outlet side is selected by wind flow velocity condition and at the outlet side is selected by pressure condition. The inlet side is changed velocity magnitude size while the outlet is used constant pressure.

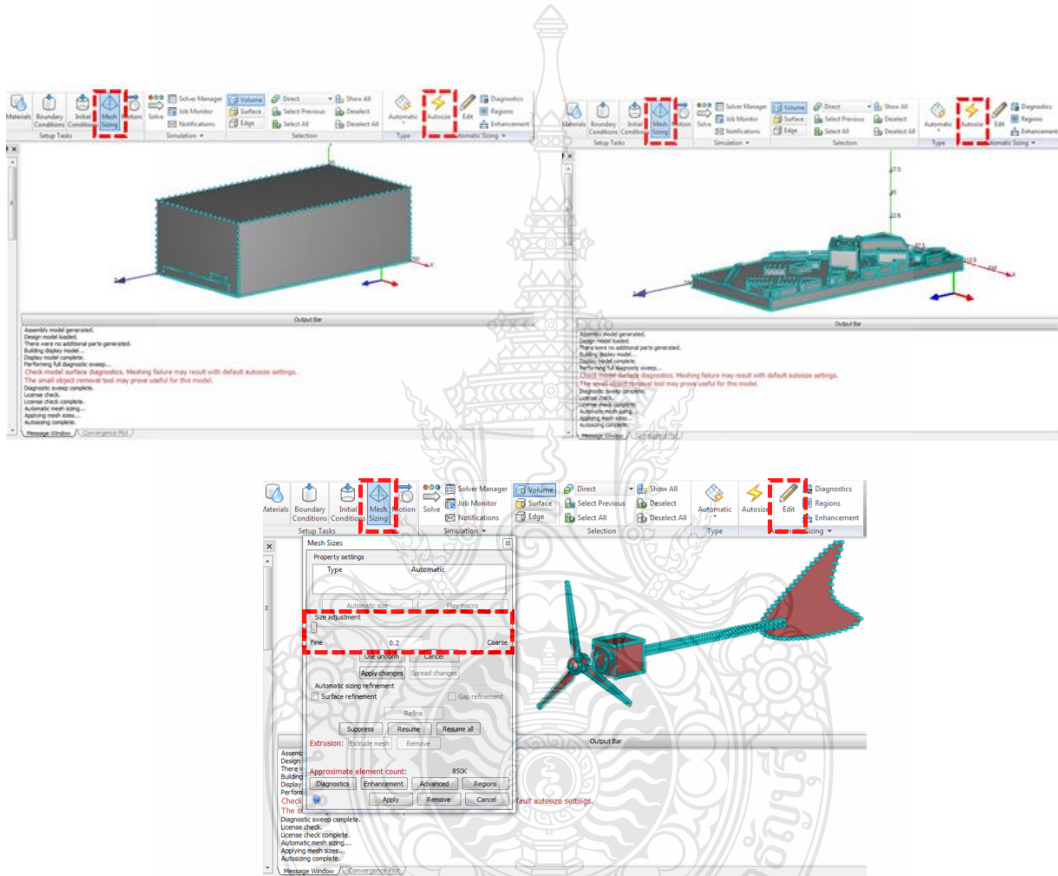


Figure 3.15 Meshing of the simulation model

Figure 3.15 shows meshing of the simulation model. One of the important features of the simulation method is the meshing method of 3D model. The suitable parts of each model and each model part can be exported for a realizable result. Some parts need high-density meshing while some parts do not need it. The air part and the building can be large meshing while the micro wind turbine must be high density meshing, the same as the rotating region, which is the dynamics part.

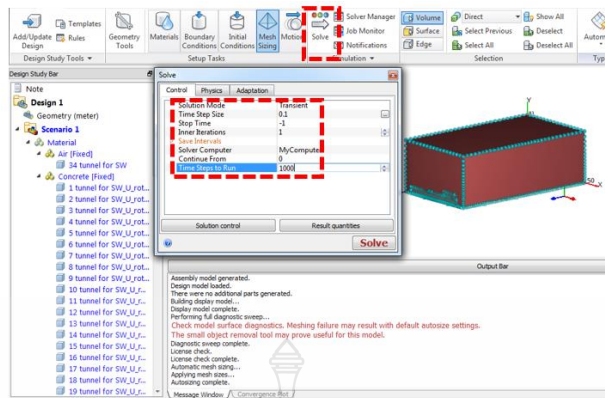


Figure 3.16 Solving the CFD method

3.2.7 Terrain of Pier 93 Building

We consider the canal in front of the PIER 93 building and the main road as a part of its terrain. The PIER 93 building is embraced by many small buildings. The Google view, 2D model, and 3D model of this terrain are shown in Figures 3.17(a)–3.17(c), respectively

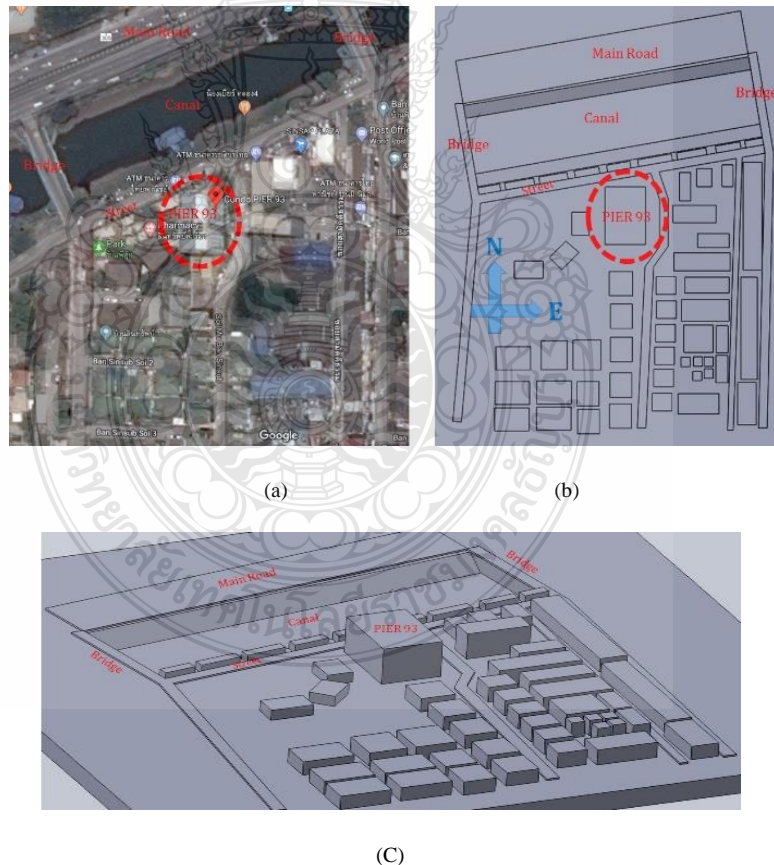
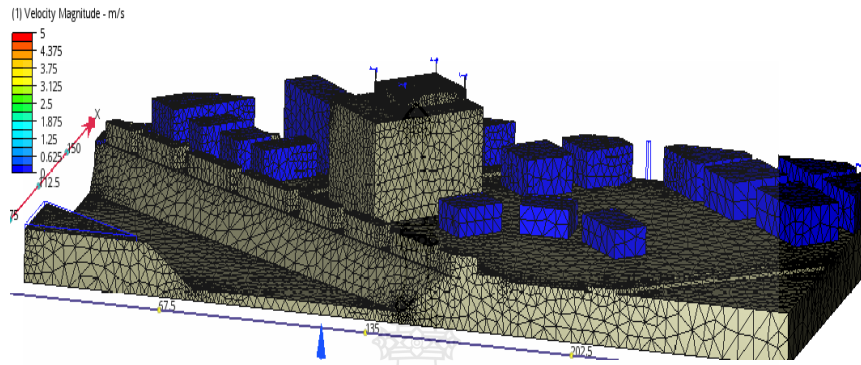
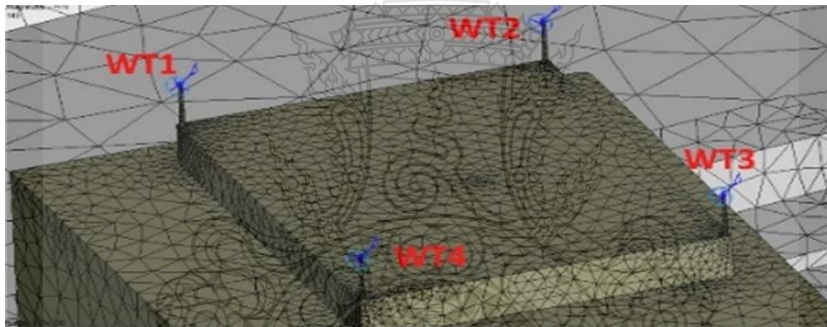


Figure 3.17 Layout of the terrain at PIER 93. (a) Google view, (b) 2D model, and (c) 3D model

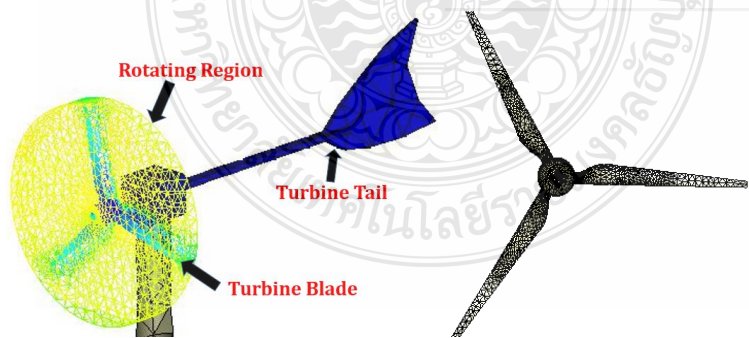
After the 3D model was created, the then grid cell of the 3D model is created, as shown in Figure 3.18(a). Grid cell is created at terrain of building, building and wind turbine. Figure 3.18(b) shows the grid cell which is generated at the building rooftop and Figure 3.18(c) shows the grid cell generated of turbine, which includes the rotating region, wind turbine tail, wind turbine blade, wind turbine nacelle, and wind turbine tower.



(a)



(b)



(c)

Figure 3.18 3D model grid cell creations. (a) Terrain, (b) Roof top of the PIER 93 building, and (c) Micro wind turbine

Figure 3.19 shows the boundary condition which set at the CFD model simulation including inlet side takings velocity is 3.82 m/s from south-southwest (SSW) and east-northeast (ENE) direction while the outlet side taking pressure zero of gage bar. This model simulation includes two mains condition that are static and dynamic parts. The static part means the part cannot move while simulation process is running which including terrain, building turbine tail and turbine nacelle. The dynamic part means the part can move while simulation process is running which including rotating region, turbine blade and air particle.

The simulation model type of the micro wind turbine in this research is simulated by the free spinning model condition. The free spinning model condition's torque is not considered in this study's simulation model.

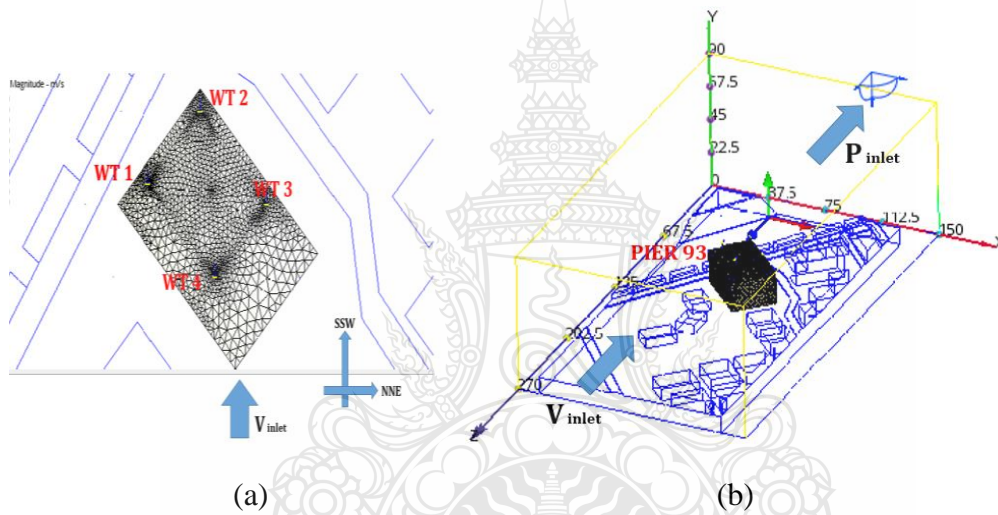


Figure 3.19 Boundary conditions. (a) Velocity inlet from the SSW direction and (b) Pressure outlet at the outlet side

The Turgo blade shape is generated from hydrodynamic theory and Bezier polynomials [53]. Further, the 3D model shape is generated using CFD simulation

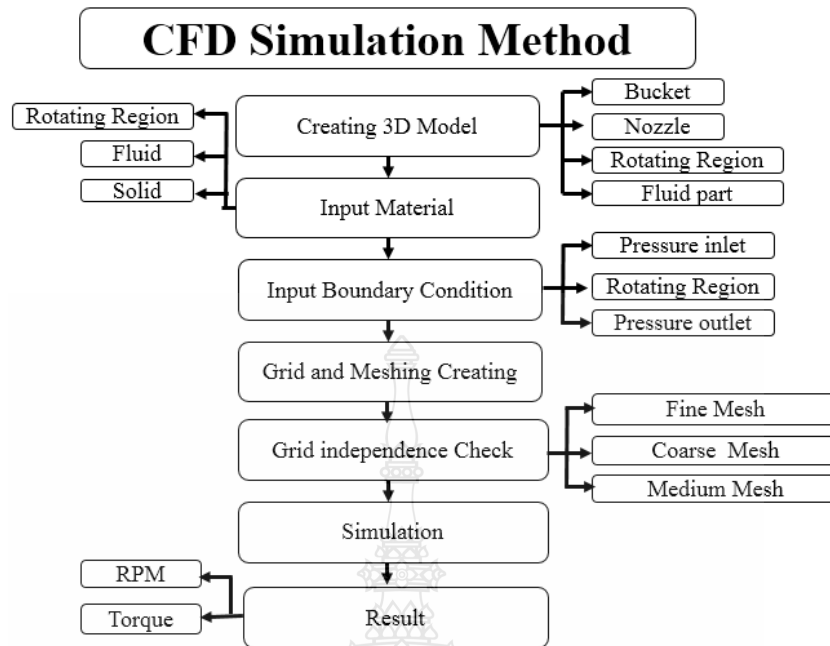


Figure 3.20 CFD simulation method

The CFD simulation method is shown in Figure 3.20. The 3D model is the first step of this process. The part of 3D model includes bucket, nozzle, rotating region and fluid part. The two main of boundary conditions include dynamics part and static part. The specific boundary conditions determine the input part of the nozzle to indicate the pressure inlets, which apply different pressures under testing, whereas the pressure outlets show the barometric pressure. In this input boundary process, the water stream from the nozzle is injected into the rotating region. The grid and mesh were created for the different parts of the study model. The mesh was determined by a grid-independent check using coarse, medium, and fine meshes to acquire the torque and rotation speed (rpm). CFD uses numerical methods to solve the governing equations describing the behavior of various fluids.

The three fundamental principles of conservation including continuity equation, momentum equation and energy equation is applied for CFD simulation method and using the Naiver–Stokes equation as below.

The Continuity equation is as follows:

$$\frac{\partial \rho}{\partial t} + \nabla \cdot (\rho \vec{u}) = 0 \quad (3.1)$$

The Momentum equation is as follows:

$$\Sigma F = ma \quad (3.2)$$

The Naiver–Stokes equation is as follows:

$$\frac{\partial}{\partial t}(\rho \vec{u}) + \rho(\vec{u} \cdot \nabla \vec{u}) = -\nabla p + \nabla \cdot \tau + S_m \quad (3.3)$$

The stress tensor τ is related to the strain rate as shown below.

$$\tau = \mu \left(\nabla \vec{u} + (\nabla \vec{u})^T - \frac{2}{3} \delta \nabla \vec{u} \right) \quad (3.4)$$

Energy equation:

$$\frac{\partial}{\partial t}(\rho h_t) - \frac{\partial \rho}{\partial t} + \nabla \cdot (\rho \vec{u} h_t) = \nabla \cdot (\vec{u} \cdot \tau) + \vec{u} \cdot S_m + S_e \quad (3.5)$$

the total enthalpy h_t is related with the static enthalpy h_s as equation below:

$$h_t = h_s + \frac{1}{2} \vec{u} \quad (3.6)$$

3.2.7 Pico Turgo turbine boundary condition for computational fluid dynamics (CFD) simulation

The principle of the CFD method should be removed in some terms of equation because the complex equation cannot solve in CFD program. The partial differentials and the discretized numerical method are used for approximate solutions of CFD method, some condition can consider as isothermal, incompressible, etc. therefore the important of CFD method is initial condition or initial boundary condition should be considered. This research condition for Pico Turgo turbine simulation, as presented in Table 3.1

Table 3.1: Boundary Conditions of the Pico Turgo turbine

Parameter name	Units	Parameter Value
Total Pressure Inlet	Bar	1–4
Total Temperature Inlet	K	320
Angular Velocity	rad/s	Free spin
Cup Number		24
Nozzle Number		4
Viscosity	Pa-s	0.001003
Specific heat	J/kg.K	4182
Working fluid		Water
Density	kg/m ³	998.2
Emissivity		1

The CFD methods can be used to analyze complex phenomena, many types of simulations, such as multiphase, highly turbulent flows, fluid solid interaction, and combustion, and reasonable timescale [93]. Recently, CFD simulation method closes to the experimental data [94], that mean can confidence and reliable the CFD result data.

The CFD software was used to conduct simulations of the Pico Turgo turbine, with a finite-volume method employed for the spatial discretization of the governing equations. The numerical results were validated by an experimental test [95]. The nozzle passage 3D model part and runner 3D model passage part are separated, then assembly together. The flow for this simulation model is simulated as steady state condition.

3.2.8 Initial condition for CFD simulations of Pico Turgo turbine

The three parts of the 3D model include a nozzle, bucket, and rotating region, as shown in Figure 3.21. In this study, we use inlet water at each nozzle and changing the pressure at the boundary water inlet condition. The blade or bucket shape is significant for the efficiency of the Pico Turgo turbine.

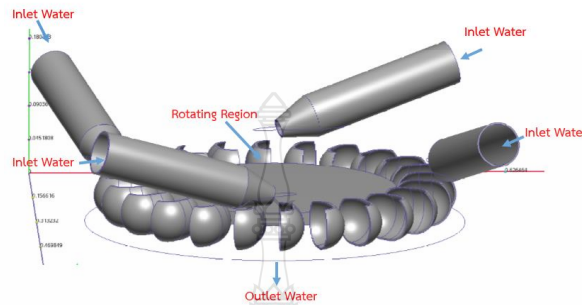


Figure 3.21 The Pico Turgo turbine computational domain and boundary conditions

This study uses the transient simulations model is applied in the simulation model and the steady state is included. The $k-\epsilon$ turbulence model which including two-part turbulent kinetic energy (k) and turbulent dissipation rate (ϵ). The homogeneous fluid is used for this simulation. The result from this CFD method includes torque and runner velocity, which will use calculate the power of turbine.

In the general single jet operation, three buckets are enough to recreate the complete runner torque. The torque is measured on the reference bucket, which is the bucket in the middle. The first bucket provides backsplash that might impact the backside of the reference bucket, and the third bucket realistically obstructs the jet from impacting the reference bucket. The most widely used turbulence models are the two-equation systems that offer a good balance between computational cost and accuracy.

3.2.9 Grid independence check

Eulerian equation is used for calculating the fluid flow field of the CFD method [59]. Before the CFD method initiates simulation, the grid or mesh must be generated. The element which generated from grid or mash obtains tetrahedral elements.

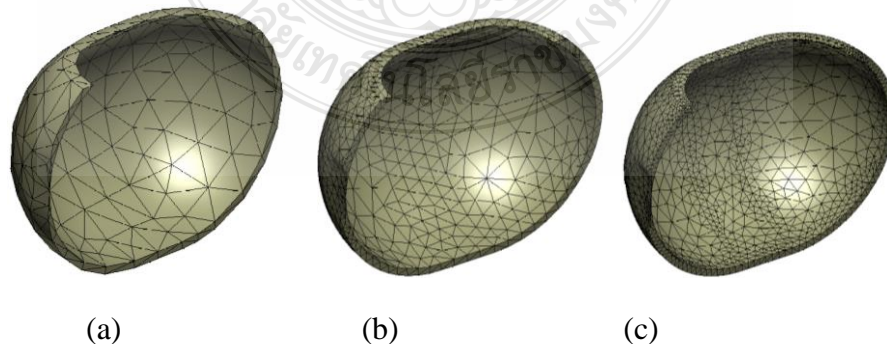


Figure 3.22 Bucket grid dependency of the Pico Turgo turbine. (a) Coarse mesh, (b) Medium mesh, and (c) Fine me

Generally, there are three types of meshing checks, which includes 'coarse mesh' (Figure 3.22(a)), 'medium mesh' (Figure 3.22(b)), and 'fine mesh' (Figure 3.22(c)). In some point or some part, the meshing density is low or high which depend on shape or force density attack to each 3D part.

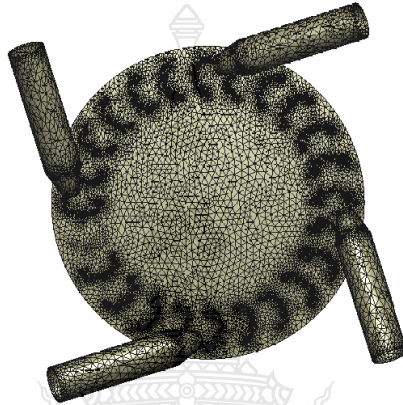


Figure 3.23 Grid density of the Pico Turgo turbine nozzle, cup, and rotating region

Generally, the CFD method includes two type for rotating simulation which is full rotating simulation type and periodic rotating simulation type. This study case is simulated in full rotating simulation type. The interface between the static and dynamics parts is adjusted by the CFD program. The part of static type includes nozzle and the dynamic part including water part, water turbine blade part and rotating part. Figure 3.24 shows grid dependence checking which used approximately 3500000 cells in the turbine model. At this value the rotating of turbine approximately 190 rpm, as presented in Table 3.2

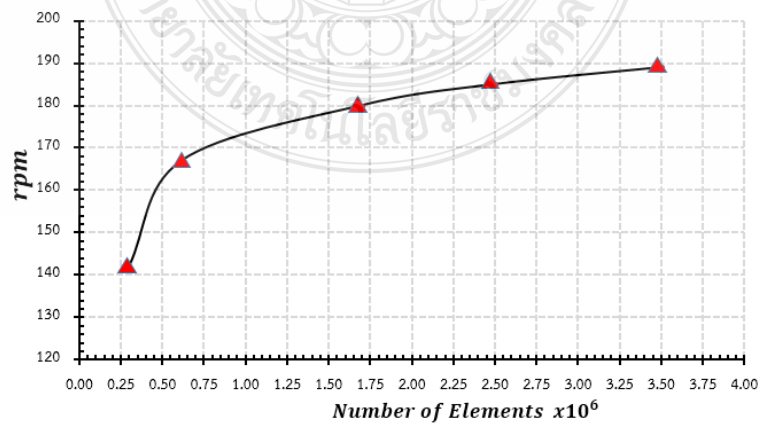


Figure 3.24 Grid dependency of the Pico Turgo turbine

Table 3.2 Grid convergence

Grid number $\times 10^6$	rpm
0.25	141
0.50	162
0.75	170
1.00	172
1.50	178
2.50	185
3.50	189

The CFD method is the first main priority for research 3D model is created and adjusting. After 3D model is approved by CFD simulation method the next method will manufacture prototype of turbine part and make this for testing apparatus



(a)

(b)

Figure 3.25 Pico Turgo turbines (a) Prototype buckets and (b) Prototype buckets with runner

The prototype of the Pico Turgo turbine blade and the runner assembly model are shown in Figures 3.25(a) and 3.25(b). The apparatus testing set is shown in Figure 3.26(a). The runner of turbine is connected to the PMG generator for measuring the electricity quantity generated. The efficiency of turbine can be measured by turbine torque and the rotating of turbine shaft; therefore, the torque sensor and rotation sensor are installed at Points A and B, respectively. Figure 3.26(b) shows the 3D model complete apparatus set including the piping line, AC motor drive for water pumping and the water circulation reservoir. Figure 3.26(c) shows the real prototype testing set with four 10 mm diameter nozzles. Figure 3.26(d) shows the water from the nozzles impacting the buckets.

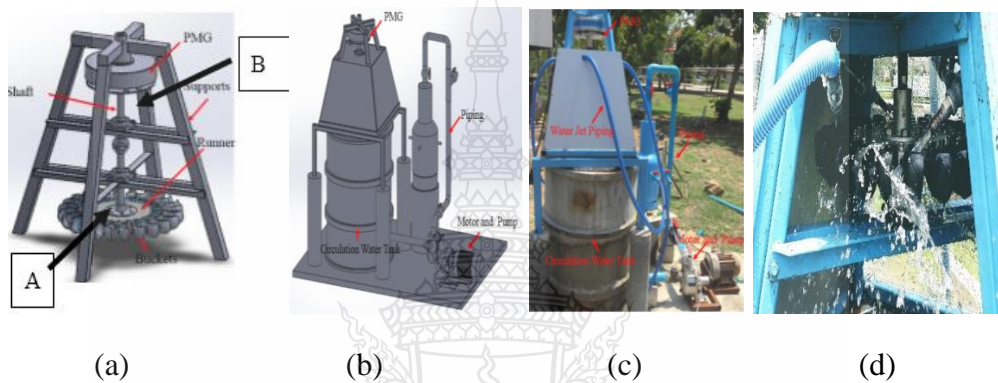


Figure 3.26 3D model of Pico turbine testing. (a) 3D model connected set connecting to PMG, (b) 3D water circulation system connecting with water pumping, (c) Real prototype testing apparatus, and (d) Water flow impacting the turbine blade

3.2.10 two hybrid renewable energy PV-wind system

The concept design of two renewable energy systems is shown in Figure 3.27 each renewable energy type wind and solar generate the electricity then the electricity is converted by converter. The system is connected grid line system in HOMER commercial program, including 4.6 kW of hybrid Wind-PV system.

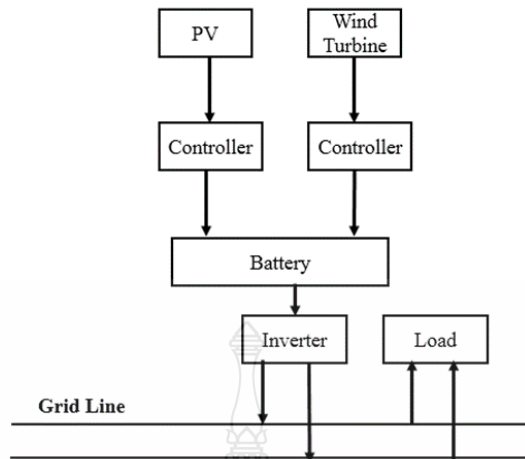


Figure 3.27 Two renewable energy system concept design

The energy from solar and wind focusing only on the rooftop of the PIER 93 building, the building height is approximately 21 m and the wind average is 3.94 m/s.

3.2.11 Power Load calculation

The concept design of two renewable energy systems is shown in Figure 3.27

Table 3.3 Load of public commonly use area electricity at the high-rise Pier 93

Floor	LED T8 2x18W	LED T8 2x18w	LED T8 2x9w	LED 7w	LED 1x 18w	LED T8 1x9w	LED 7w
1	19	25	7	21	-	2	10
2	-	5	-	11	1	-	-
3	-	5	-	11	1	-	-
4	-	5	-	11	1	-	-
5	-	5	-	11	1	-	-
6	-	5	-	11	1	-	-
7	-	5	-	11	1	-	-
Total	38	55	14	87	6	2	10
kW	0.684	0.99	0.126	0.609	0.108	0.036	0.07
24h/d	12	8	24	8	24	24	24
kWh/d	8.208	7.92	3.024	4.872	2.592	0.864	1.68
Total kwh/d				29.16			

Table 3.3 shows the public commonly load use area of PIER 93 building, including totally bulbs LED 18 W amount 115 sets and LED 9 W amount 24 sets, overall loaded amount 29.16 kWh/d. The STC condition testing for solar cell is under considered.

3.3 Homer Commercial Program Calculations

In this study, a renewable hybrid system comprising PV and micro wind turbines was modelled

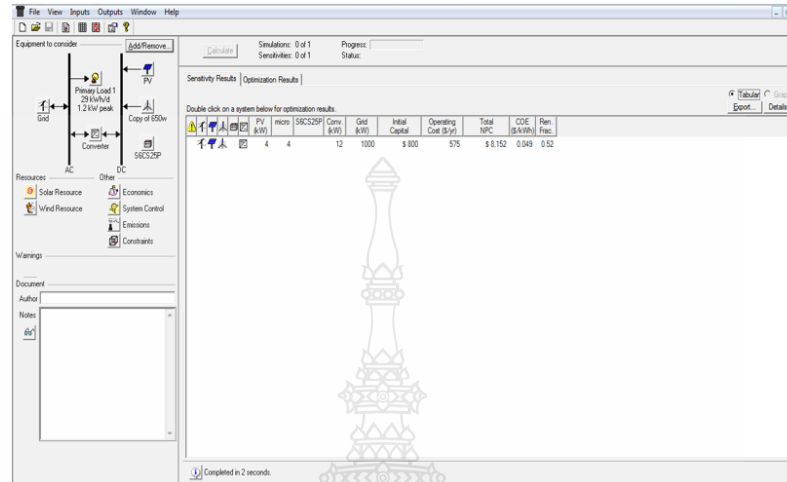


Figure 3.28 HOMER commercial programs

The HOMER commercial Program is shown in Figure 3.28, the tool condition device of program including Grid line connected, Primary Load 1 which approximately 29 kWh/d and 1.2 kW peak. The model uses a converter tool device to convert the power type from DC to AC and vice versa, depending on the device sources. The model includes two type of renewable type which is wind sources and solar sources.

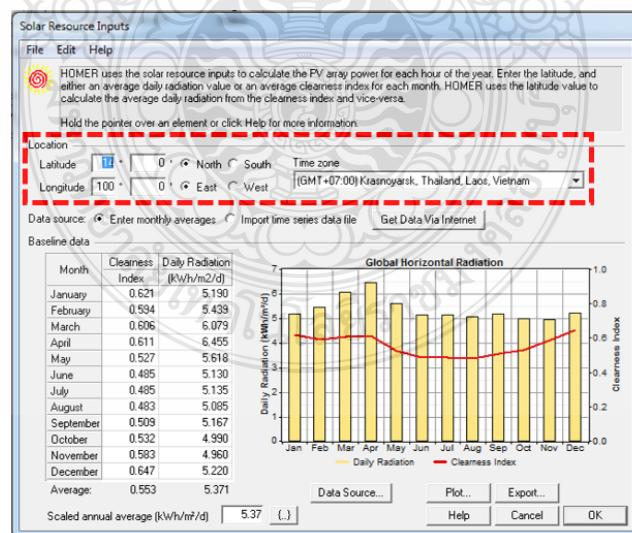


Figure 3.29 Select the real side location of the PIER 93 building

Figure 3.29 shows the solar resources input, using the location of the real site PIER 93 building data. The building location is Latitude 14 °N and Longitude is 100 °E, which is in the GMT+07.00 time zones.

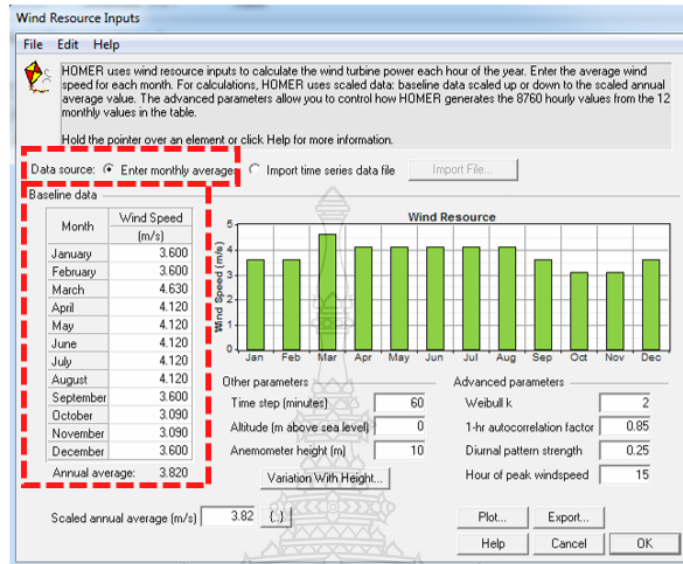


Figure 3.30 Monthly input average of the wind velocity

Figure 3.30 shows the wind velocity resources input, using the wind monthly average in each month which is collected by the Wind finder website. At the baseline data input 3.6 m/s in January, 3.6 m/s in February, etc. the value of annual average wind velocity is approximately 3.82 m/s.

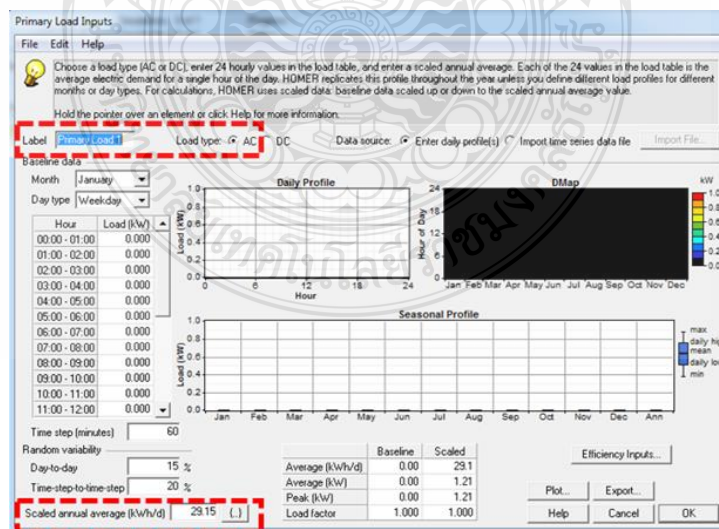


Figure 3.31 Input primary load input of the PIER 93 building

The input primary load input of the PIER 93 building in Figure 3.31 shows the load type is AC load. The primary AC load input includes two types for data input: hour loading, which means we can input load demand at each hour and another one can input annual average load demand (kWh/d) of approximately 29.15 kWh/d.

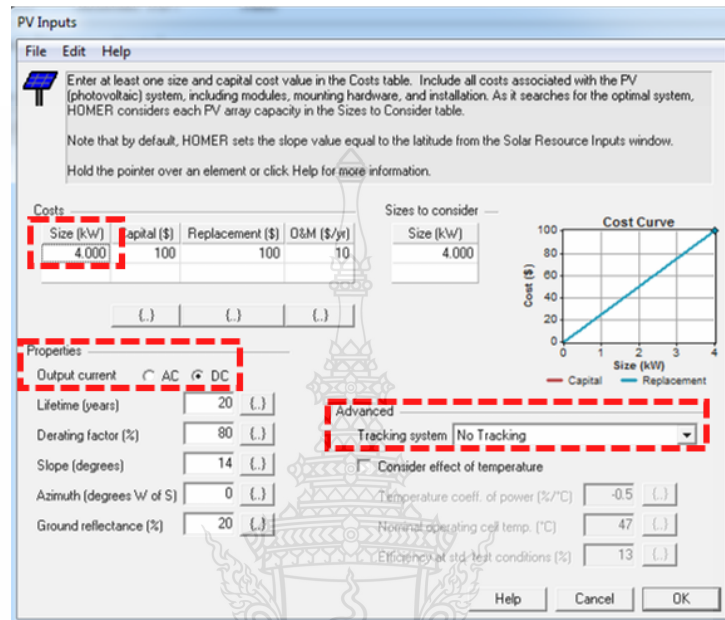
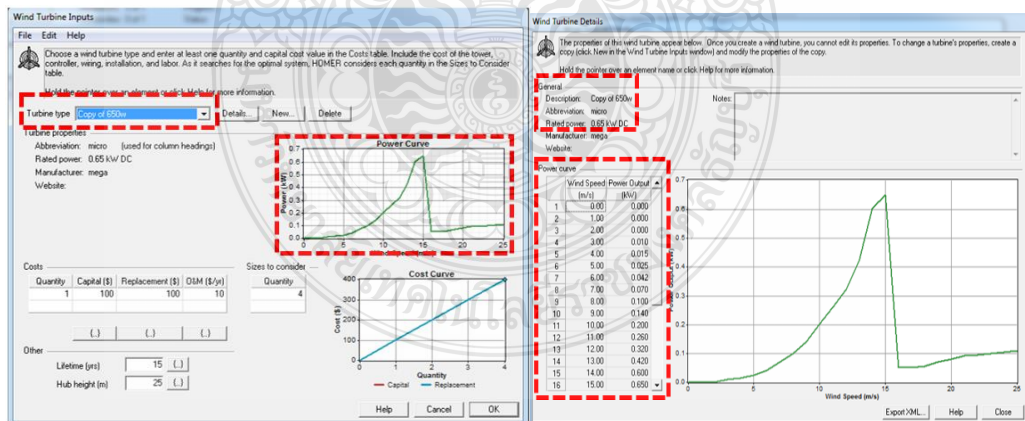


Figure 3.32 Specifications of the PV inputs

Figure 3.32 shows the specifications of the PV Inputs and the total PV capacity (approximately 4.0 kW), and the output current is DC current with no tracking type.



(a)

(b)

Figure 3.33 Input specifications of a wind turbine

Figure 3.33 shows the specifications of a wind turbine. The turbine power is 650 W and totally four sets. At difference wind speed, wind turbine can generate the electricity as shown in wind turbine power curve.

The daily wind speed profile for each month is shown in Figure 3.34. The modelling program (HOMER) that was used for simulation had values entered for various conditions: load demand, of about 21 kWh/d; PV of 4 kW; four sets of micro wind turbines, at 650 W each; and 16 sets of 12 V, 200 Ah batteries

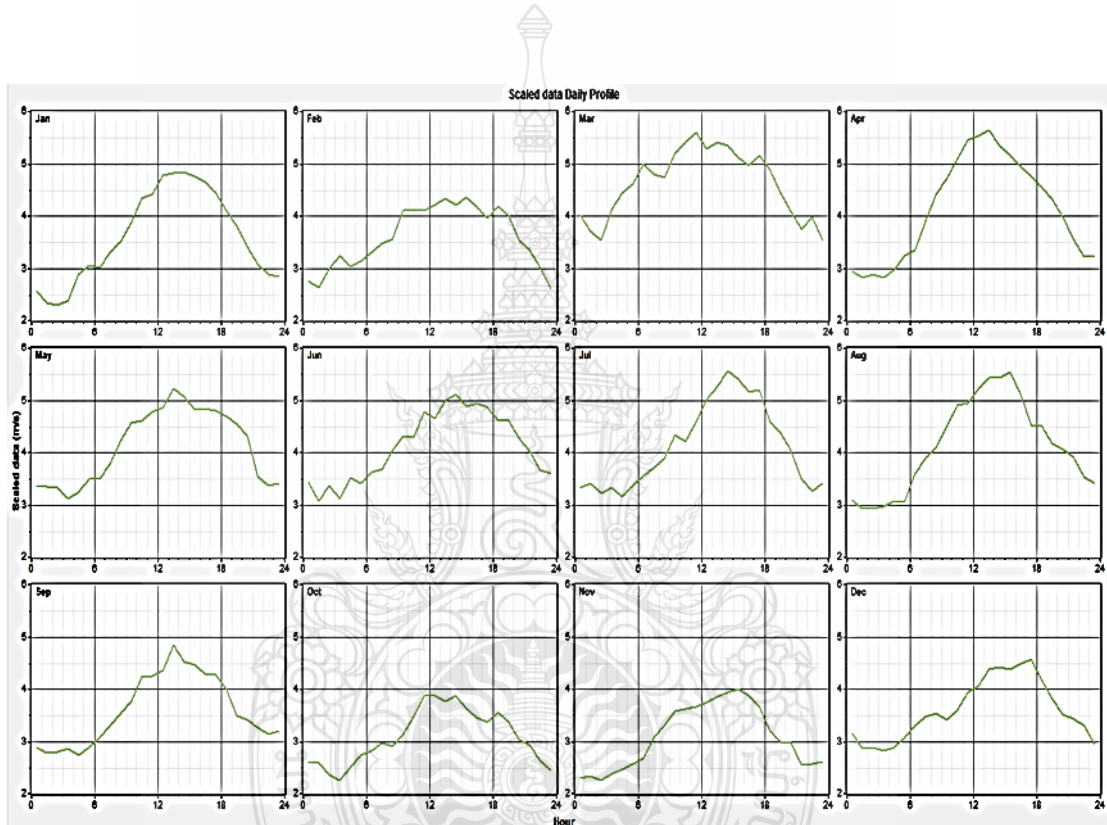


Figure 3.34 Wind speed daily profile of the HOMER program at 14 °N, 100 °E

The PV-wind hybrid simulation model is shown in Figure 3.35. In addition to the micro wind turbines and PV array, the system also includes the battery storage used to increase the reliability of the system. Primarily, renewable sources feed the energy demand and the excess energy is stored in batteries.

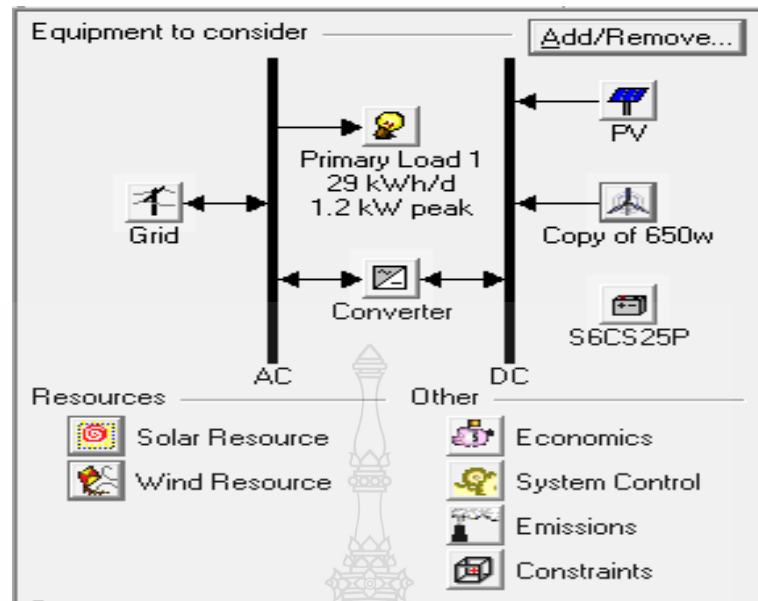
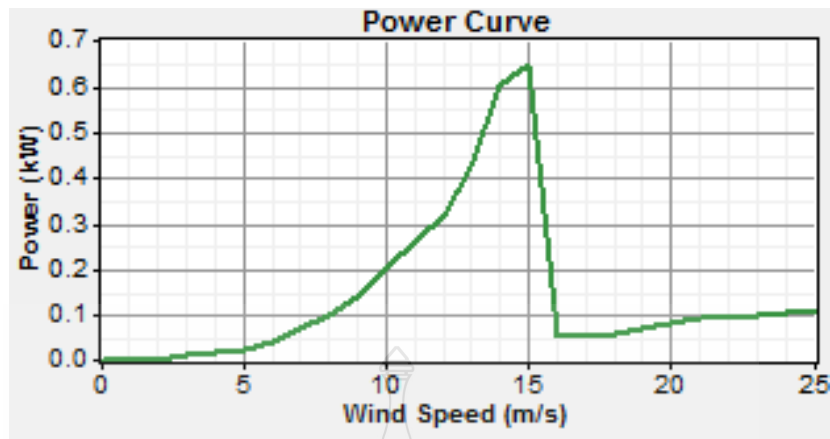


Figure 3.35 Simulation model of the hybrid PV and wind system

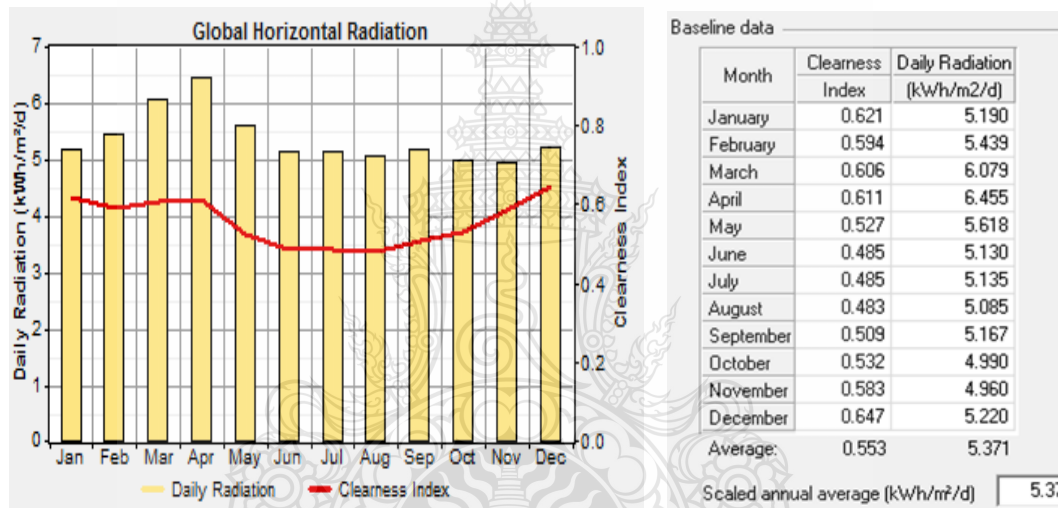
When renewable sources are not available, the batteries supply electricity to the system. In this system, a converter is used to convert DC power to AC power. Consequently, grid electricity can be used as an energy source to supplement renewable sources when required. However, as a stand-alone operation strategy has been adopted, this model does not transmit any power to the grid.

Figure 3.35 shows the simulation model of the hybrid PV and wind system. The overall PIER 93 building load demand is 29.15kWh/d and the model include 4 kW of PV system and micro wind turbine 650 W with battery. The simulation system runs on a grid system type, solar resources using global solar radiation at the study site (14 °N, 100 °E), and wind resources from Table 2.1

The micro wind turbine power curve is shown in Figure 3.36(a), illustrating that at 15 m/s incoming wind speed, the rated power of the turbine is 650 W. Figure 3.36(b) shows the monthly averages of daily solar radiation and the clearness index for the study site over one year. Typical solar radiation at the site is found to be 5–6 kWh/m².d. At the site location 14 °N, 100 °E, the HOMER computes the scaled annual average of daily solar radiation as 5.37 kWh/m².d with an average sky clearness of 0.553.



(a)



(b)

Figure 3.36 Energy inputs for the wind turbine and solar photovoltaic array (a) Power curve of the micro wind turbine and (b) Global solar radiation at the study site (14 °N, 100 °E)

As expected, solar radiation is available throughout the year, with the highest monthly average radiation in Pathum Thani Province (about 6.11 kW/m²·d) occurring in April, which is during the summer season. The lowest monthly average radiation values (about 4.96 kW/m²·d) were recorded in November, which is rainy season in Thailand.

Any system that contains both AC and DC elements requires a converter. A converter can be an inverter (to convert DC to AC), a rectifier (to convert AC to DC), or both. The size of the converter required to satisfy peak demand in the study system was 3 kW, with a lifetime of 15 years. The inverter efficiency was 90% and rectifier efficiency was 85%.

The studied renewable-based hybrid system utilized grid connectivity, which was conceptualized as a back-up energy source to compensate for the intermittency of solar and wind resources at the site. However, the model is stand-alone, which means any excess energy generated by it is not sold back into the grid

3.4 Experimental Site Testing

3.4.1 Photo Voltaic Array Installation

Figure 3.37 shows that the PV array is a collection of PV modules, which generates DC electricity by collecting solar radiation. The lifetime of the PV arrays was assumed to be 25 years and no tracking system was included in the PV system. The specifications of the PV rooftop panel used in the on-site experimental testing are presented in Table 3.4.

Table 3.4 Technical specifications of a PV panel

	Specifications
Rated Maximum Power at STC	250W
Maximum Power Voltage (Vmp)	30.5V
Maximum Power Current (Imp)	8.22A
Module Efficiency	15.4%
Cell Type	Poly-crystalline
	156x156mm (6inch)
Application Class	A



Figure 3.37 PV array installations at the PIER 93 building

3.4.2 Micro Wind Turbine Installation

Table 3.5 presents the specifications of micro wind turbine. The wind turbine rated power approximately 650 kW at wind speed 10 m/s and cut in at 2.2 m/s. Figure 3.38 shows the micro wind turbine installed at the PIER 93 building. The rotor diameter is 1.8 m

Table 3.5 Technical specifications of the micro wind turbine

	Specifications
Weight	15 kg
Rotor Diameter	1.8 m
Rated power	650w@15m/s
Cut in	3.0 m/s
Number of blade	3
Generator	3Ø PMG



Figure 3.38 Micro wind turbine installed at the PIER 93 building

3.4.3 Hybrid Inverter of PV-Wind Installation

Figure 3.39 shows the PV-wind hybrid power generating system installed on the rooftop of the PIER 93 building was comprised of a micro wind turbine of $650\text{ W} \times 4$ sets, PV array of 4 kW, backup storage batteries, inverter and was integrated with the grid. Occasionally, power from the grid was provided to the hybrid system, either to equalize the charge of the batteries or to meet site power demand during prolonged unfavorable weather conditions. The hybrid system was equipped with data logging capacity to monitor various parameters, namely solar current, wind current, load current, load power, PV power, and wind power, at regular intervals of 1 min.

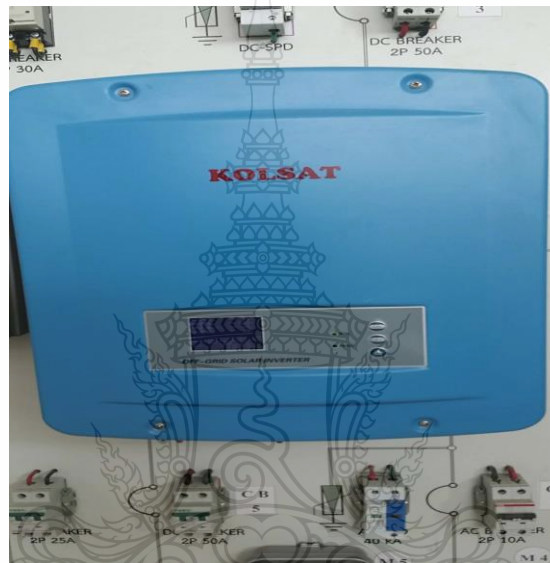


Figure 3.39 PV-Wind hybrid inverter

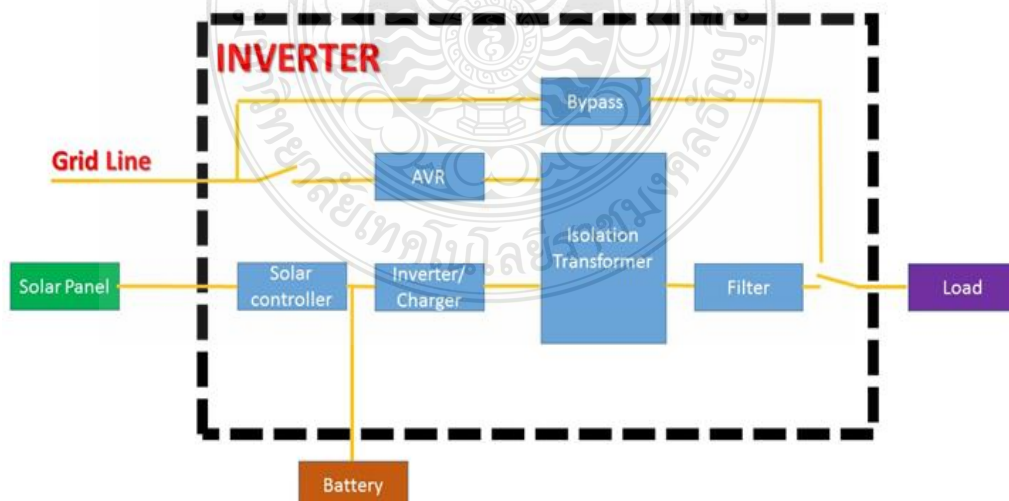


Figure 3.40 PV-wind hybrid inverter circuits

Figure 3.40 shows a PV-wind hybrid inverter circuit; the electricity from grid line can be bypass to the load or pass through AVR and then into isolation transformer after that input the load. While the electricity which is generated from the solar cell panel through solar controller that included in inverter unit can be charged or through isolation transformer then through the filter and finally input the load.

3.4.4 Hybrid PV-wind System Installation

Figure 3.41 shows the hybrid system on the rooftop at the site. Figure 3.41(a) shows the micro wind turbine 400 W which totally 4 sets. Figure 3.41(b) shows the PV panel which is installed on the rooftop of a high-rise building and Figure 3.41(c) shows the hybrid control panel using the control PV and micro wind turbine systems.

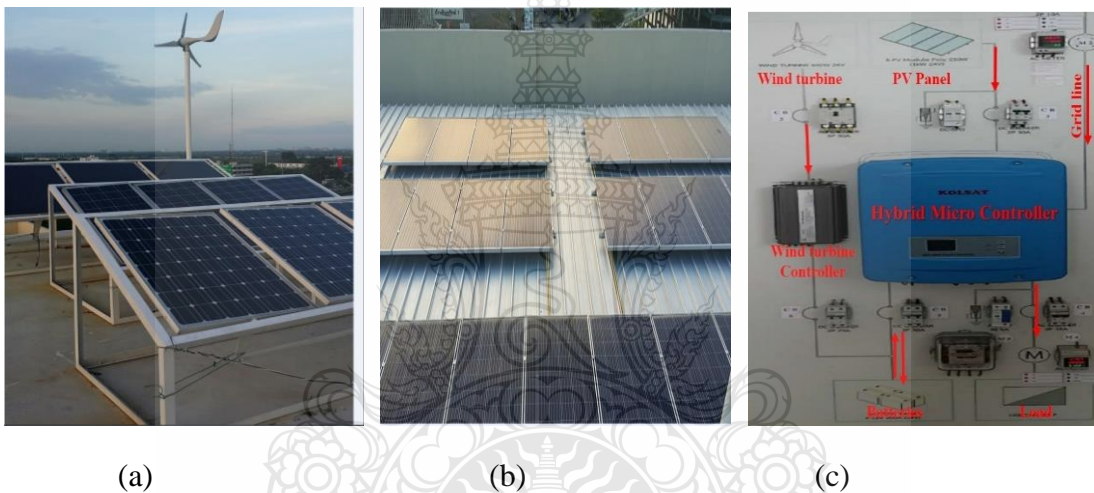
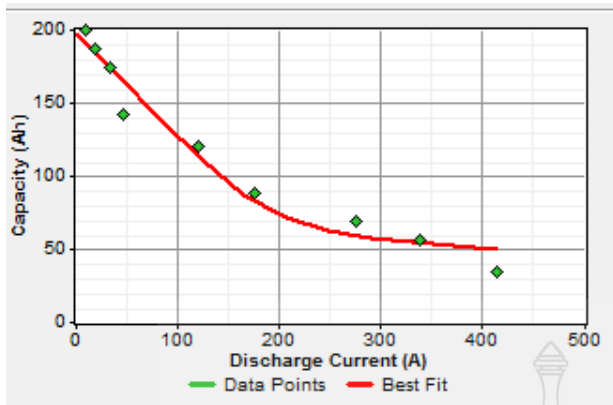


Figure 3.41 Experimental hybrid system installed on PIER 93 building rooftop
 (a) Hybrid system on the rooftop, consisting of wind turbine and solar PV panels, (b) PV panels installed on the building rooftop, and (c) Hybrid system control panel

3.4.5 Battery Bank for Hybrid PV-wind System Installation

The specification of battery bank is 200 Ah and 12 V. The efficiency is 80% approximately at 40% minimum state of charging. The power life time is 917 kWh approximately according to the capacity curve shown in Figure 3.42(a), and the real battery set at the testing site is shown in Figure 3.42(b).



(a)

(b)

Figure 3.42 Battery bank. (a) Battery capacity curve and (b) Battery sets



CHAPTER 4

RESULTS AND DISCUSSION

4.1 Pico-Water Turbine Energy Result

Table 4.1 presents the result of Pico Turgo water turbine which using 10 mm nozzle diameter, the electricity which is turbine generated depends on flow rate and water head. The testing result is depicted theory value at the lowest height of 5m; the flow rate of 11.21m³/h is approximately 152.24 W while the CFD simulation is showed 138.54 W and finally 101.39 W in practical experiments.

Table 4.1 Power of the Pico Turgo water turbine from theoretical calculations, CFD simulations, and experimental tests

Nozzle Dia. (mm)	Head (m)	Flow rate (m ³ /h)	Power Theory (W)	Power CFD (W)	Power Exp. (W)
10	5	11.21	152.24	138.54	101.39
	7	13.21	252.19	229.49	182.86
	9	15.02	367.66	334.57	266.59
	11	16.61	496.78	452.07	360.22
	13	18.05	638.25	580.81	462.80
	15	19.39	791.07	719.87	573.61
	17	20.64	954.45	868.55	692.07
	19	21.83	1127.74	1026.24	817.72
	21	22.95	1310.41	1192.47	950.18

From the result in table above, the Pico Turgo water turbine including maximum head 21 m which obtain flow rate of 22.95m³/h. the result shows 1310.41 W from theory calculation while the power from CFD method approximately 1192.47 W and the prototype testing approximately 950.18 W. At the CFD method simulate for finding rotation of the runner (ω) and the torque (T) of the turbine then using the power formula $P=T\omega$ finding to power generating. The difference between CFD result and the prototype testing is approximately 6.7%. Therefore, the CFD result can be used to assist the design.

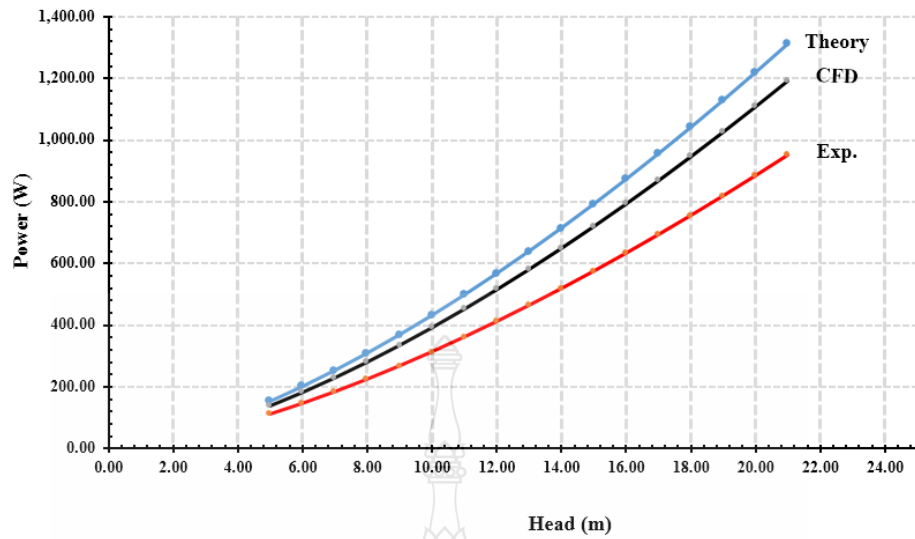


Figure 4.1 Comparison of power output between theoretical, CFD, and experimental results

The Pico Turgo water turbine power generation is investigated by three methods, first, using the theoretical analyze method; second, using CFD simulation method; and third, using the apparatus testing. The CFD method and apparatus method difference approximately 20.31% while the CFD method and theoretical difference approximately 8.32% w, as shown in Figure 4.1.

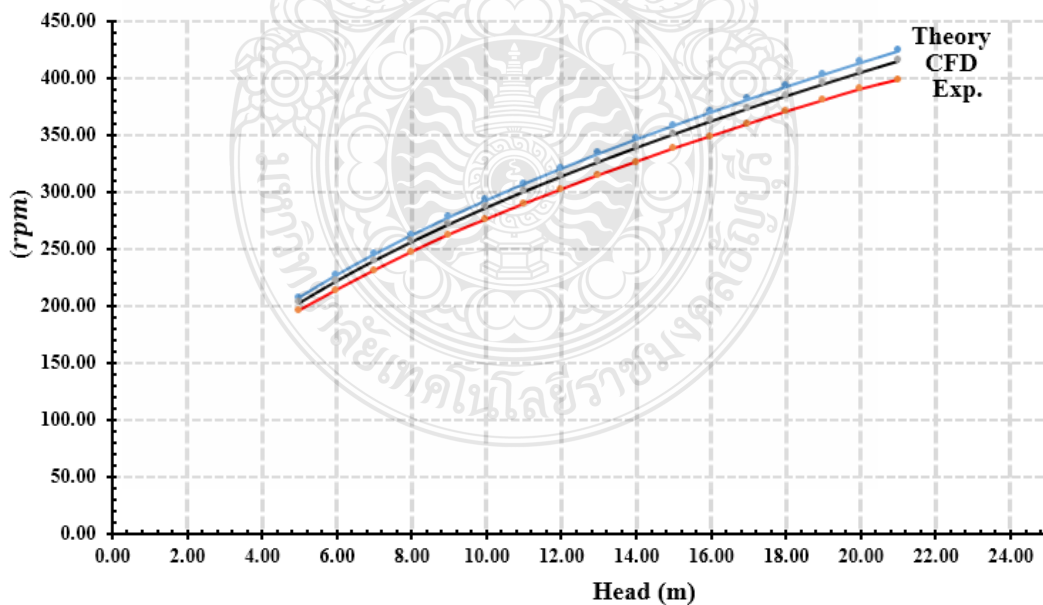


Figure 4.2 Rotation of runner and water head

The Pico Turgo water turbine is operated at approximately 200–420 rpm and the relationship operating between the rotation of the runner and the water head is shown in Figure 4.2. The result shows 206.86 rpm for the theoretical analysis, 202.48 rpm for CFD simulation testing, and 195.53 rpm for apparatus testing.

At the PIER 93 rooftop, can collect approximately 350 m³ rain water annually. The electricity power generated is approximately 950.18 W x 15.87 h=15.08 kWh/y.

In addition, waste water from each room from PIER 93 building can apply to electricity generation. The waste water of shower, hand washing is selected for driving the turbine. The PIER 93 building room totally 79 unit and assume the facility using approximately 150 L, Table 4.2 shows for various water head and flow rate and turbine power.

Table 4.2 Power from wastewater

Head (m)	Floor	Volume (m ³ /year)	Power (kWh/day)	Power (kWh/year)
6	3	711.75	0.0231	8.42
9	4	711.75	0.0424	15.47
12	5	711.75	0.0652	23.82
15	6	711.75	0.0912	33.29
18	7	711.75	0.1198	43.76
Total				124.76

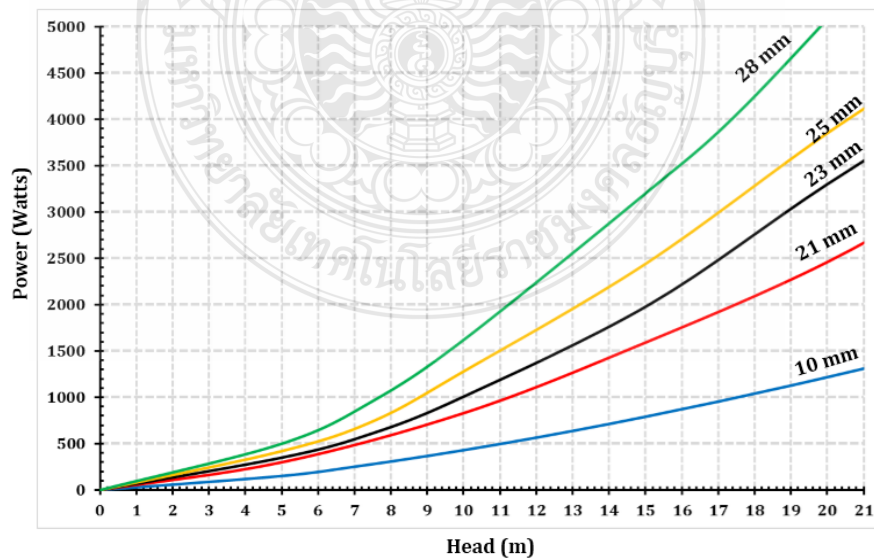


Figure 4.3 Power curve of Pico Turgo water turbine on differences nozzle diameter

Nozzle Dia. (mm)	Head (m)	Flow rate (m ³ /h)	Power CFD (W)
10	0	0	0
	5	11.21	152.24
	7	13.21	252.19
	9	15.02	367.66
	11	16.61	496.78
	13	18.05	638.25
	15	19.39	791.07
	17	20.64	954.45
	19	21.83	1127.74
	21	22.95	1310.41
25	0.00	0.00	0
	5.00	56.30	420
	7.55	68.80	750
	10.00	81.40	1280
	15.00	100.80	2440
	20.00	117.40	3850
	24.00	126.60	4860
28	0.00	0.00	0
	5.00	61.20	500
	7.50	89.10	960
	10.00	105.00	1620
	15.00	130.00	3200
	17.50	141.00	4050
	21.00	150.00	5500
21	0.00	0.00	0
	5.00	46.50	300
	10.00	56.50	830
	14.50	68.50	1510
	20.00	80.00	2460
	25.00	89.60	3580
	28.80	95.80	4440

The power curve of water turbine from different nozzle diameter as shown in Figure 4.3 and. When used 28 mm of nozzle diameter the power of water turbine can up to 5000 watts at about 20-meter head.

4.1.1 Flow Modelling of Pico-water Turbine CFD Result

Figure 4.4 shows the streamlines of water jets 10 mm diameter nozzle, the flow of water contour attack to the blade on top side pushing turbine runner and the velocity and torque of turbine will be investigated

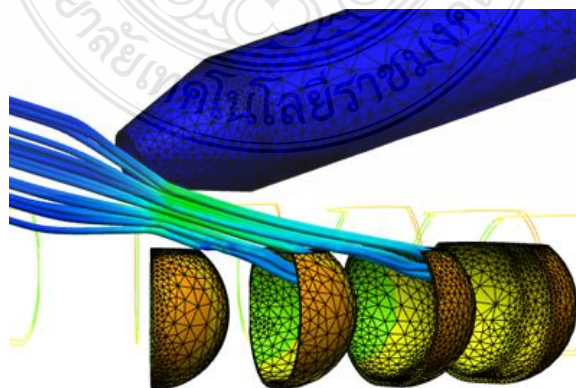


Figure 4.4 Streamline of water flow in a bucket

The particle equations can be solved by a second-order predictor-corrector scheme in the rotating frame of reference, using a sufficiently small time-step (0.002 s) to produce independent results. The particle path along the bucket surface is computed at each time step from its velocity vector and the known local surface slope, and the path terminates when the particle flows out of the bucket, as shown in Figures 4.5 and 4.6. Particles that pass by the reference blade or impinge on the next blade are not counted.

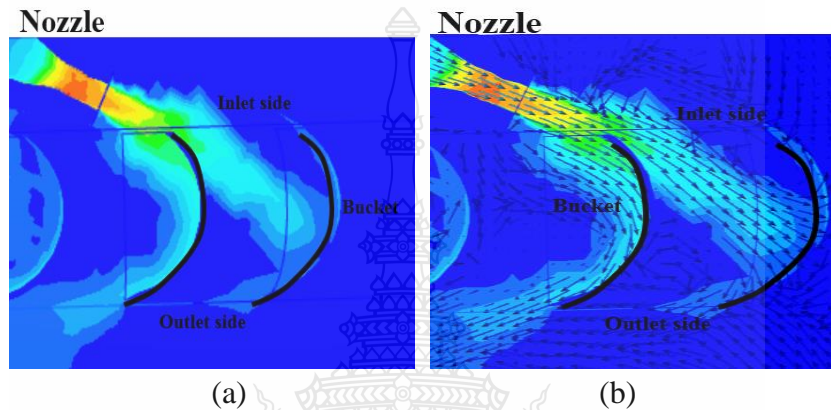


Figure 4.5 Velocity contours on pico turgo water turbines. (a) Flow and (b) Vector velocities

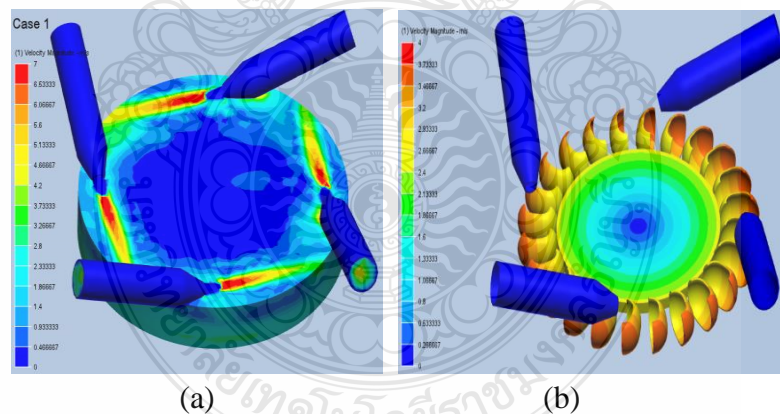


Figure 4.6 Velocity distributions. (a) Rotating region and (b) Buckets

Figure 4.7 shows the velocity distribution of Pico Turgo water turbines with the flow velocity contours of water on the buckets. The highest velocity impacts on the middle bucket, because the nozzles are adjusted for water streamlines to impact on this bucket. The counter-clockwise vector direction of the velocity profile contours is shown in Figure 4.7.

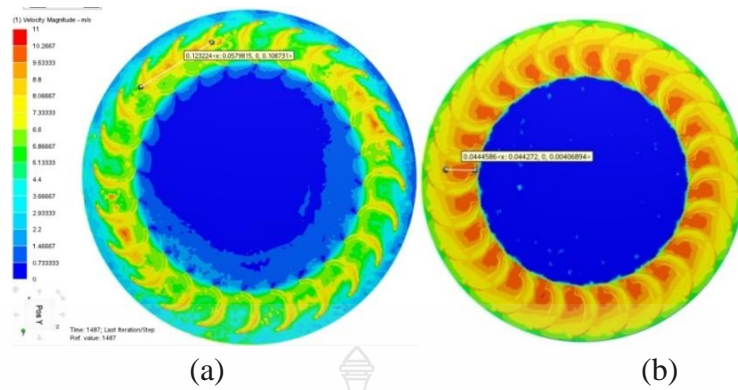


Figure 4.7 Flow velocity contours of Pico Turgo turbines. (a) Top, (b) Middle, and (c) Bottom buckets

Figure 4.8 shows the water velocity distribution in the inner bucket surfaces resulting from the water jets from the nozzles. The distribution of water velocity can be seen using the ISO surfaces function of the CFD method, which depicts the top of the bucket.

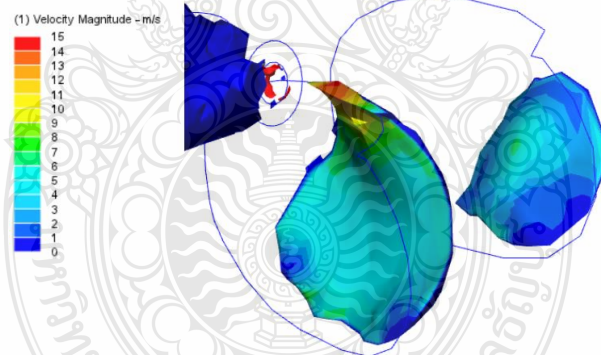
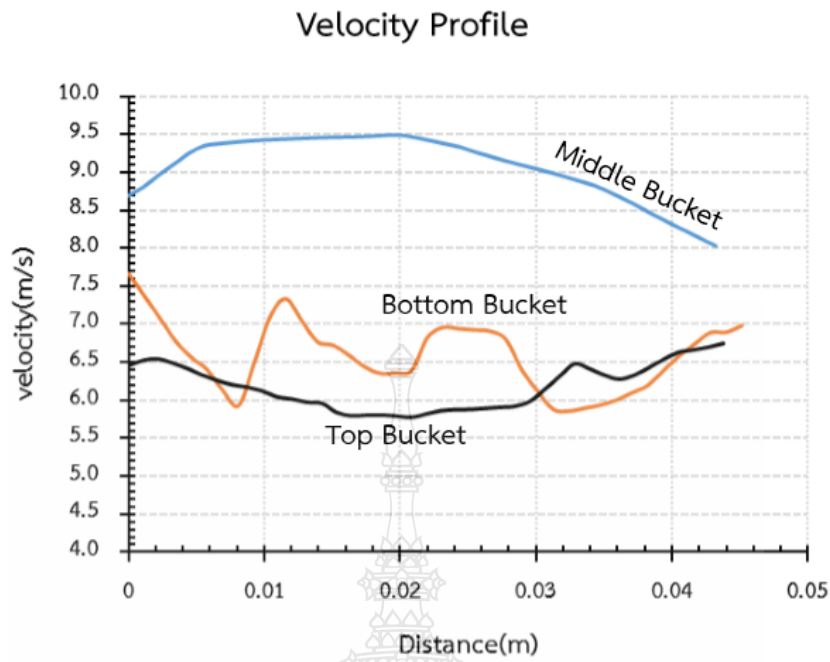
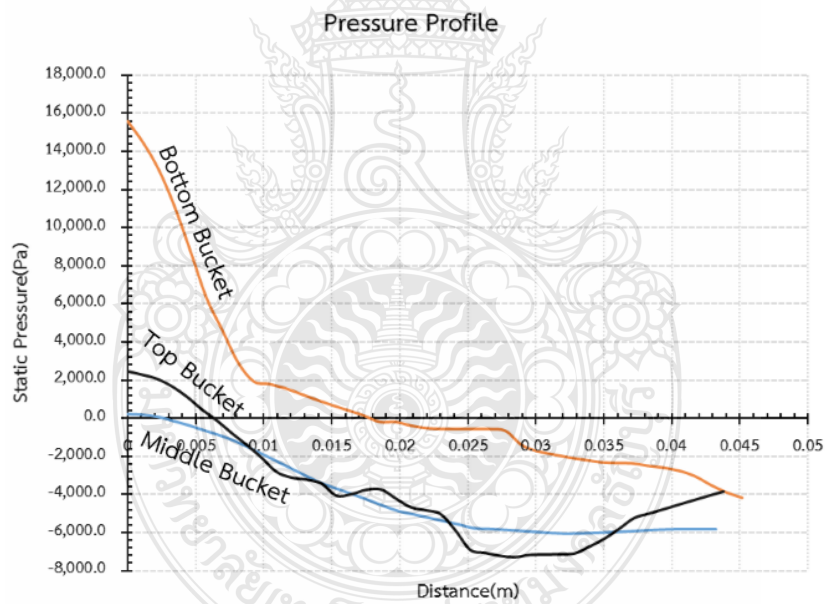


Figure 4.8 Iso surfaces of velocity in the bucket

Figure 4.9(a) shows the velocity profile in the bottom, middle, and top buckets. The velocity in the bottom bucket has the highest turbulence; therefore, this velocity is unstable.



(a)



(b)

Figure 4.9 Pressure and velocity profiles for the top, middle, and bottom buckets
 (a) Velocity and (b) Pressure profiles

High pressure acts on the back bucket and decreases through the front of the next bucket, as shown in Figure 4.9(b). The highest pressure occurs on the bottom bucket, whereas the lowest pressure and highest velocity occur on the middle bucket. Figure 4.10 shows the flow velocity contours on the top, middle, and bottom buckets

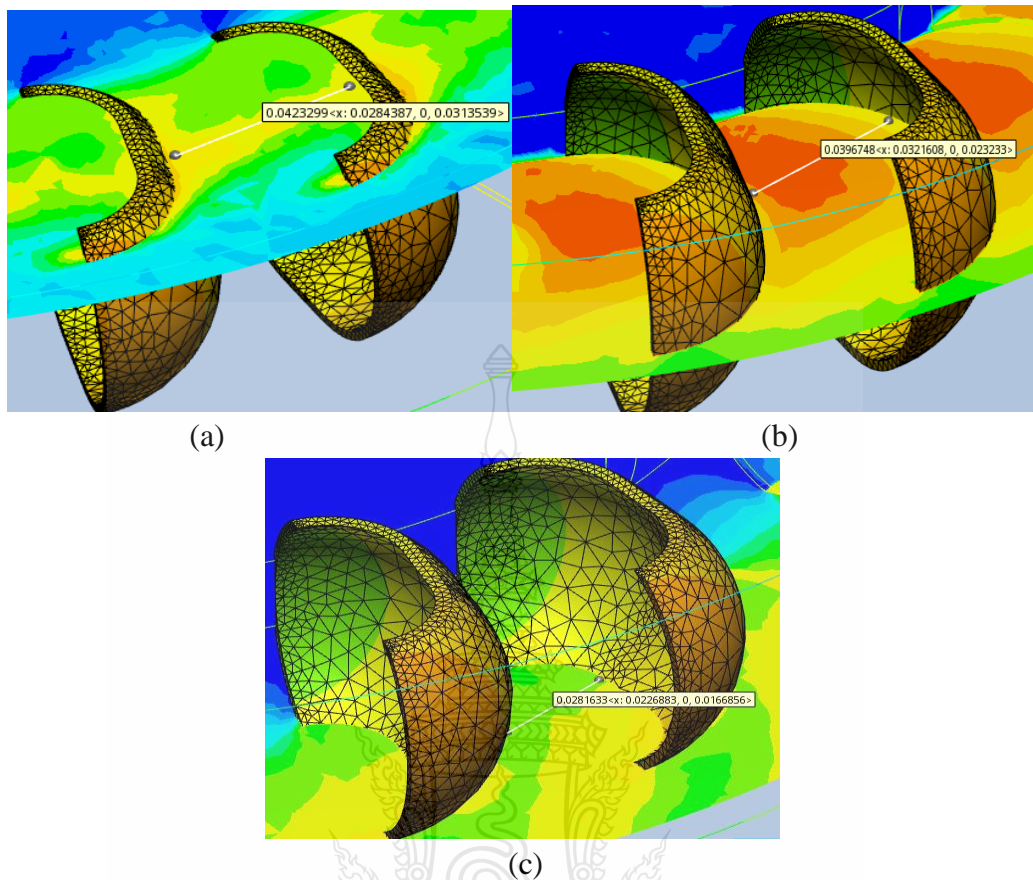


Figure 4.10 Flow velocity contours of the Pico Turgo water turbine. (a) Top, (b) Middle, and (c) Bottom buckets

4.1.2 Computational Fluid Dynamics (CFD) Result of Terrain

Figure 4.11 shows the overall points of velocity investigation, which includes point A–K. The magnitude velocity versus height is shown in Figure 4.12. The height is between 0–26 m from rooftop level. The tower of micro wind turbine is 3 m in height; thus, the only height that can be considered is between 0–3 m on the rooftop of the velocity profile, as shown in Figure 4.12(b).

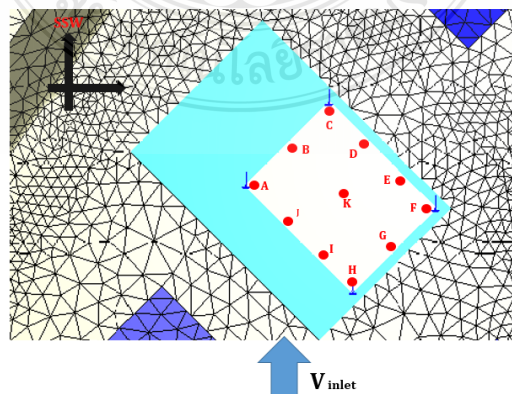
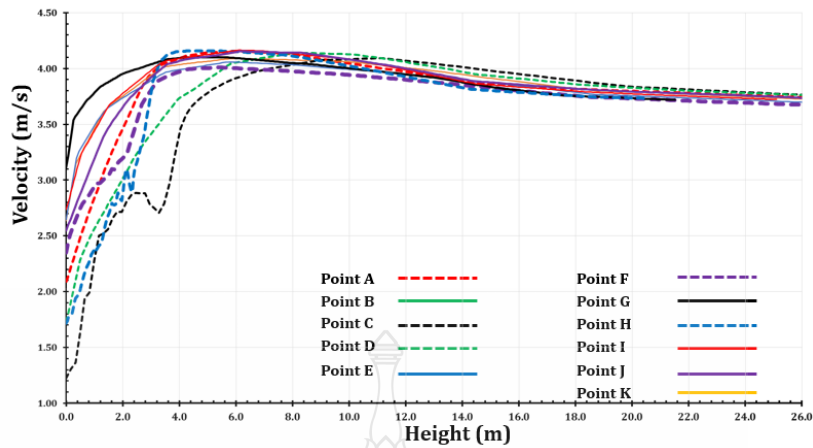
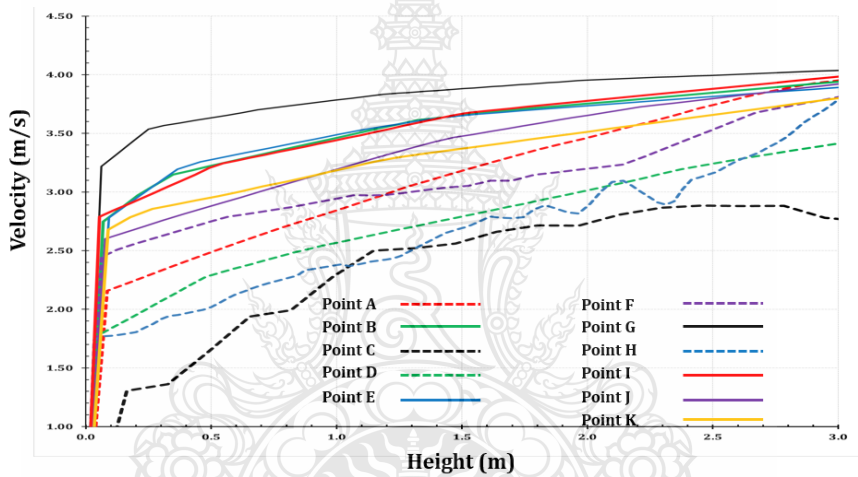


Figure 4.11 Velocity investigation point on the rooftop



(a)



(b)

Figure 4.12 Velocity distribution on the rooftop from the SSW wind flow direction
 (a) Height 0–26 m from the rooftop and (b) Height 0–3 m from the rooftop

The magnitude velocity at investigation points A–K, as presented in Table 4.3. The velocity at 3 m height from rooftop level of CFD simulation shows results point G > I > E > B > J > K > H > F > D > C respectively. Due to the total wind turbine which are 4 sets therefore selected 4 points for the good location installation point which is point A, E, G, I respectively.

If considering only wind turbine installing point, WT1, WT2, WT3, and WT4 are installed at point A, C, F, and H, respectively. The magnitude velocity is at 3 m height from the rooftop level, the highest velocity is point G, while the lowest velocity is point C. When considering the magnitude velocity, which is the micro wind turbine installation point, the result of wind velocity is shown as WT1 > WT3 > WT4 > WT2.

Table 4.3 Velocity magnitude from SSW wind flow direction at point (A-K) of 3 m from rooftop level

Point	V(m/s)	Point	V(m/s)
A(WT1)	4.05	B	4.02
C(WT2)	2.92	D	3.61
E	4.10	F(WT3)	3.82
G	4.33	H(WT4)	3.91
I	4.13	J	4.01
K	3.94		

Figure 4.13 shows the cross-section velocity area of the East-Southeast (ESE) and South-Southwest (SSW) directions at each WT installation point which inlet wind flow from SSW direction and the velocity magnitude is 3.82 m/s. Figure 4.14 shows the velocity contour of the SSW section at WT1, WT2, WT3, and WT4.

The wake flow region is generated at downstream of building area, as shown in Figure 4.15, the velocity contour and vector contour direction of the ESE section at WT1, WT2, WT3, and WT4. From this simulation results show that the magnitude velocity generated on rooftop is higher than on building ground.

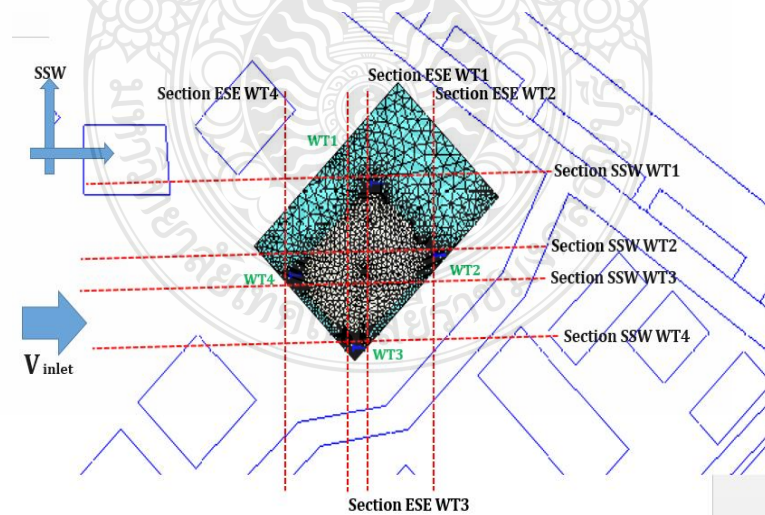


Figure 4.13 Cross-section velocity areas of the ESE and SSW directions at each WT installation point

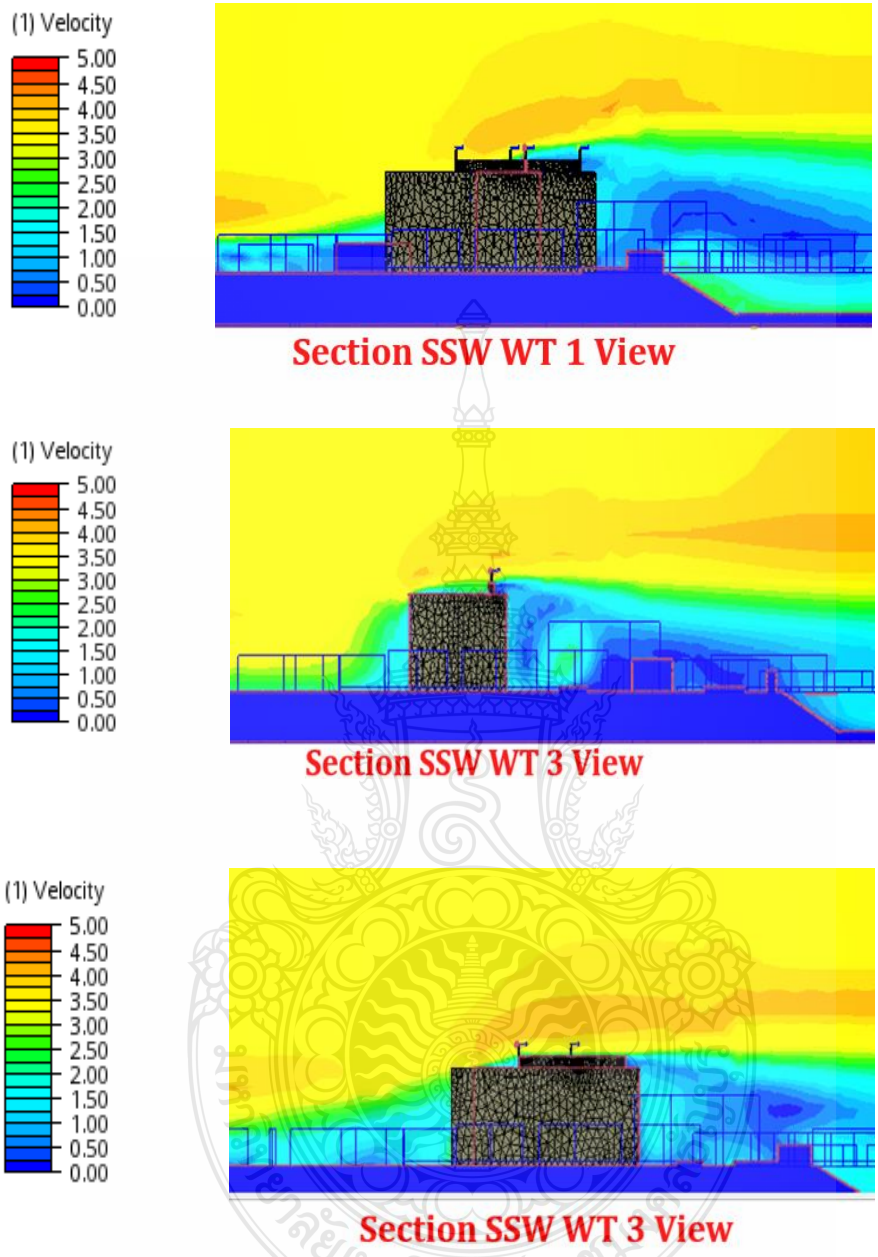


Figure 4.14 Velocity contour of the cross-section area of the SSW section from the SSW wind flow direction

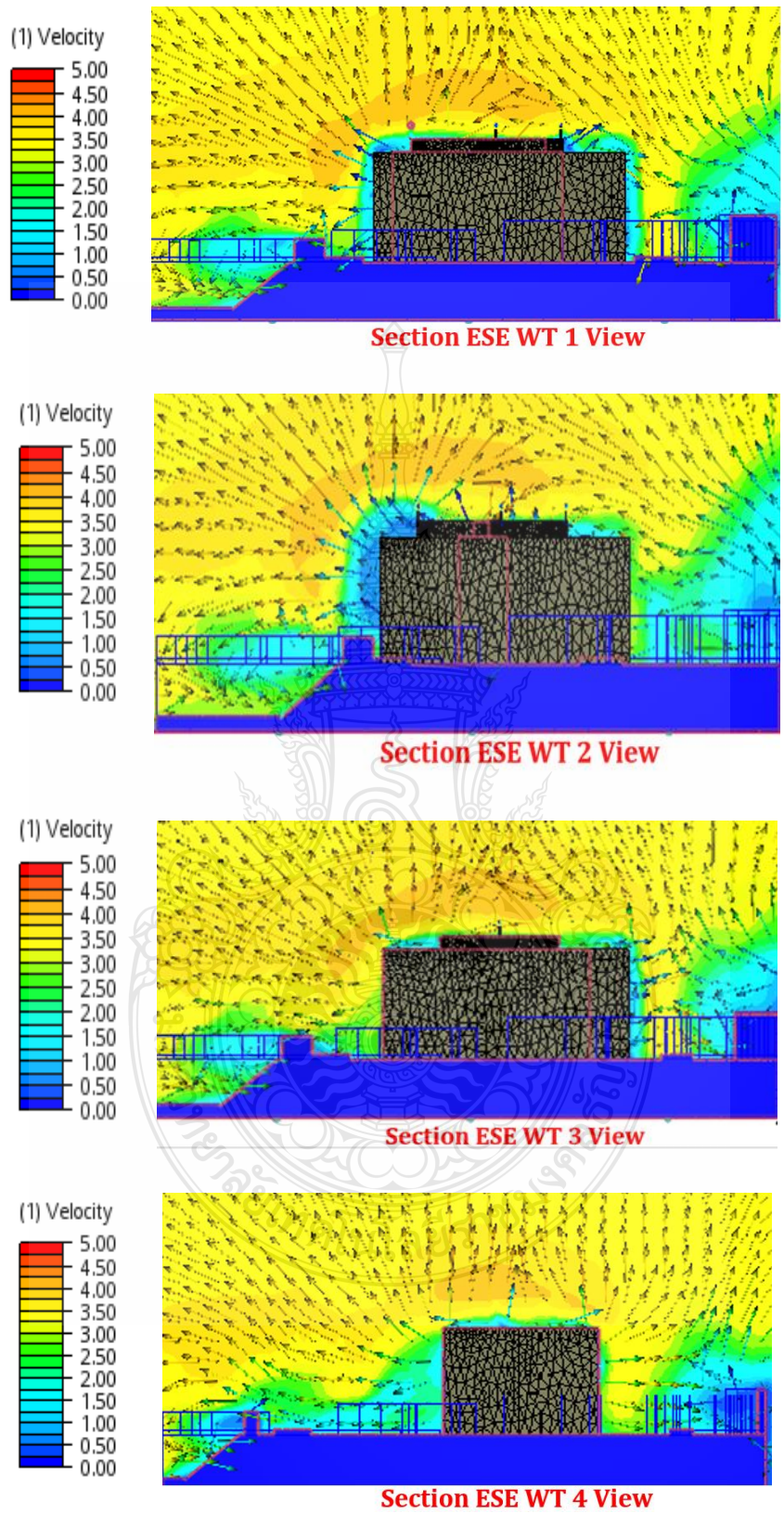


Figure 4.15 Velocity and vector contour of the cross-section wind flow area of the ESE section from the SSW wind flow direction

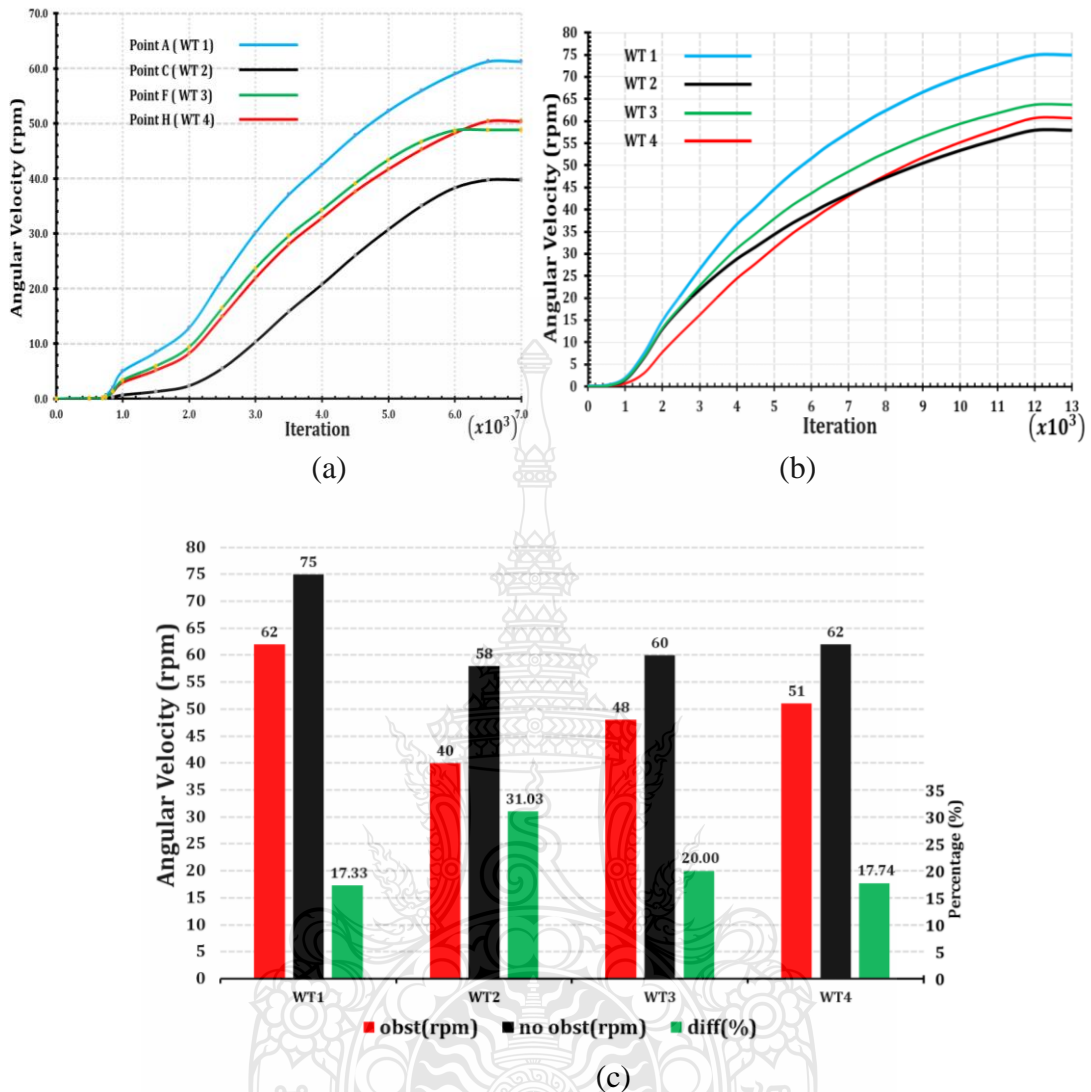


Figure 4.16 Wind turbine velocity curve from the SSW wind flow direction of WT1, WT2, WT3, and WT4 (a) Including terrain obstacle, (b) Not including terrain obstacle, and (c) Percentage of angular velocity differences

Figure 4.16 shows the result of the wind turbine velocity of WT1, WT2, WT3, and WT4 which Figure 4.16(a) shows result of micro wind turbine when including terrain obstacle while Figure 4.16(b) shows result of micro wind turbine when not including terrain obstacle and Figure 4.16(c) shows the percentage of velocity differences from micro wind turbine.

Although the rooftop of PIER 93 building, which includes terrain, can be generating velocity higher than no terrain landscape area (inlet velocity condition 3.82 m/s); however, the rotation of the micro wind turbine is lower than that with no obstacle, as presented in Table 4.4.

Table 4.4 Rotation of micro wind turbine between including terrain obstacle and not including terrain obstacle from the SSW wind flow direction

Point	Obst (rpm)	No obst (rpm)	Diff (%)
WT1	62	75	-17.33
WT2	40	58	-31.03
WT3	48	60	-20.01
WT4	51	62	-17.74

4.1.3 New Location Installation Point

The original micro wind turbine installation point, as shown in Figure 4.17(a) WT1, WT2, WT3, and WT4 are installed at the corners of the rooftop points A, C, F, and H, respectively. At the end of simulation, the simulation result show the good point which is high velocity including point A, E, G, and I and will used this point for installing micro wind turbine WT1, WT2, WT3, and WT4, respectively, as shown in Figure 4.17(b).

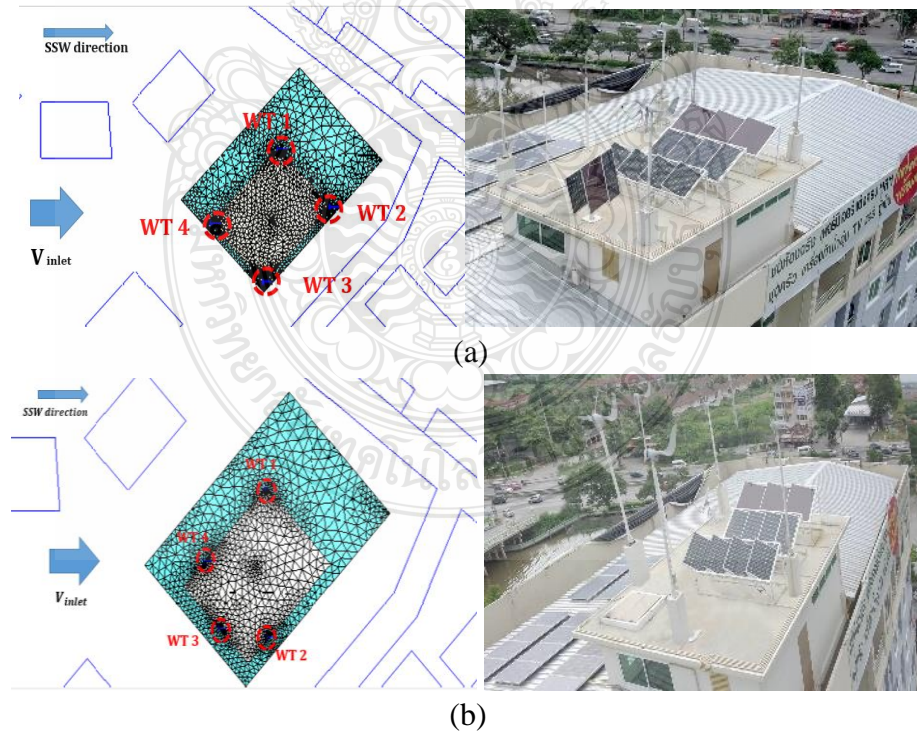


Figure 4.17 Micro wind turbine installation points (a) Original and (b) New location points

Result of the rotation of micro wind turbine at new location installation as presented in Table 4.5 and shown in Figure 4.18. This simulation result, the rotational of turbine at new location installation point including WT1, WT2, and WT3 higher than the original location installation point and lower than the no obstacle simulation result. While the rotational result of simulation of WT4 shows higher than original location point and higher than no obstacle simulation result.

$$\begin{aligned} &WT1_{ori} < WT1_{new} < WT1_{no\ obst} \\ &WT2_{ori} < WT2_{new} < WT2_{no\ obst} \\ &WT3_{ori} < WT3_{new} < WT3_{no\ obst} \\ &WT4_{new} > WT4_{no\ obst} > WT4_{ori} \end{aligned}$$

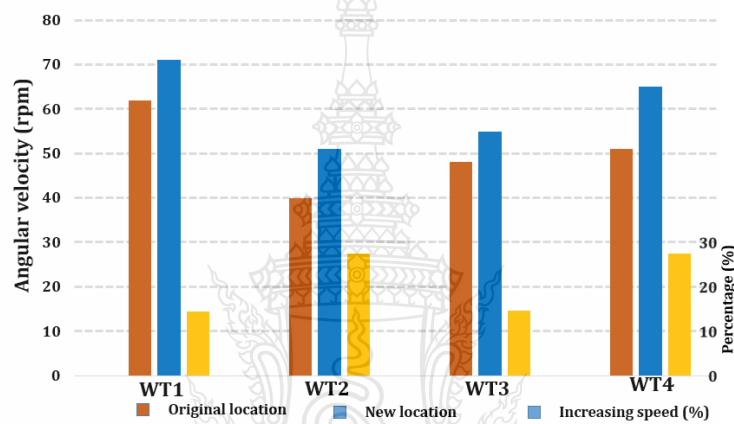


Figure 4.18 Percentage of angular velocity differences from the SSW wind flow direction

At wind turbine number four (WT4), the building creates both magnitude velocity and vector direction therefore the angular velocity (rpm) is increased ($WT4_{new} > WT4_{no\ obst} > WT4_{ori}$) about +27.45% while WT1, WT2, and WT3 are decreased about -14.52, -27.51, and -14.58, respectively.

Table 4.5 Rotation of micro wind turbine between the original and new locations from the SSW wind flow direction

Point	Original (rpm)	New (rpm)	Increasing (%)
WT1	62	71	-14.52
WT2	40	51	-27.51
WT3	48	55	-14.58
WT4	51	65	+27.45

4.2 Homer Hybrid System Simulation Result

4.1.1 PV and Wind Hybrid System

Simulation Results								
System Architecture:		1,000 kW Grid	12 kW Inverter					
		4 kW PV	12 kW Rectifier					
		4 Copy of 650w						
Cost Summary	Cash Flow	Electrical	PV	micro	Converter	Grid	Emissions	Time Series
		Quantity	Value	Units		Quantity	Value	Units
		Total rated capacity	2.60	kW		Minimum output	0.00	kW
		Mean output	0.13	kW		Maximum output	2.46	kW
		Capacity factor	4.86	%		Wind penetration	10.4	%
		Total production	1,108	kWh/yr		Hours of operation	7,473	hr/yr

(a)

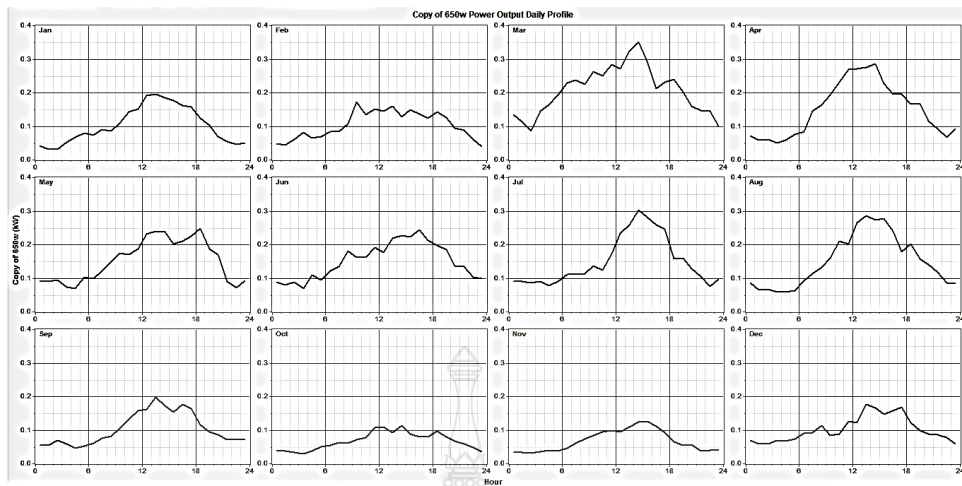
Cost Summary	Cash Flow	Electrical	PV	micro	Converter	Grid	Emissions	Time Series
		Quantity	Value	Units		Quantity	Value	Units
		Rated capacity	4.00	kW		Minimum output	0.00	kW
		Mean output	0.74	kW		Maximum output	3.93	kW
		Mean output	17.7	kWh/d		PV penetration	60.7	%
		Capacity factor	18.4	%		Hours of operation	4,402	hr/yr
		Total production	6,460	kWh/yr				

(b)

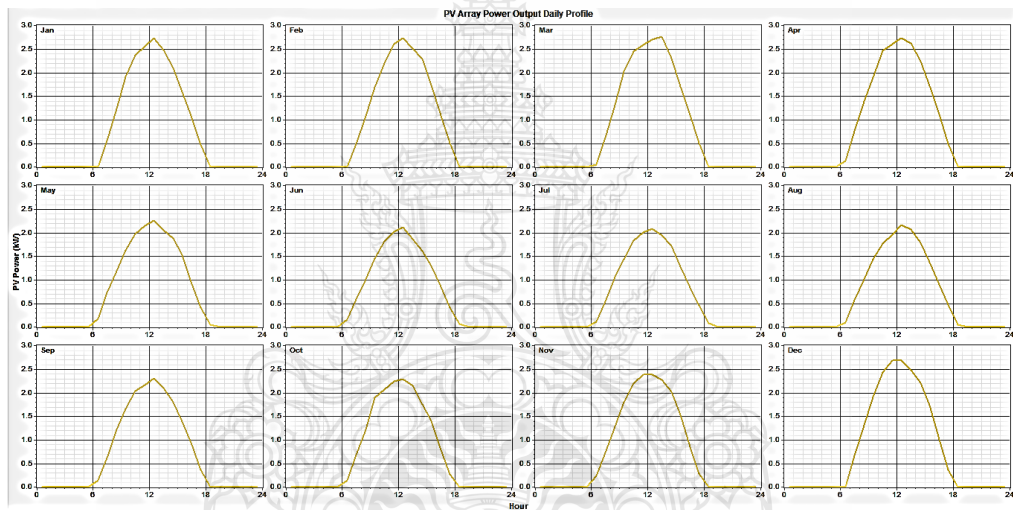
Figure 4.19 Electricity production of HOMER simulation result of hybrid PV-wind system. (a) Wind turbine and (b) PV simulation results

The wind turbine which used for this study is 650 W and 4 sets, totally 2.6 kW; while the PV panel system is 4 kW, which is shown for wind turbine and PV in Figures 4.19(a) and 4.19(b), respectively.

An average daily profile for power output of the wind turbine and PV for each month is shown in Figure 4.20. As shown in Figure 4.10(a), the highest wind energy was generated in March (about 0.35 kW), while the lowest was generated in October (about 0.1 kW). Throughout the year, the PV power output remained relatively constant, as shown in Figure 4.10(b)



(a)



(b)

Figure 4.20 Average daily power output profiles by month for case study hybrid power
(a) Wind turbine power output (b) PV power output

4.1.2 Electricity Production

The monthly average electricity production of the entire PV-wind hybrid system, as calculated using HOMER, is shown in Figure 4.21.

Tables 4.6 and 4.7 show the results indicating that the annual electrical energy from the hybrid system, which is available to meet the demand, is 10640 kWh. 47% (6460 kWh/y) of this electricity is produced by the solar panels, while 8 % (1108 kWh/y) and 45% (6,187kWh/y) are supplied by the wind turbine units and the grid, respectively. The mean PV and wind turbine outputs were observed to be 740 and 130 W, respectively. The overall renewable contribution to the total electricity share was observed to be 52.4%.

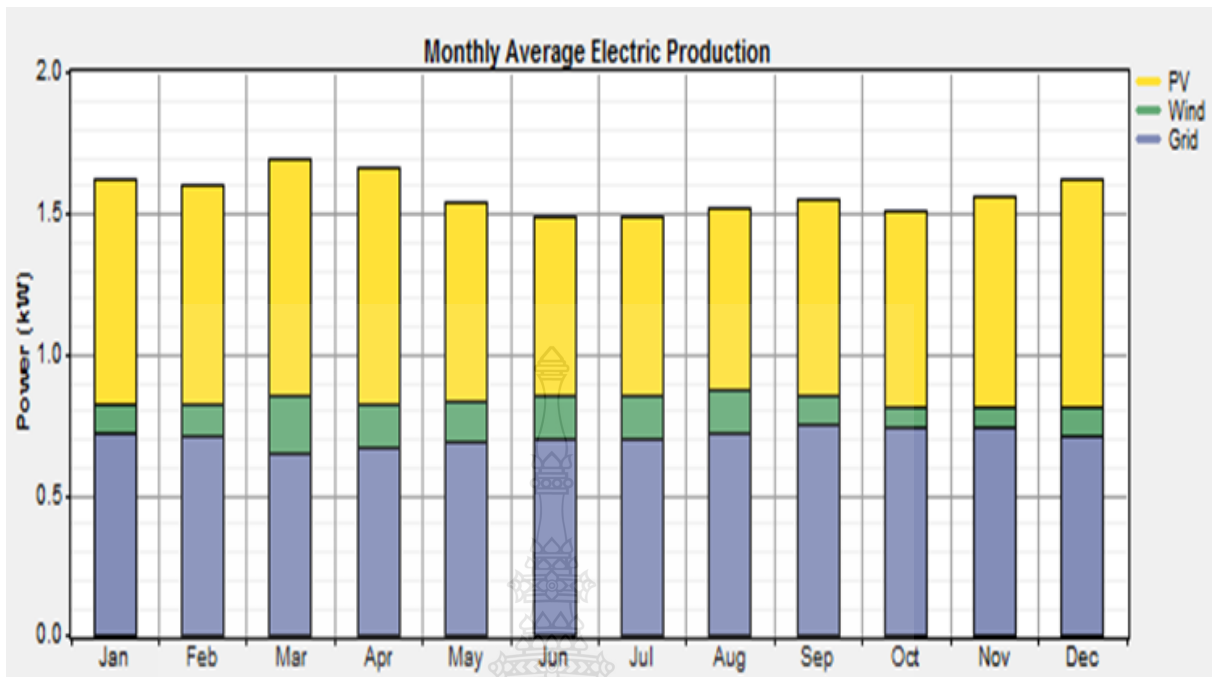


Figure 4.21 Monthly averages of energy output from the case study HRES, as calculated using HOMER

Table 4.6 Results of a simulation of a hybrid PV-wind energy system operating on the PIER 93 building

Parameter	Value
<i>PV array</i>	
Rated capacity	4 kW
Mean output	0.74 kW, 17.77 kWh/day
Capacity factor	18.4%
Total production	6,460 hr/y
PV penetration	60.7%
Hours of operation	4,402 hr/y

Table 4.7 Results of a simulation of a hybrid PV-wind energy system operating on the PIER 93 building

Parameter	Value
<i>Wind Turbine</i>	
Total rated capacity	2.6 kW
Mean output	0.13 kW, 3.04 kWh/day
Capacity factor	4.86 %
Total production	1,108 kWh/y
Wind penetration	10.4%
Hours of operation	7,473 hr/y

Table 4.8 presents the HOMER simulation results of the monthly energy purchased. The maximum value is 386 W in October, which is in the rainy season that has very less radiation from the sun. The minimum value is 232 W in April, which is in the summer season and has high radiation from the sun

The estimated wind turbine power production from the HOMER simulation was consistently higher than the measured values on-site throughout the year, with an average difference of 26.65%. This can be attributed to the fact that the real site has many parameter effects, such as gusts of wind, building obstruction, and Venturi effects; although the micro wind turbine does respond to changes in wind direction.

The simulated and experimental result values for energy production from each of the renewable energy sources in the studied system are shown in Table 4.9. The power from the PV energy is approximately 6460 kWh/y and 5825 kWh/y for the simulation and experimental results, respectively. The power result from the wind turbine energy is approximately 1108 kWh/y and 812 kWh/y from the simulation and experimental respectively. The difference of power production is approximately 9.87% and 26.65% from PV power and wind power, respectively.

Table 4.8 HOMER simulation results of monthly energy purchased

Month	Energy purchased (kWh)	Month	Energy purchased (kWh)	Month	Energy purchased (kWh)
Jan	303	May	330	Sep	357
Feb	276	Jun	364	Oct	386
Mar	203	Jul	375	Nov	345
Apr	232	Aug	366	Dec	291
			Annual	3,829 kWh	

Table 4.9 Power production (simulated with HOMER and experimental) of the renewable energy sources in a hybrid wind-PV energy system installed on the PIER 93 building

Type	Simulated (kWh/y)	Experimental (kWh/y)	Difference (%)
PV	6,460	5,825	9.87
Wind turbine	1,108	812	26.65

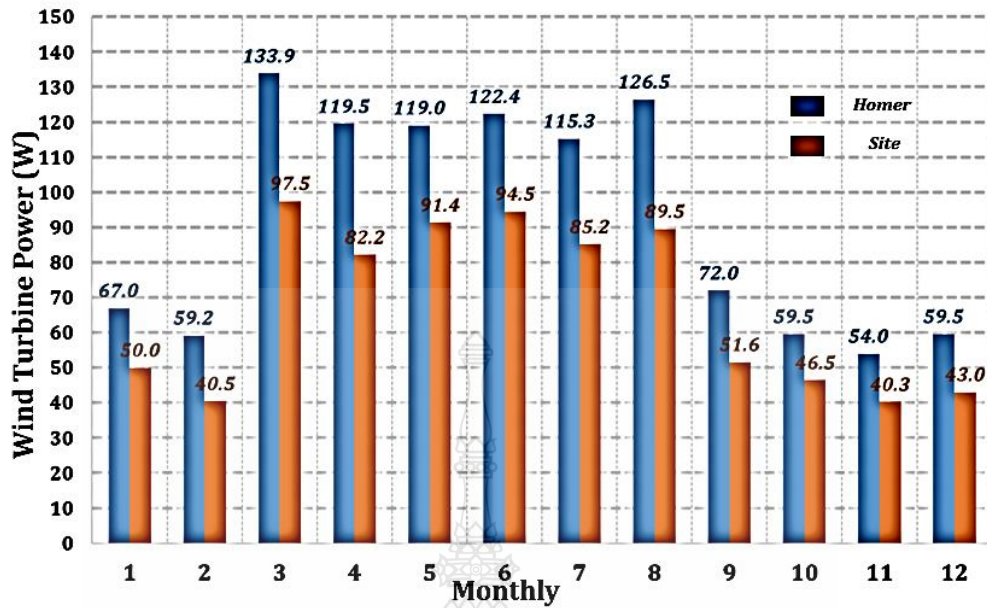


Figure 4.22 Comparison between HOMER simulation and experimental on-site values for monthly micro wind turbine power production (Feb. 2016–Jan. 2017)

Figure 4.22 shows the comparison of the HOMER simulation results with experimental on-site values recorded for the wind turbine. This data was recorded from February 2016–January 2017. In general, the average micro wind turbine power production was observed to be relatively higher from October–February as compared to that produced in the rest of the year.

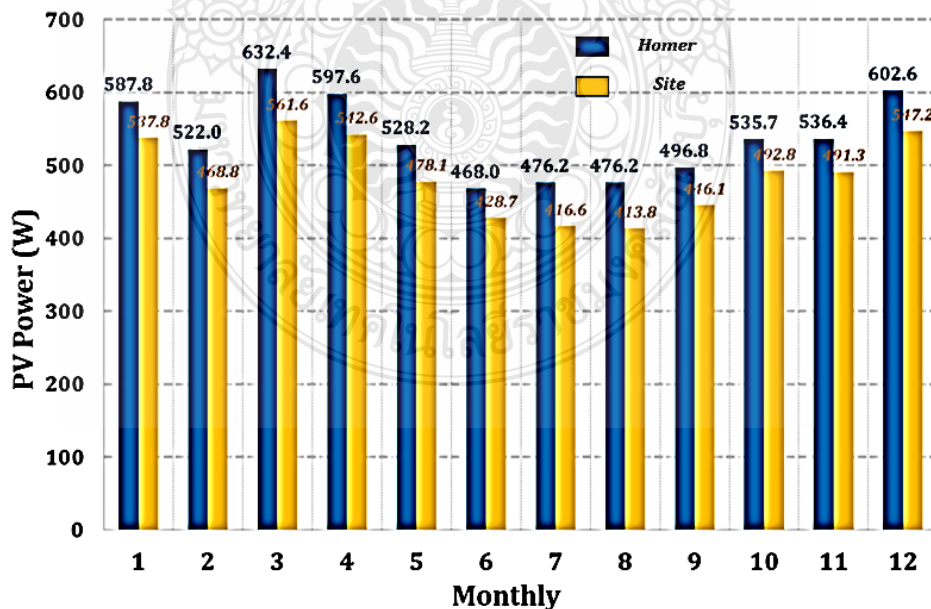


Figure 4.23 Comparison between HOMER simulation and experimental on-site values for monthly solar photovoltaic power production (Feb. 2016–Jan. 2017)

Figure 4.23 shows a comparison between the values estimated by a HOMER simulation and on-site experimental values of power produced by PV. This data was recorded from February 2016–January 2017. The HOMER-estimated PV power production was higher than the actual recorded values on-site throughout the year, with an average difference of 9.87%. The monthly average electricity production of the entire PV-wind hybrid system is shown in Figure 4.23, as measured on-site for one year.

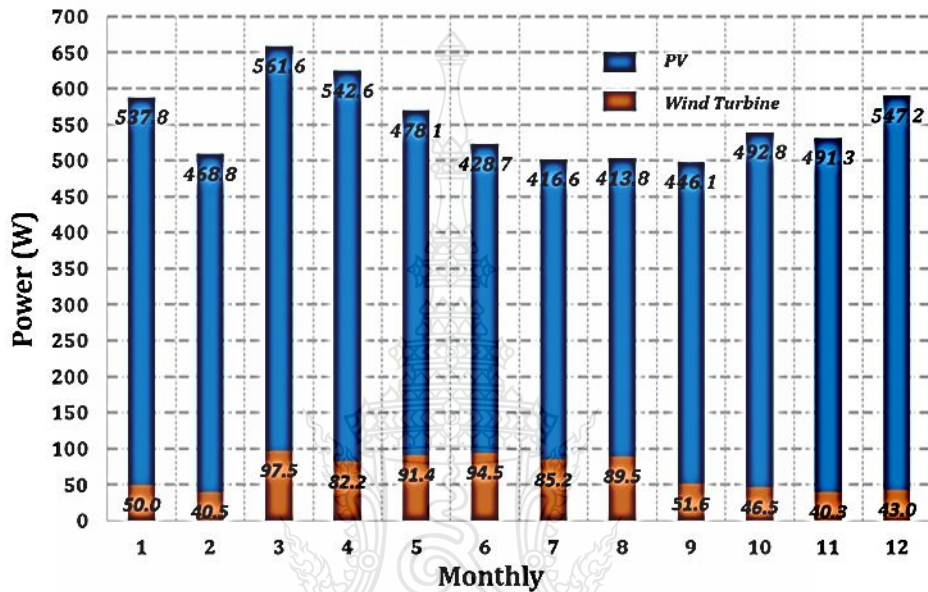


Figure 4.24 Site measurement data of monthly average electricity production, measured on-site of a hybrid PV-wind energy system installed at the PIER 93 building

The above figure shows that PV power generation is efficient almost throughout the year. The annual average power production from the combination of renewable energy sources was 18.19 kWh/d of which PV and wind turbine outputs were observed to contribute on an average 662.86 W and 92.35 W, respectively. The annual average renewable contribution to the total electricity share was observed to be 52.4%, which reinforces the idea that solar and wind power production have good monthly complementarity.

Figure 4.25 show the monthly power purchased from the grid to supplement the renewable energy in the hybrid system. The lowest level of support from the grid was in April, which is because of the high solar radiation and wind that occurs in that month at the study site.

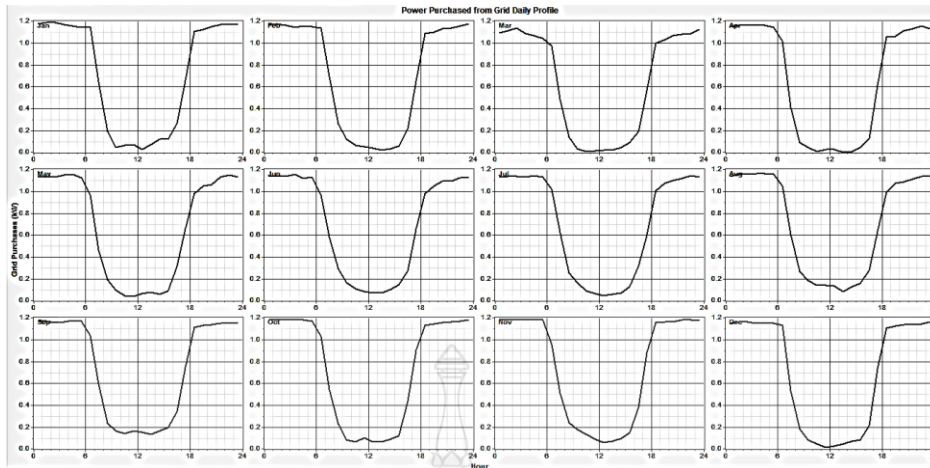


Figure 4.25 HOMER result of monthly profiles of power purchased from the grid into a hybrid wind-PV energy system installed on the PIER 93 building

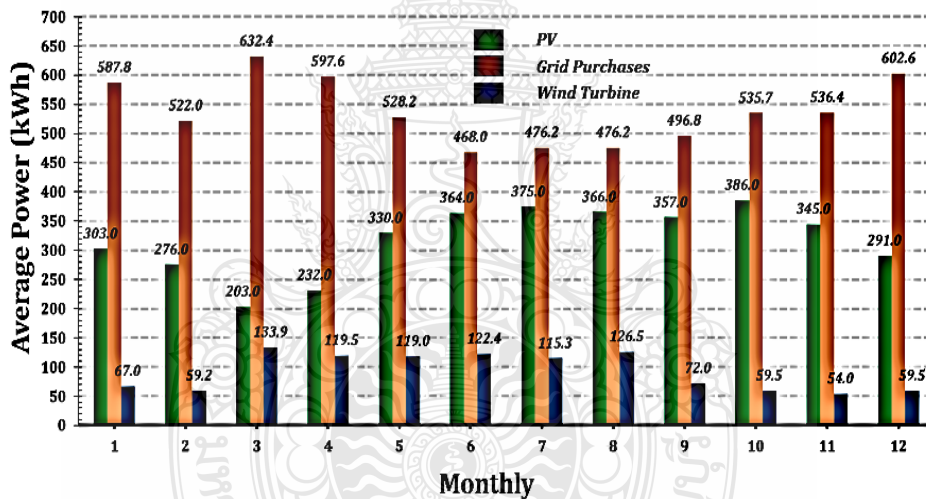


Figure 4.26 Monthly profile of power production hybrid PV-wind energy system from HOMER simulation result

Figure 4.26 shows the monthly profile of power production in hybrid PV-wind energy system from the HOMER simulation result. The highest grid purchase is shown in March, which is about 632.4 kWh, and the lowest in June, which is about 468.0 kWh.

Electricity Cost Analysis

The electricity cost analysis as shown in Figure 4.27 the lowest cost for system installation is single PV system while the highest installation cost is water turbine. When compared the return cost between the hybrid system and single system, the result show that single system better than hybrid system.

	Energy Generate (Kwh/y)	Investment Cost (Baht)	Electricity Cost (Baht/Unit)	Total Value (Baht/y)	Return of Investment (y)
Wind	1,108.00	200,000.00	5	5,540.00	36.10
Water	15.00	300,000.00	5	75.00	60,000.00
PV	6,460.00	140,000.00	5	32,300.00	4.33
Wind+PV+Water	7,583.00	640,000.00	5	37,915.00	16.88
Wind+PV	7,568.00	340,000.00	5	37,840.00	8.99
Wind+Water	1,123.00	500,000.00	5	5,615.00	89.05
PV+Water	6,475.00	440,000.00	5	32,375.00	13.59

Figure 4.27 Cost comparison of renewable energy system

The installation cost of PV system about 140,000 bath, wind system 200,000 bath and water system 300,000 baths. If assume the electricity fee about 5 bath/unite the best return cost is single system of PV while the highest return cost is water system.

CHAPTER 5

CONCLUSIONS

In this study, we presented the three HRES that are applied to a PIER 93 building, where the case study is set up on a high-rise building located at the Pathum Thani province. The three renewable energy sources include solar, wind, and water energies. The solar energy using 4 kW of a PV cell panel, wind energy from four sets of micro wind turbine of 650 W, and water energy using 1 kW of Pico-water turbine was collected, and electricity power was generated.

The feasibility of electric power generation is tested using two primary methods: CFD and HOMER commercial simulation methods. Furthermore, the prototype of Pico Turgo water turbine and PV-wind system are installed at the designate site and test. The CFD technique is using to simulate the micro wind turbine, building and building terrain. The result from CFD shows the effect of building and building terrain increase the magnitude of wind velocity. The rotational speed of micro wind turbine from CFD simulation result shows decreasing speed, because of the rotational speed is vector type which depends on magnitude and wind direction. The CFD software simulation indicates the complex flow of urban terrain resulting in the suitable location to install wind turbine. The HOMER software program verifies electricity output results produce from hybrid renewable energy system compare to single renewable energy system from actual data record.

The space on roof top area can install the HRES from wind, water and solar energy to generate electricity. The electrical energy output cost conscious produce from HRES was proved unsatisfied cost compare to single renewable energy system. The limitation of building height and roof-top reservoir create head and flow suitable for the Pico Turgo turbine type. The efficiency of the experimental Pico turbine is 72.51% while the efficiency from the CFD simulation is 79.21%. From these efficiencies of turbine indicate the enough energy deliver.

The simulation result also indicate the rotational of wind turbine $WT_{ori} < WT_{new} < WT_{no\ obst}$, but the result of WT4 is $WT4_{new} > WT4_{no\ obst} > WT4_{ori}$ that indicate some point on rooftop can increase both magnitude velocity and vector direction.

For the micro wind turbine and building terrain of CFD simulation, the CFD simulation result shows the rotational speed of micro wind turbine, although terrain and PIER 93 building can be increasing magnitude wind velocity but the rotational of micro wind turbine decreasing because the rotational is vector type which depend on magnitude and direction that the CFD boundary of rotating condition type is important and should be use for wind turbine simulation. Generally, the rotational of wind turbine $WT_{ori} < WT_{new} < WT_{no\ obst}$ but the result of WT4 is $WT4_{new} > WT4_{no\ obst} >$

WT4ori that indicate some point on rooftop can increase both magnitude velocity and vector velocity direction.

For the Pico water turbine CFD simulation, result of the rotation of the runner (ω) and the torque (T) of the turbine is analysed then compute the power of the turbine ($P=T\omega$). For a maximum head of 21 m and flow rate of 22.95m³/h the power generated is approximately 1192.47 W, and the power generation difference between the CFD and theoretical methods is approximately 8.32%. The power generation difference between the CFD and apparatus methods is approximately 20.31% while at the PIER 93 rooftop; we can collect approximately 350 m³ of rain water annually. The electricity power generated is approximately 950.18 W x 15.87 h=15.08 kWh/y.

The hybrid PV-wind experimental system is grid-connected and was designed using the HOMER software, considering the selected location data, such as global solar radiation, wind speed, and daily load demand. The HOMER simulation results of the system output show that 47% of the electricity is produced from the solar PV panels, while 8% is produced from wind energy, which together indicates that 45% of the electricity required from the grid can be replaced with renewable energy. The experimental results recorded on-site show that 42.38% of the energy supplied to the hybrid system comes from the PV panels, while an average of 5.87% of the energy is produced by the wind turbine system annually. This indicates that this hybrid PV-wind energy system can reduce the annual dependence on grid electricity by 51.75%.

5.1 Recommendation and Contribution

5.1.1 The contribution for the condominium entrepreneurs and investors who interest to get use of high-rise building roof top space should study more in term of the energy quantitative produce from hybrid renewable energy system (HRES) and single renewable energy system (SRES), investment effectiveness which related to the building characteristics.

5.1.2 The more discussion of the advantage and disadvantage of the HRES compare to the SRES, to prove the optimum electrical energy output.

5.1.3 The more study by using HOMER commercial program to optimize the load demand in the building public area and electrical supply from the efficiently selected type of HRES, in term of production cost and investment cost.

5.2 The Interesting Knowledge found in this study

5.2.1 The Pico Turgo turbine type is chosen because of the limitation of building height and roof-top reservoir, from this experimental it deliver satisfy high efficiency electrical output but it is not appropriated to install in the building resulting from lacking of the adequate water supply and high installation cost.

5.2.2 The wind turbine is not appropriated to install on building roof top resulting from the CFD simulation.

5.2.3 The HRES may suitable for land use but it is not appropriated to install on high-rise building

5.2.4 The roof top area of the high-rise building can be used to install HRES from wind, water and solar energy to produce small amount of electricity, but this electrical energy is worthless in value.

5.2.5 The suitable HRES on roof top building is only for the small watt size electricity and hybrid only wind and solar energy with definitely not hybrid with water energy.

5.2.6 The PV system on single technology is the most economical investment for electrical energy produced from roof top space of the building.



List of Bibliography

- [1] Volker Quasching.(2005). Understanding Renewable Energy System, First Edition, Carl Hanser Verlag GmbH & Co KG.
- [2] Aldo V. Da Rosa, (2005). Fundamentals of Renewable Energy Processes, Elsevier Inc.
- [3] European Commission, 2001, "Guidebook on the RES Power Generation Technologies," Athens, 2001
- [4] Mukund R., "Wind and Solar Power Systems: Design, Analysis and Operation," Second Edition, Taylor & Francis, 2006.
- [5] IRENA. (2012). Renewable Energy Technologies: cost analysis series-Wind Power. International Renewable Energy Agency.
- [6] Small Hydro Power, [Online] <http://www.small-hydro.com>
- [7] <http://www.geni.org/globalenergy/library/renewable-energy/resources/world/asia/wind-asia/wind-thailand.shtml>
- [8] Small Hydro Power, [Online] <http://www.small-hydro.com>
- [9] Bent Sorenson.(2010) Renewable Energy: Its physics, engineering, use of environmental impacts, economy and planning aspects, Third Edition.
- [10] KTH DSEE Educational Materials for Renewable Energy Technology. (2012)
- [11] Hydroelectric Power. (2006)A Guide for Developers and Investors; International Finance Corporation (IFC), World Bank Group.
- [12] Bent Sorenson, "Renewable Energy: Its physics, engineering, use of environmental impacts, economy and planning aspects," Third Edition.
- [13] Twidell, J., Weir, T. (2015). Renewable Energy Resources. Taylor & Francis.
- [14] International Energy Agency. (2015). Renewable energy medium-term market report.
- [15] Flavin, C., Hull Aeck, M. (2005). Energy for Development, The Potential Role of Renewable Energy in Meeting the Millennium Development Goals. REN21 Netw. 4–39.
- [16] Energy situation report of Chaiyaphum Province, (2013).
- [17] <https://www.windfinder.com/#3/49.5042/9.5421>
- [18] Mukund R.(2006). Wind and Solar Power Systems: Design, Analysis and Operation, Second Edition, Taylor & Francis.
- [19] Regulation PEA on the terms of network connectivity, the year (2008).
- [20] Small Hydro Power, [Online] <http://www.small-hydro.com>
- [21] B. S. Lissaman Robert E. Willson, (1974). Applied Aerodynamics of Wind Power Machine. Oregon State.
- [22] Fugsang and Helge A. Madsen. (1995). Optimization of Stall Regulated Rotor, Wind Energy, vol. 16.

List of Bibliography (Continued)

- [23] Desire LE GOURIERES. (1982). Wind Power Plants Theory and Design. Headington Hill Hall: Pergamon Press Ltd.
- [24] Bent Sorenson, "Renewable Energy: Its physics, engineering, use of environmental impacts, economy and planning aspects," Third Edition.
- [25] L. Battisti, L. Zanne, S. Dell'Anna, V. Dossena, G. Persico, B. Paradiso. (2011). Aerodynamic measurements on a vertical Axis wind turbine in a large scale wind tunnel, J. Energy Resour. Technol. 133.
- [26] Gipe, P. (2010). Urban Wind Energy A Review by Paul Gipe. from:<http://www.winndworks.org/LargeTurbines/UrbanWindEnergyAReviewbyPaulGipe.html>
- [27] Mathew, S. (2006). Wind Energy: Fundamentals, Resource Analysis and Economics. Berlin, Germany: Springer.
- [28] International Energy Agency. (2015). Renewable energy medium-term market report.
- [29] Gipe, P. (2004). Wind Power: Renewable Energy for Home, Farm and Business. White River Junction, USA: Chelsea Green Publishing Company.
- [30] Post HN, Thomas MG. (1988). Photovoltaic systems for current and future applications. Sol Energy, 465–73.
- [31] Mahmoud M. (1990). Experience results and techno-economic feasibility of using Photovoltaic generators instead of diesel motors for water pumping from rural Desert wells in Jordan. IEEE Proc, 391–4.
- [32] Global Trends in Renewable Energy Investment; 2016. (<http://www.fs-unepcentre.org>) (Frankfurt am Main), Frankfurt School of Finance & Management gGmbH
- [33] Richard NC. (1989). Development of sizing nomograms for stand-alone photovoltaic/storage systems. Sol Energy, 71–6.
- [34] Traca A, et al. (1983). Source reliability in a combined wind–solar–hydro system. IEEE Trans Power Appar Syst, 1515–20.
- [35] Solar - World Energy Council, (<https://www.worldenergy.org>).
- [36] Sawle Y, Gupta SC. A novel system optimization of a grid independent hybrid renewable energy system for telecom base station. Int J Soft Comput, Math Control 2015;4(2):49–57.
- [37] <http://www.pilkington.com/en/global/commercial-applications/types-of-glass/solar-energy/solar-technologies/crystalline-silicon-photovoltaics>
- [38] Abhijit Date, Ashwin Date, Aliakbar Akbarzadeh. (2012). Performance Investigation of a Simple Reaction Water Turbine for Power Generation from Low Head Micro Hydro Resources, Smart Grid and Renewable Energy, pp 239-245

List of Bibliography (Continued)

- [39] Deepak Bisen, Shuneel Kumar Shukla, P.K. Sharma. (2014). Review Paper on Nozzle in Hydro-Turbine. International Journal of Advanced Technology in Engineering and Science, Volume No.02, Issue No. 08.
- [40] S.J. Williamson, B.H. Stark, J.D. Booker. (2001). Low Head Pico Hydro Turbine Selection using a Multi-Criteria Analysis”, World Renewable Energy Congress.
- [41] Hermod Brekke. (2001). Hydraulic Turbines Design, Erection and Operation, Endringsdato.
- [42] A.H. Elbatran, O.B. Yaakob, Yasser M. Ahmed, H.M. Shabara. (2015). Operation performance and economic analysis of low head micro-hydropower turbines for rural and remote areas: A review, Renewable and Sustainable Energy Reviews, , pp 40-50 .
- [43] Bryan Patrick Ho-Yan. (2002). Design of a Low Head Pico Hydro Turbine for Rural Electrification in Cameroon, Master Thesis.
- [44] Kyle Gainer, Paul Erickson, Pieter Stroeve, Jean-Pierre. (2016). An experimental investigation of design parameters for pico-hydro Turgo turbines using a response surface methodology”, Renewable Energy Renewable Energy pp.406-418.
- [45] Gilbert Gilkes & Gordon Ltd. Gilkes Turgo Impulse Hydro Turbine, (2016).
- [46] Bryan R. Cobb, Kendra V. Sharp. (2013). Impulse (Turgo and Pelton) turbine performance characteristics and their impact on pico-hydro installations”, Renewable Energy 50 (2013) pp.959-964.
- [47] Cobb, B. R. and K. V. Sharp. (2011). Impulse (Turgo and Pelton) turbine performance characteristics and their impact on pico-hydro installations. Renewable Energy. vol. 36, no. 5, pp. 1379–1391.
- [48] John S. Anagnostopoulos, and Dimitrios E. Papantonis. (2007). Flow Modeling and Runner Design Optimization in Turgo Water Turbines, International Journal of Mechanical, Aerospace, Industrial, Mechatronic and Manufacturing Engineering Vol:1, No:4.
- [49] Wilson, P. N.(1967). A High Speed Impulse Turbine.
- [50] Anagnostopoulos, J. H. (2011). Development and laboratory testing of improved Action and Matrix hydro turbines designed by advanced analysis and optimization tools” Small Hydro Going Smart Conference.
- [51] Crewdson, E. (1922). Design and Performance of a New Impulse Water-Turbine, Minutes of Proceedings of the Institution of Civil Engineers.
- [52] Audrius Židonis, DavidS.Benzon, GeorgeA. Aggidis. (2011). Development of hydro impulse turbines and new opportunities, Renewable and Sustainable Energy Reviews 51 pp.1624–1635.

List of Bibliography (Continued)

- [53] Audrius Židonis, George A. Aggidis.(2012). Identifying the Optimum Number of Buckets Using CFD, Lancaster University Renewable Energy Group and Fluid Machinery Group, Engineering Department.
- [54] Yang H, Lu L, Burnett J. Weather data and probability analysis of hybrid photovoltaic–wind power generation system in Hong Kong. *Renew Energy* 2003;28:1813–24. [http://dx.doi.org/10.1016/S0960-1481\(03\)00015-6](http://dx.doi.org/10.1016/S0960-1481(03)00015-6).
- [55] Hybrid Energy System, [Online] <http://exploringgreentechnology.com/solar-energy/hybrid-energy-systems/>
- [56] Ghosh B. (2004). towards modernized bio-energy – a first hand book for the stakeholders, School of Energy Studies, Jadavpur University, Kolkata, India, Technical Backup Unit on Biomass Gasifier Promotion (A Unit of Ministry of Non-Conventional Energy Sources, Govt. of India).
- [57] Ramakumar R. (1993). Economic aspects of advanced energy technologies proceedings of the ieee. vol. 81. no. 3.
- [58] Arifujjaman Md, Tariq M, Iqbal E, John M, Quaicoe, Khan. Jahangir. (2005). Modeling and control of a small wind turbine IEEE transaction, pp. 778–781.
- [59] Deshmukh MK, Deshmukh SS. (2008). Modeling of hybrid renewable energy systems. *Renew Sustain Energy*, 235–49.
- [60] Maghraby HAM, Shwehdi MH, Al-Bassam GK. (2002). Probabilistic assessment of photovoltaic (PV) generation systems. *IEEE Trans Power Syst*, 205–208.
- [61] Al-Ashwal AM, Moghram IS. (1997). Proportion assessment of combined PV–wind generating systems. *Renew Energy*, 43–51.
- [62] Luna-Rubio R, Trejo-Perea M, Vargas-V_quez D, Ríos-Moreno GJ. (2012). Optimal sizing of renewable hybrids energy systems: a review of methodologies. *Sol Energy*, 107-788.
- [63] Heinz. (2014). Facilities Management: The History of Carleton’s First Wind Turbine | Carleton College, Carleton College. [Online]. Available: https://apps.carleton.edu/campus/facilities/sustainability/wind_turbine/.
- [64] ETAP Powering Success. Photovoltaic Array | Solar Panel | Solar Farms | Solar Irradiance. ETAP Powering Success. [Online]. Available: <https://etap.com/product/s/distribution-network-analysis/renewable-energy/photovoltaic-array-solar-panel>.
- [65] Hybrid Energy System, [Online] <http://exploringgreentechnology.com/solar-energy/hybrid-energy-systems/>
- [66] SANDIA. Stand-alone photovoltaic systems: a handbook of recommended design practice’ SAND87-7023, printed; 1995.

List of Bibliography (Continued)

- [67] Bhuiyan MMH, Asgar M Ali. Sizing and stand-alone photovoltaic power system at Dhaka. *Renew Energy* 2003;28:929–38.
- [68] Ming J, Buping L, Zhegen C. Small scale solar PV generating system-the household electricity supply used in remote area. *Renew Energy* 1995;6:501–5.
- [69] Ofry E, Braunstein A.(1983). The loss of power supply probability as a technique for designing stand-alone solar electric photovoltaic system. *IEEE Trans Power Appar Syst* ;Vol. PAS-102(5).
- [70] Klein SA, Beckman WA. (1987). Loss-of-load probability for stand-alone photovoltaic systems. *Sol Energy* 39(6):449–512.
- [71] Rodolfo Dufo-Lopez, Bernal-Augustin Jose L. (2005). Design and control strategies of PV diesel using genetic algorithm. *Sol Energy* , 33–46.
- [72] Bogdan S, Borowy , Salameh Ziyad M. (1996). Methodology for optimally sizing the combination of battery Bank and PV array in a wind/PV hybrid system. *IEEE Trans Energy Convers*, 367–75.
- [73] Bagul AD, Salameh Ziyad M. (1996). Sizing of stand-alone hybrid wind- PV system using three events probability density approximation. *Sol Energy*, 323–35.
- [74] Beyer Hans Georg, Langer Christian. (1996). A method for identification of configurations of PV/wind hybrid systems for the reliable supply of small loads. *Sol Energy*, 381–91.
- [75] Seeling-Hochmuth GC. (1997). A combined optimization concept for the design and operation strategy of hybrid-PV energy systems. *Sol Energy*, 77–87.
- [76] Erhard K, Dieter M. (1991). Sewage plant powered by combination of photovoltaic, wind and bio-gas on the island of Fehmarl, Germany. *Renew Energy*, 745–8.
- [77] Diaf S, Notton G, Belhamel M, Haddadi M, Louche A. (2008). Design and techno economical optimization for hybrid PV/wind system under various meteorological conditions. *Appl Energy*, 968–87.
- [78] (<http://www.nrel.gov/HOMER>).
- [79] Erdinc O, Uzunoglu M. (2012). Optimum design of hybrid renewable energy systems: overview of different approaches. *Renew Sustain Energy Rev*; 16:1412–25.
- [80] BajpaiP, DashV.(2012). Hybrid renewable energy systems for power generation in stand-alone applications : Areview. *Renew Sustain Energy Rev*; 16:2926–39.
- [81] Bernal-AgustínJL, Dufo-LópezR. (2009). Simulation and optimization of stand-alone Hybrid renewable energy systems. *Renew Sustain Energy*; 13:2111–8.
- [82] Bhattacharyya S C. (2012). Review of alternative methodologies for analyzing off-grid electricity supply. *Renew Sustain Energy*; 16:677–94.

List of Bibliography (Continued)

- [83] Fathima A H, Palanisamy K. (2015). Optimization in microgrids with hybrid energy Systems —a review. *Renew Sustain Energy*; 45:431–46.
- [84] HOMER energy modeling software. National Renewable energy laboratory. 522 <http://en.openei.org/wiki/HOMER>.
- [85] Ramli MAM, Hiendro A, Twaha S.(2015). Economic analysis of PV/diesel hybrid System with flywheel energystorage. *RenewEnergy*;78:398–405.
- [86] Mudasser M, Yiridoe E K, Corscadden K. (2015). Cost-benefit analysis of grid-connected wind–biogas hybrid energy production ,by turbine capacity and site. *RenewEnergy*; 80:573–82.
- [87] Lujano-Rojas Juan M, Dufo-López Rodolfo, José , Bernal-Agustín L. (2014). Technical and economic effects of charge controller operation and coulombic efficiency on stand-alone hybrid power systems. *Energy Convers Manag*, 709–16.
- [88] Olatomiwa Lanre, Mekhilef Saad, Huda a ASN, Ohunakin Olayinka S. (2015). Economic evaluation of hybrid energy systems for rural electrification in six geo-political zones of Nigeria. *Renew Energy*, 435–46.
- [89] Giraud F, Salameh ZM. (2001). Steady-state performance of a grid-connected rooftop hybrid wind–photovoltaic power system with battery storage. *IEEE Trans Energy Convers*, 1–7.
- [90] Xu D, Kang L, Chang L, Cao B. Optimal sizing of stand alone hybrid wind/PV power systems using genetic algorithms. *Electrical and computer engineering, Canadian conference on: IEEE*; 2005. (<http://dx.doi.org/10.1109/CCECE.2005.1557315>).
- [91] Dawoud SM, Lin X, Sun J, Mohsin QK, Flaih FM, Long P. (2015). Reliability study of hybrid PV-wind power system to isolated micro-grid. *Intelligent Control and Information Processing (ICICIP), 2015 Sixth International Conference on: IEEE*; p. 431(<http://dx.doi.org/10.1109/ICICIP.2015.7388210>).
- [92] Yang H, Zhou W, Lu L, Fang Z. (2008). Optimal sizing method for stand-alone hybrid solar–wind system with LPSP technology by using genetic algorithm. *Sol Energy*; 82:354–67. <http://dx.doi.org/10.1016/j.solener>.



Appendices

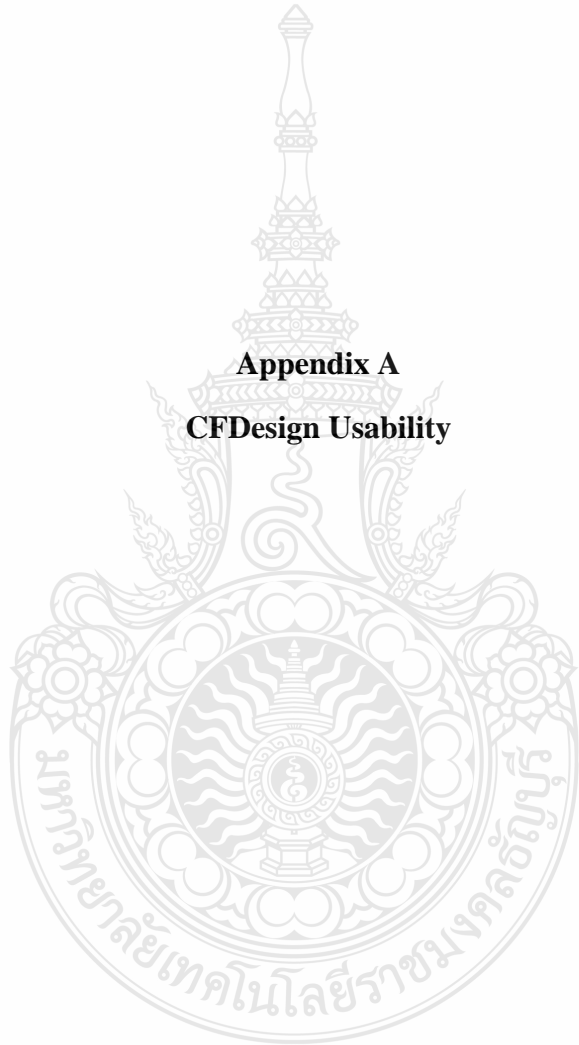
Appendix A CFDesign Usability

Appendix B CFD Result as Wind Flow from the SW of New Installation Point

Appendix C CFD Result as Wind Flow from the SW of Original Installation Point

Appendix D List of Publications

Appendix A
CFDesign Usability



CFDesign Usability

Step 1 In the menu bar select the “New” for use the new model as shown in Figure 1

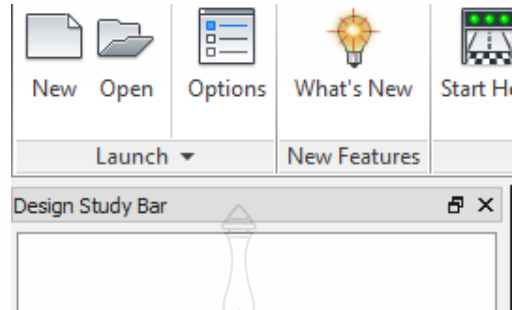


Figure 1 CFDesign menu bar

Step 2 In the “New Design Study” select “Browse” import the model file as shown in Figure 2

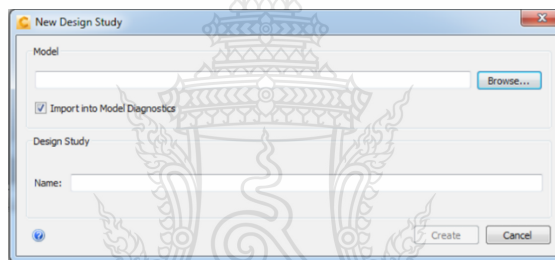


Figure 2 CFDesign import file

Step 3 The model assessment will check the model compatible “Edge lengths, Surface sliver, Model slivers, Part gaps, Model gaps, and interference” for preparing CFD solving, as shown in Figure 3

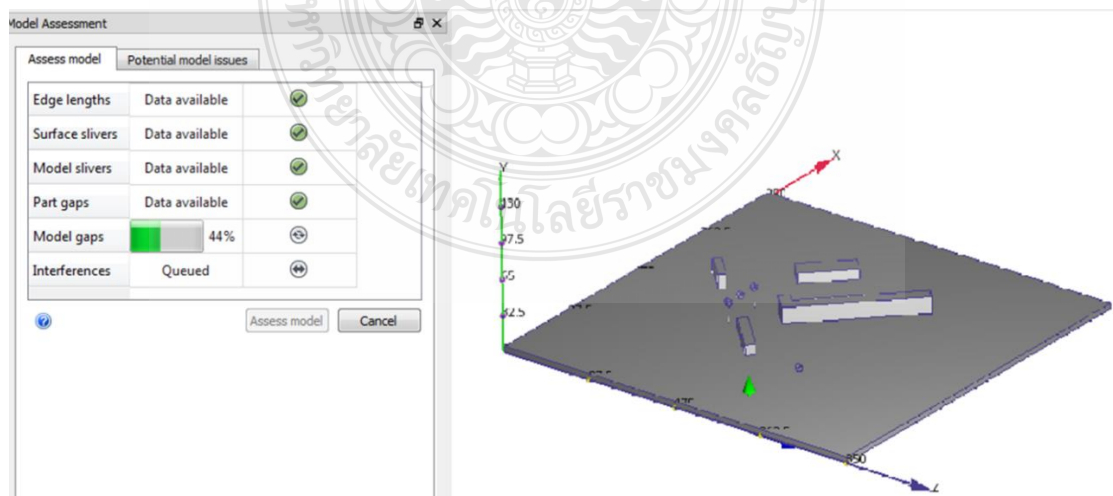


Figure 3 CFDesign model assessment

Step 4 Overall, the model part must be selected by the material, the wind turbine be selected by the solid part, and the air be selected by air fluid material, as shown in Figure 4

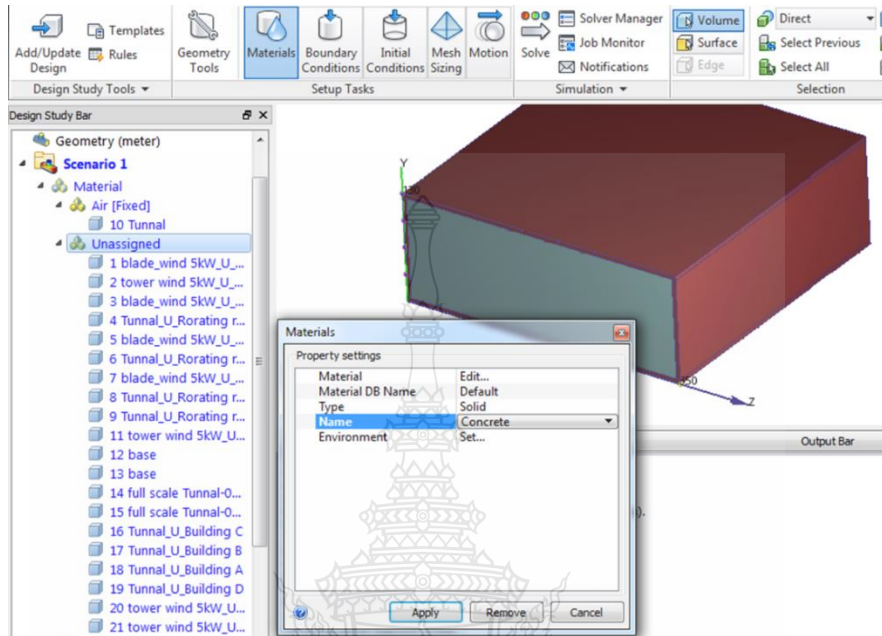


Figure 4 CFDesign material selected

Step 5 Select the boundary condition of the model; the inlet side of model should be selected by 4.5 m/s of air flow and the outlet side by 0 Pa of pressure, as shown in Figure 5

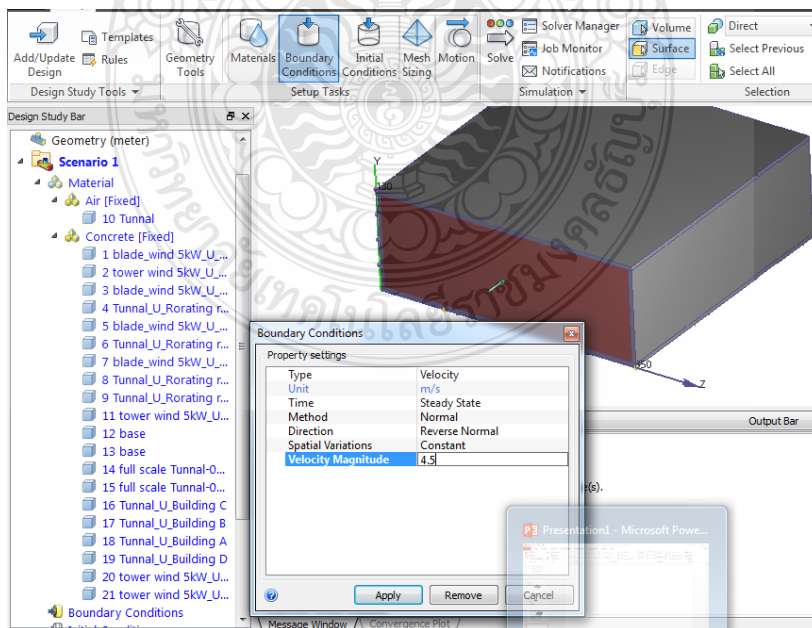


Figure 5 CFDesign boundary condition of the model

Step 6 After selecting the boundary condition, the “Mashing” will be created as shown in Figure 6

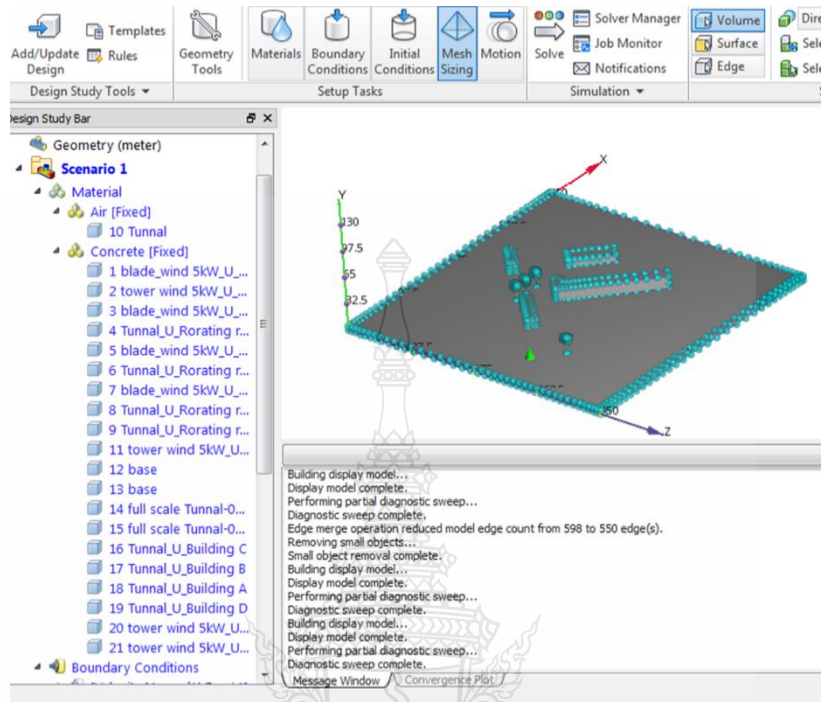


Figure 6 CFDDesign meshing

Step 7 After the model part is meshed, the model will be solved and can be changed to the “turbulence model”, including the $k-\epsilon$, $k-\omega$, and RNG turbulence model, as shown in Figure 7

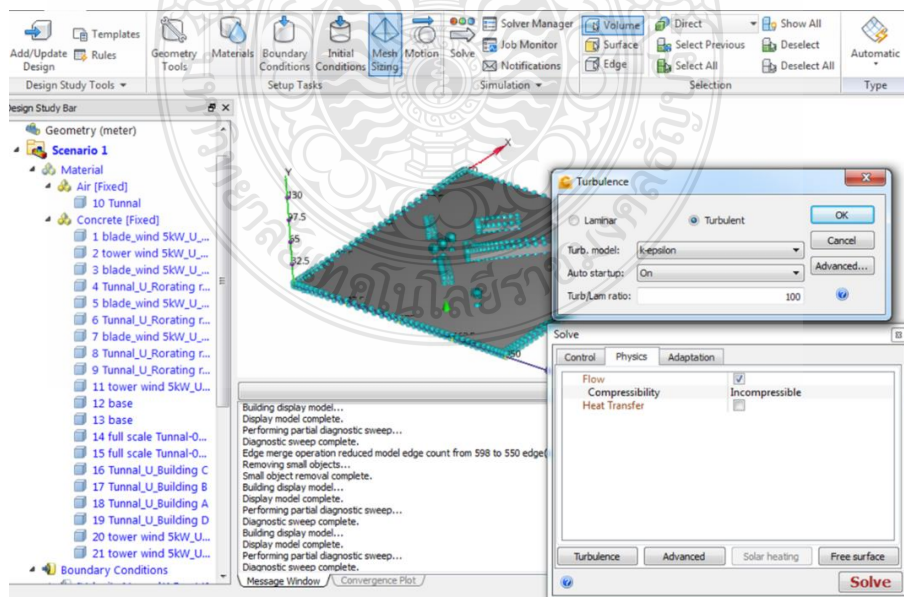


Figure 7 CFDDesign turbulent model selection

Step 8 After all steps are finished, the model will be solved, as shown in Figure 8

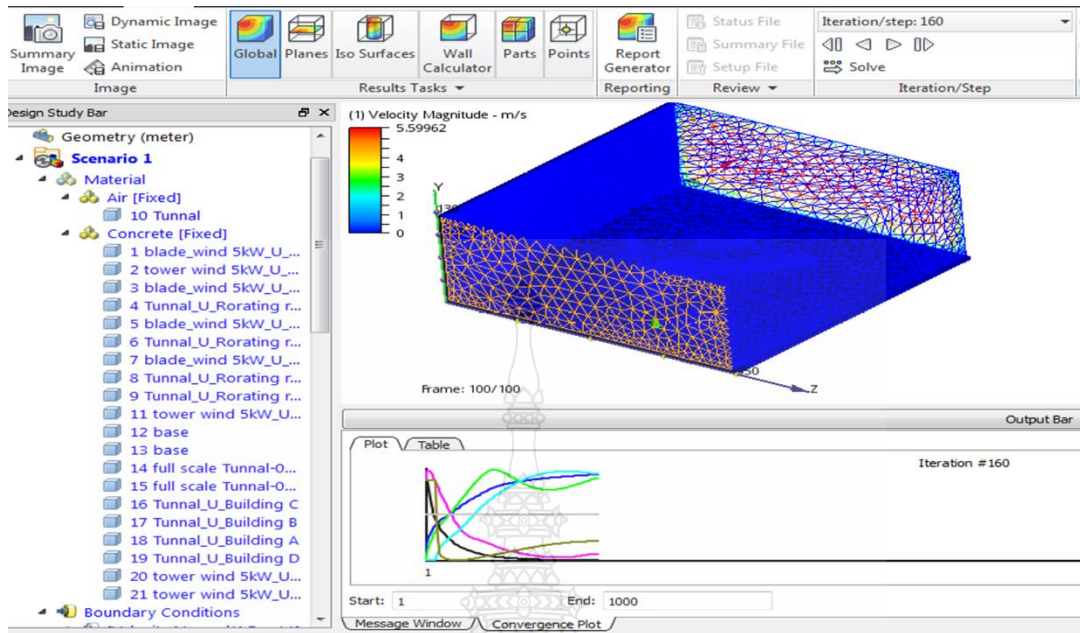


Figure 8 CFDesign solver

Step 9 After completely solving, torque and angular velocity can be found in summary result file in the CFD solver, as shown in Figure 9

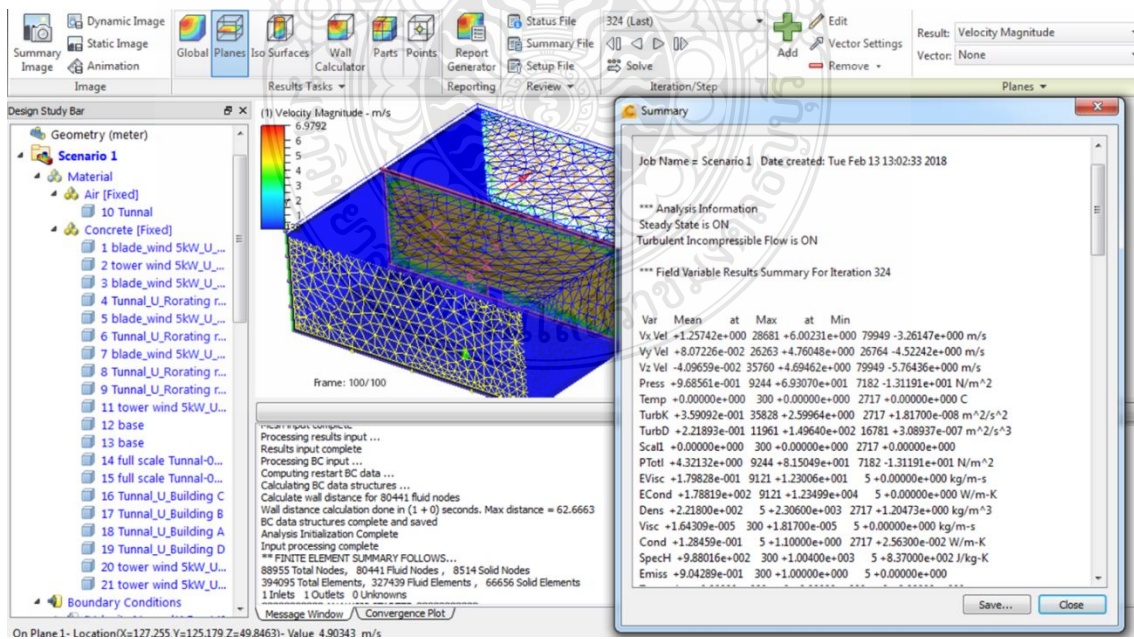


Figure 9 CFDesign solver result



APPENDIX B

CFD Result as Wind Flow from the SW of New Installation Point

CFD Result as Wind Flow from the SW of New Installation Point

Time (sec)	Rotating Speed (RPM)	Hydraulic Force_X (N)	Hydraulic Force_Y (N)	Hydraulic Force_Z (N)
0.50	0.0000	3.246E-06	2.707E-06	4.571E-05
0.50	0.0000	-1.272E-05	-2.670E-06	3.054E-05
0.50	0.0000	-5.387E-05	2.135E-04	-2.422E-04
0.50	0.0000	-6.022E-05	2.927E-04	-2.660E-04
1.00	0.0000	5.916E-05	5.185E-05	1.011E-03
1.00	0.0000	1.637E-04	5.587E-05	7.686E-04
1.00	-0.0002	-5.732E-05	2.812E-04	1.230E-03
1.00	-0.0002	-1.021E-04	4.223E-04	1.632E-03
1.50	0.0001	8.888E-05	6.903E-05	1.908E-03
1.50	0.0000	2.963E-04	1.055E-04	1.640E-03
1.50	-0.0003	-7.414E-06	3.022E-04	2.745E-03
1.50	-0.0004	-8.861E-05	4.834E-04	3.331E-03
2.00	0.0002	9.763E-05	7.176E-05	2.573E-03
2.00	0.0001	3.568E-04	1.357E-04	2.339E-03
2.00	-0.0003	5.833E-05	2.694E-04	3.966E-03
2.00	-0.0004	-5.618E-05	4.709E-04	4.527E-03
2.50	0.0003	9.654E-05	6.683E-05	3.026E-03
2.50	0.0002	3.701E-04	1.500E-04	2.840E-03
2.50	-0.0003	1.157E-04	2.312E-04	4.845E-03
2.50	-0.0004	-2.653E-05	4.444E-04	5.271E-03
3.00	0.0005	9.161E-05	5.863E-05	3.325E-03
3.00	0.0004	3.576E-04	1.550E-04	3.192E-03
3.00	-0.0001	1.612E-04	1.984E-04	5.470E-03
3.00	-0.0003	-1.276E-06	4.197E-04	5.724E-03
3.50	0.0006	8.565E-05	4.984E-05	3.526E-03

CFD Result as Wind Flow from the SW of New Installation Point (Continued)

Time (sec)	Rotating Speed (RPM)	Hydraulic Force_X (N)	Hydraulic Force_Y (N)	Hydraulic Force_Z (N)
1496.000	70.385	-0.003	-0.001	1.069
1496.000	67.348	-0.002	-0.005	0.907
1496.000	85.145	-0.003	-0.004	1.314
1496.500	62.626	-0.004	0.000	0.522
1496.500	70.360	0.002	-0.004	1.068
1496.500	67.325	0.002	-0.001	0.913
1496.500	85.137	0.003	-0.001	1.320
1497.000	62.557	-0.001	0.002	0.519
1497.000	70.335	-0.004	-0.005	1.066
1497.000	67.302	0.000	-0.006	0.903
1497.000	85.130	0.006	-0.007	1.328
1497.500	62.486	-0.003	0.001	0.519
1497.500	70.312	0.001	-0.002	1.066
1497.500	67.278	0.000	-0.001	0.900
1497.500	85.121	-0.001	-0.008	1.322
1498.000	62.417	-0.002	0.002	0.516
1498.000	70.290	0.000	-0.007	1.069
1498.000	67.256	0.002	-0.006	0.908
1498.000	85.114	0.001	-0.002	1.309
1498.500	62.346	-0.003	0.001	0.515
1498.500	70.264	-0.002	-0.001	1.067
1498.500	67.234	-0.001	-0.002	0.904
1498.500	85.104	0.005	-0.004	1.301
1499.000	62.276	-0.002	0.002	0.513
1499.000	70.237	0.001	-0.005	1.064



APPENDIX C

CFD Result as Wind Flow from the SW of Original Installation Point

CFD Result as Wind Flow from the SW of Original Installation Point

Time (sec)	Rotating Speed (RPM)	Hydraulic Force_X (Newton)	Hydraulic Force_Y (Newton)	Hydraulic Force_Z (Newton)
0.5000	0.0000	0.0000	0.0000	0.0000
0.5000	0.0000	0.0000	0.0000	0.0000
0.5000	0.0000	-0.0001	0.0003	-0.0003
0.5000	0.0000	-0.0001	0.0002	-0.0003
1.0000	0.0000	0.0001	0.0000	0.0009
1.0000	0.0000	0.0001	0.0001	0.0008
1.0000	-0.0002	-0.0001	0.0004	0.0012
1.0000	-0.0002	-0.0001	0.0004	0.0008
1.5000	0.0000	0.0001	0.0001	0.0018
1.5000	0.0001	0.0003	0.0001	0.0016
1.5000	-0.0004	-0.0001	0.0005	0.0026
1.5000	-0.0003	-0.0002	0.0004	0.0019
2.0000	0.0001	0.0001	0.0001	0.0026
2.0000	0.0002	0.0003	0.0001	0.0021
2.0000	-0.0005	-0.0001	0.0005	0.0037
2.0000	-0.0004	-0.0001	0.0004	0.0028
2.5000	0.0003	0.0001	0.0001	0.0031
2.5000	0.0003	0.0003	0.0002	0.0025
2.5000	-0.0005	-0.0001	0.0004	0.0043
2.5000	-0.0005	-0.0001	0.0003	0.0034
3.0000	0.0004	0.0001	0.0001	0.0035
3.0000	0.0004	0.0003	0.0002	0.0028
3.0000	-0.0005	0.0000	0.0004	0.0048
3.0000	-0.0005	0.0000	0.0003	0.0039
3.5000	0.0006	0.0001	0.0001	0.0037

CFD Result as Wind Flow from the SW of Original Installation Point (Continued)

Time (sec)	Rotating Speed (RPM)	Hydraulic Force_X (Newton)	Hydraulic Force_Y (Newton)	Hydraulic Force_Z (Newton)
1713.5000	77.9113	0.0007	0.0012	0.8106
1713.5000	66.2024	-0.0004	0.0015	0.7799
1714.0000	64.1293	0.0022	0.0004	0.7001
1714.0000	60.7872	-0.0016	-0.0034	0.6984
1714.0000	77.9179	0.0006	-0.0018	0.8146
1714.0000	66.2076	0.0012	-0.0006	0.7685
1714.5000	64.1372	-0.0018	-0.0006	0.6998
1714.5000	60.7923	0.0016	0.0033	0.7007
1714.5000	77.9237	-0.0022	-0.0001	0.8141
1714.5000	66.2121	-0.0015	0.0005	0.7697
1715.0000	64.1456	0.0012	0.0005	0.7026
1715.0000	60.7982	-0.0014	-0.0036	0.7002
1715.0000	77.9288	0.0007	0.0012	0.8102
1715.0000	66.2172	0.0015	-0.0003	0.7851
1715.5000	64.1527	-0.0010	-0.0006	0.7016
1715.5000	60.8035	0.0016	0.0033	0.7007
1715.5000	77.9343	0.0006	-0.0019	0.8092
1715.5000	66.2213	-0.0016	-0.0001	0.7732
1716.0000	64.1598	0.0007	0.0010	0.7007
1716.0000	60.8087	-0.0015	-0.0037	0.6957
1716.0000	77.9399	-0.0019	0.0008	0.8107
1716.0000	66.2253	0.0013	0.0007	0.7755
1716.5000	64.1674	-0.0005	-0.0012	0.7017
1716.5000	60.8135	0.0016	0.0041	0.6964
1716.5000	77.9446	0.0021	0.0010	0.8054



APPENDIX D

List of Publications

List of Publications

International Journal (ISI)

1. Wichai Pettongkum, W.Roynarin and D.Intholo
“Investigation of PV and Wind Hybrid System for Building Rooftop”
International Energy Journal (2018) .

Impact Factor 2017 = 0.434

Quarties 2016 = Q3

<https://www.rericjournal.ait.ac.th>

2. Wichai Pettongkum, W.Roynarin and D.Intholo
“Investigation of a Pico Turgo Turbine for High-Rise Buildings Using
Computational Fluid Dynamics”

Journal of sustainable development (2018) .

Impact Factor 2017 = 3.25

Quarties 2017 = Q3

<http://www.ccsenet.org/journal/index.php/jsd>

International Conferences

Wichai Pettongkum, Wirachai Roynarin Ph.D., Decha Intholo
“Feasibility using HOMER Software Estimation For Hybrid Wind-PV
System on High-Rise Building
14th Eco-Energy and Materials Science and Engineering Symposium,
Kyoto, Japan, April 03-06, 2018

Biography

Name-Surname	Mr. Wichai Pettongkam
Date of Birth	20 January 1953
Address	99/1 Ngamwongwan 26 Tungsonghong Laksi District Bangkok 10210
Education	-Master of Engineering Program Textile Rajamangala University of Technology Thanyaburi, (2011) -Master of Art Political Science Program Political Management Ramkhamhaeng University, (2005)
Experience Work	-Aeronautical radio Technician, Department of Aviation Ministry of Transport (1973-1976) -Manager, Aviation and Electronics Department, Siam Aviation Company Limited (1976-1978) -Director, Special Project Sale and Service Nitipattana Co., Ltd (1978-1980) - Establish the Private Engineering Business Firm, The Donner co, ltd. Import, Sale, Installation and Services to State Enterprise and Government Sectors, Communication and Navigation Equipment VHF FM Transceiver, HF SSB Transceiver (1980-1985) -Establish the Private Real Estate Business Firm, Buying Selling Land Property and Developing Residential Housing and Condominium Project The Gardenhome Land Management co, ltd The Tri Homes Property co, ltd The Four Homes co, ltd The pitaya Property co, ltd The Sinpattana Enterprises co, ltd (1985-Present)
Telephone Number	08 1633 7082
Email Address	Wichai_p@mail.rmutt.ac.th